DTIC
ELECTE
NOV 16 1990
S E D

STRUCTURAL ENGINEERING

School of Civil and Environmental Engineering

CORNELL UNIVERSITY

ITHACA, NEW YORK

PROBABILISTIC FRACTURE MECHANICS

A VALIDATION OF PREDICTIVE CAPABILITY

Final Report for AFOSR Project
Contract # F49620-87-C-0054

Dr. Spencer Wu, Project Monitor

Drs. Anthony R. Ingraffea
and Mircea Grigoriu
Principal Investigators

August 1990   Report 90-8

Structural Engineering
School of Civil and Environmental Engineering
Cornell University
Ithaca, New York 14853

REPORT DOCUMENTATION PAGE

Form Approved
OMB No. 0704-0188

PORT SECURITY CLASSIFICATION unclassified	1b. RESTRICTIVE MARKINGS
CURITY CLASSIFICATION AUTHORITY	3. DISTRIBUTION / AVAILABILITY OF REPORT unclassified Approved for public release, distribution unlimited
CLASS'FICATION / DOWNGRADING SCHEDULE	
FORMING ORGANIZATION REPORT NUMBER(S) Report 90-8	5. MONITORING ORGANIZATION REPORT NUMBER(S) AFOSR-TR· 90 1074

AME OF PERFORMING ORGANIZATION Dept. of Civil & Env. Engrg., Cornell Univ.	6b. OFFICE SYMBOL (If applicable)	7a. NAME OF MONITORING ORGANIZATION USAF, AFSC, Air Force Office of Scientific Research
DRESS (City, State, and ZIP Code) Ithaca, New York 14853-3501		7b. ADDRESS (City, State, and ZIP Code) Building 410, Bolling AFB Washington, D.C. 20332-6448

AME OF FUNDING / SPONSORING RGANIZATION AFOSR	8b. OFFICE SYMBOL (If applicable) NA	9. PROCUREMENT INSTRUMENT IDENTIFICATION NUMBER F49620-87-C-0054

DRESS (City, State, and ZIP Code) ·Building 410, Bolling AFB Washington, D.C. 20332-6448	10. SOURCE OF FUNDING NUMBERS			
	PROGRAM ELEMENT NO. 61102F	PROJECT NO. 2302	TASK NO. C2	WORK UNIT ACCESSION NO.

TLE (Include Security Classification)
Probabilistic Fracture Mechanics: A Validation of Predictive Capability
(unclassified)

RSONAL AUTHOR(S)
Ingraffea, Anthony R. and Grigoriu, Mircea

TYPE OF REPORT Final	13b. TIME COVERED FROM 4/1/87 TO 30/12/89	14. DATE OF REPORT (Year, Month, Day) August 1990	15. PAGE COUNT 153

JPPLEMENTARY NOTATION

COSATI CODES			18. SUBJECT TERMS (Continue on reverse if necessary and identify by block number)
IELD	GROUP	SUB-GROUP	Probability, Fracture, Fracture Mechanics

BSTRACT (Continue on reverse if necessary and identify by block number)

A two-phase task was undertaken to the Probabilistic Fracture Analysis Code (PROFRANC) developed under this project. Phase one consisted in predicting deterministically the outcome of a subset of a larger number of experiments in which variability in geometry and material parameters was purposely minimized. The purpose of this phase was to verify that PROFRANC could predict nearly deterministic events accurately. This phase was shown to be highly successful.

This verification was based on experimental results which had to be obtained within this project due to a paucity of comprehensive mixed-mode fracture propagation data in the open literature. -) OV over
(continued on back)

ISTRIBUTION / AVAILABILITY OF ABSTRACT UNCLASSIFIED/UNLIMITED ☐ SAME AS RPT. ☐ DTIC USERS	21. ABSTRACT SECURITY CLASSIFICATION unclassified	
NAME OF RESPONSIBLE INDIVIDUAL Dr. Spencer Wu	22b. TELEPHONE (Include Area Code) (202)767-6962	22c. OFFICE SYMBOL AFOSR/NA

orm 1473, JUN 86   Previous editions are obsolete.   SECURITY CLASSIFICATION OF THIS PAGE

In Phase two all currently available data involving inherent uncertainties in some material and geometrical parameters was assembled in a probabilistic framework and subsequently compared to the probabilistic predictions of PROFRANC qualitatively and quantitatively. These comparisons were shown to be very successful. The quantitiative comparison was performed by hypothesis testing, which is a mathematical rule deciding whether to except or reject PROFRANC predictions using experimental data.

Results to date show in particular that:

1. PROFRANC can predict deterministically load to fracture initiation, initial direction of crack extension, complete trajectory to failure, and various load-displacement relationships in arbitrary two-dimensional structures.

2. PROFRANC can accurately predict probabilistic characteristics of fracture phenomena for systems including uncertainties in geometrical and material parameters. This predictive capability includes not only means and variances of all relevant fracture-based responses, but also their full probabilistic descriptions. Two independent hypothesis tests namely, Kolmogorov-Smirnov and Wilcoxon tests, validated these descriptions.

3. It is possible to create a controlled, scientifically designed database for both deterministic and probabilistic response of two-dimensional mixed-mode fracture propagation. Such a database currently cannot be found in the open literature and has been critical in the validation of PROFRANC.

4. A previously unanticipated source of uncertainty was uncovered during the experiments and simulations: variability in supposed boundary conditions. This source of uncertainty has been shown to affect significantly trajectory of curvilinear fracture, and can have a profound effect on the reliability of fail-safe design of structures sensitive to such cracking.

PROBABILISTIC FRACTURE MECHANICS:

A VALIDATION OF PREDICTIVE CAPABILITY

TABLE OF CONTENTS

1.0 INTRODUCTION

This document is the final report for the research project entitled, "Probabilistic Fracture Mechanics". Its principal objective is to demonstrate validation, via recent unique experiments, of previously reported theoretical, analytical, and numerical developments on this project. These developments are focused on the creation of a new capability to predict probabilistically fracture initiation and complete history of propagation under general mixed-mode conditions in arbitrary two-dimensional structures. This new capability integrates classical mixed-mode fracture mechanics and advanced concepts of reliability within a state-of-the-art computational mechanics code, PROFRANC, housed in an engineering workstation.

The validation efforts reported herein concentrated on predictions of load to fracture initiation, initial angle of propagation, total trajectory to structural failure, and load-versus-displacement and load-versus-CMOD relationships. These predictions had to be compared to observations which, because they are absent from the literature, had to be generated within this project. Consequently, an experimental program was designed to develop a broad database for mixed-mode fracture involving uncertainties in material and geometrical parameters.

Section 2 of this report reviews the scarce available experimental results, while Section 3 presents details of the experimental program. A two-phase task was undertaken to validate PROFRANC. Phase one consisted in predicting

deterministically the outcome of a subset of a larger number of experiments in which variability in geometry and material parameters was purposely minimized. This subset included the experiments with variable initial crack length and crack location. The purpose of this phase was to verify that PROFRANC could predict nearly deterministic events accurately. Section 4 shows that this phase was highly successful. Moreover, a more realistic structure has been tested and deterministic validation performed. The structure has holes of variable location relative to initial crack location. Section 5 highlights these results. In Phase two, all currently available data involving inherent uncertainties in some material and geometrical parameters was assembled in a probabilistic framework and subsequently compared to the probabilistic predictions of PROFRANC. A quantitative comparison between the available data and PROFRANC preditions was performed by hypothesis testing. These comparisons are shown to be successful in Section 6. Furthermore, this section includes an immediate practical application of the newly developed technology.

2.0 PRELIMINARY VALIDATION EFFORTS

2.1 Validation of Data from Literature.

An extensive literature search has been conducted on experimental data for crack stability, initial direction of crack extension and crack trajectory. From a very limited number of such available data, a reliable set of nine specimens (Figure 2.1) was found [1] for a preliminary validation of our theoretical model. There are two groups of specimens in this set of nine corresponding to two different loading conditions. The groups are designated as 800 series consisting of six specimens and 900 series containing the remaining three.

Data reported in this study show that geometrical parameters such as initial crack length, specimen thickness, loading angle, and material fracture toughness K_{IC} exhibit statistical variation. Therefore these parameters were modeled as random variables.

The PRobabilistic FRacture ANalysis Code (PROFRANC), developed at Cornell by this research team, was applied to predict the probability of load at fracture initiation and of initial direction of crack extension. Probability distribution of the fracture initiation load was in excellent agreement with the experimental results (Figures 2.2 and 2.3). The experimentally measured values of these loads are very close to the peak of the corresponding probability density curve predicted by PROFRANC. Sensitivity studies show that fracture toughness is the critical
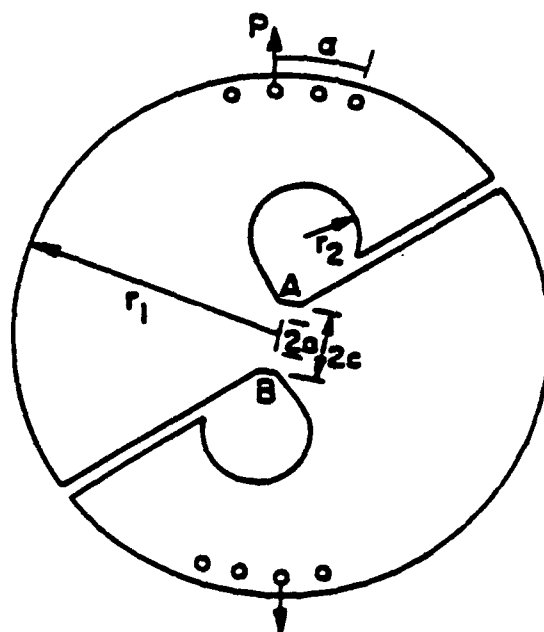
Figure 2.1 Mixed-Mode fracture specimen (r_1 = 95 mm, r_2 = 20 mm), loading angle controls the ratio K_I/K_{II} (from Ref. [1])
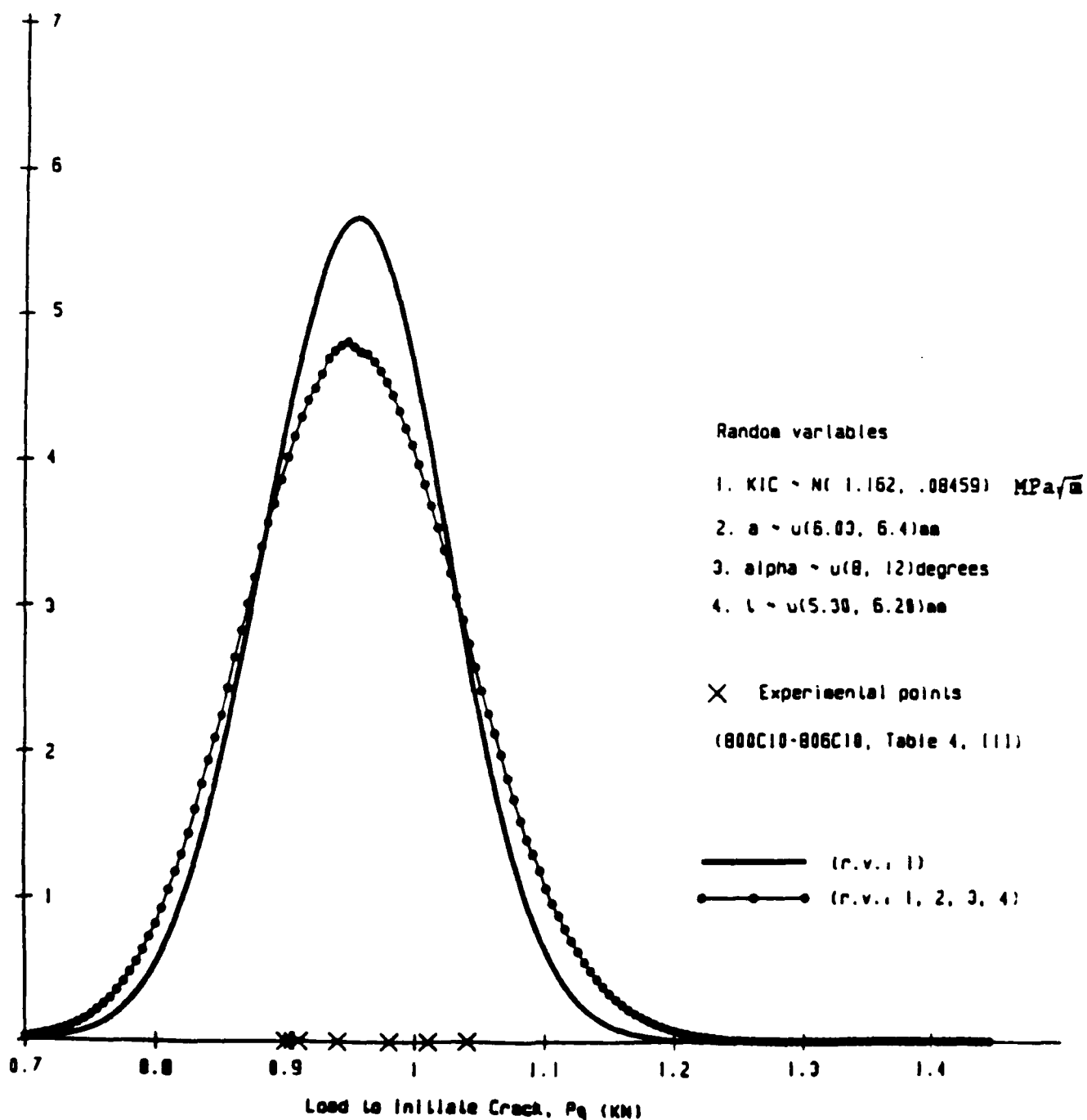
Figure 2.2 Probability density curve of the load to initiate fracture for the 800 series specimens. Experimental results are also shown.

Random variables:

1. KIC ~ N(1.162, .08459) MPa√m̄

2. a ~ u(5.14, 6.28)mm

3. alpha ~ u(18, 22)degrees

4. l ~ u(5.62, 6.22)mm

✕ Experimental points

(902C20-906C20, Table 4, [1])

——————— (r.v.: 1)

●—●—●—● (r.v.: 1, 2, 3, 4)

Load to Initiate Crack, Pq(KN)

Figure 2.3 Probability density curve of the load to initiate fracture for the 900 series specimens. Experimental results are also shown.

parameter for fracture initiation load. Measured crack initiation directions varied by about two degrees from predicted directions (Tables 2.1 and 2.2).

The distribution of a random variable, e.g., angle of or load to fracture initiation, predicted by PROFRANC is based upon a mathematical model derived in [3]. As in case of any theoretical model, this model also re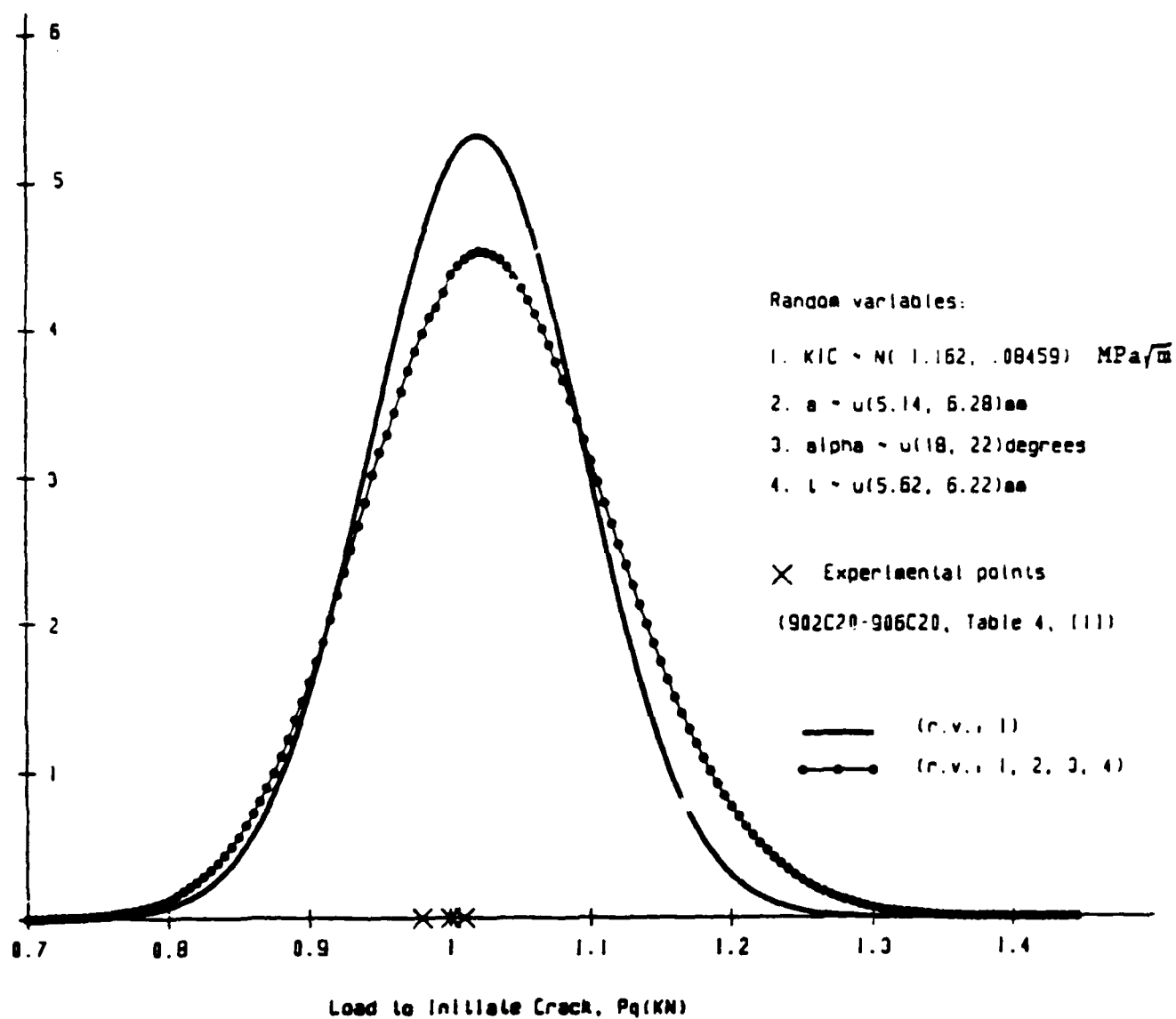lies on certain assumptions and approximations. It is thus essential to ascertain qualitatively and quantitatively the performance of the model by comparing the results predicted by the model with those of the field experiments. In this section we have studied the qualitative comparison between the results predicted by PROFRANC and laboratory experiments from literature. For completeness of the model validation study, we will perform, in the next section, quantitative comparison between the theoretical and experimental results, referred to as hypothesis testing. The central idea of hypothesis testing is as follows. We have a random variable, e.g., load to fracture initiation. From the theoretically predicted (i.e., hypothesized) distribution of this load we can generate its samples. On the other hand, we can generate samples of the load by laboratory experiments. We want to compare these two sets of samples in order to ascertain whether the theoretical samples belong to the same random variable as that of the experiment. There are standard methods of comparison based upon sound mathematical judgment. We shall use some of these methods as tools of our hypothesis testing.

Case	800	Series
	90%	98%
r.v.: a, K_{Ic}	(-67.54, -67.56)	(-67.54, -67.57)
r.v.: a, t, α, K_{Ic}	(-67.20, -67.92)	(-67.17, -67.96)

Table 2.1 Confidence intervals in degrees on initial direction of crack extension for the specimen in Figure 2.1 using the parameters of the 800 series, Table 4, [1]

Case	900	Series
	90%	98%
r.v.: a, K_{Ic}	(-65.49, -65.56)	(-65.48, -65.57)
r.v.: a, t, α, K_{Ic}	(-65.10, -65.91)	(-65.04, -65.96)

Table 2.2 Confidence intervals in degrees on initial direction of crack
extension for the specimen in Figure 2.1 using the parameters
of the 900 series, Table 4, [1]

2.2 Hypothesis Testing

The probability density curves for load to fracture initiation are quantitatively validated in this section by two established statistical tests of hypothesis. Here hypothesis is referred to a statement about the probability distribution of a random variable, namely, the load to fracture initiation. The test of hypothesis is a rule deciding quantitatively whether to accept or reject the hypothesis using the sample data of the random variable.

2.2.1 Kolmogorov-Smirnov Test [33]

This procedure uses individual sample points to perform the test and hence is effective for both small and large number of sample data. The test compares the sample (empirical) cumulative density function (CDF) of the random variable with the corresponding predicted density. The test consists of the following steps.

1. order n samples of experimental loads

   $P_{q1} \leq P_{q2} \leq \cdots \leq P_{qn}$

   Sample CDF: $F_{Exp}(P_{qj}) = j/n$, $j = 1, \ldots n$.

2. Null hypothesis, H_0: r.v P_q has predicted CDF $F_{Pred}(P_q)$ given by PROFRANC

   Alternative hypothesis, H_1: r.v P_q does not have CDF $F_{Pred}(P_q)$

3. select γ, the level of significance of the test

4. specify the rejection region:

   $R = \{D_{max} | D_{max} > D_\nu{}^\gamma\}$

D_n^γ are provided in statistics Tables.

5. calculate

$$D_{max} = \max_{1 \leq i \leq n} \{|F_{Pred}(P_{qi}) - F_{Exp}(P_{qi})|,$$
$$|F_{Pred}(P_{qi}) - F_{Exp}(P_{qi-1})|\}$$

6. if $D_{max} > D_n^\gamma$, reject H_0, accept H_1.

The results of Kolmogorov-Smirnov test for load to fracture initiation are given in Tables (2.3) and (2.4).

2.2.2 Wilcoxon's Test [34]

Suppose we have randomly and independently drawn n observations from the population of experimental loads to fracture and m observations (m ≥ n) from the population of the load predicted by PROFRANC. Wilcoxon test checks the null hypothesis, H_0, that the two populations are identical against the alternative hypothesis, H_1, that they are nonidentical. The test consists of the following steps.

1. Draw m samples of P_q from its predicted distributions $F_{Pred}(P_q)$. Let n be the number of its experimental observations.

2. Order these m + n observations.

3. H_0: r.v P_q has predicted CDF $F_{Pred}(P_q)$

    H_1: r.v P_q does not have CDF $F_{Pred}(P_q)$

4. select γ, the level of significance of the test

5. specify the rejection region:

    $$R = \{W|W < W_{m,n}^\gamma\}$$

    $W_{m,n}^\gamma$ are provided in statistics Tables.

Confidence Limit, γ	D_6^γ(800 series)	Test Results	D_3^γ(900 series)	Test Results
.01	.618	Accepted	.828	Accepted
.05	.521	Accepted	.708	Accepted
.1	.470	Accepted	.642	Accepted
.15	.436	Accepted	.597	Accepted
.2	.410	Accepted	.565	Accepted

$$D_{max} = \left\{ \begin{array}{ll} .22 & 800 \text{ series} \\ .548 & 900 \text{ series} \end{array} \right\}$$

Table 2.3   Results of analyses by Kolmogorov-Smirnov Test. Random Variable: K_{IC}

Confidence Limit, γ	D_6^{γ}(800 series)	Test Results	D_3^{γ}(900 series)	Test Results
.01	.618	Accepted	.828	Accepted
.05	.521	Accepted	.708	Accepted
.1	.470	Accepted	.642	Accepted
.15	.436	Accepted	.597	Accepted
.2	.410	Accepted	.565	Rejected

$$D_{mas} = \left\{ \begin{array}{ll} .25 & 800 \text{ series} \\ .581 & 900 \text{ series} \end{array} \right\}$$

Table 2.4   Results of analyses by Kolmogorov-Smirnov Test. Random Variable: K_{IC}, α, a, t

6. calculate

$W = \sum R_i$ = sum of the ranks of experimental observations among m + n samples.

7. if $W < W_{m,n}{}^{\gamma}$, reject H_0, accept H_1.

The results of Wilcoxon's test for load to fracture initiation and initial direction of crack extension are given in Tables (2.5) and (2.6) respectively.

The tables show that the predicted distribution of load to fracture initiation is accepted by two independent tests of hypothesis for almost all levels of confidence. This validates the model quantitatively and completes the preliminary validation studies.

Successful validation of a probabilistic model depends upon the number of experimental data of the random variable used for the test. The credibility of a hypothesis test increases with the number of experimental data. In the above studies, the number of experimental data used from literature was limited. Our extensive search shows that very limited amount of experimental data are available in literature. This necessitated the additional experiments be conducted to validate current analytical developments.

Confidence Limit, γ	$W_{6,6}^{\gamma}$(800 series)	Test Results	$W_{6,3}^{\gamma}$(900 series)	Test Results
.005	23	Accepted		
.01	24	Accepted		
.025	26	Accepted	7	Accepted
.05	28	Accepted	8	Accepted
.1	30	Accepted	9	Accepted

$$W = \left\{ \begin{array}{ll} 14 & 800 \text{ series} \\ 40 & 900 \text{ series} \end{array} \right\}$$

Table 2.5 Results of analyses by Wilcoxon Test. Random Variable: K_{IC}

Confidence Limit, γ	$W_{6,6}^7$(800 series)	Test Results	$W_{6,3}^7$(900 series)	Test Results
.005	23	Accepted		
.01	24	Accepted		
.025	26	Accepted	7	Accepted
.05	28	Accepted	8	Accepted
.1	30	Accepted	9	Accepted

$$W = \left\{ \begin{array}{ll} 14 & \text{800 series} \\ 38 & \text{900 series} \end{array} \right\}$$

Table 2.6   Results of analyses by Wilcoxon Test. Random Variable: K_{IC}, α, a, t

3.0 MIXED-MODE FRACTURE EXPERIMENTS

3.1 Objective of Experiments

The very limited number of data in the literature necessitates that further experiments be conducted for validation of the present analytical developments. The parameters affecting mixed-mode fracture initiation and trajectory are length, inclination, and location of initial crack, and ratio and orientation of principal material toughnesses. The objective of the experiments is to investigate sensitivities of load to fracture initiation and crack trajectory due to uncertainty in the selected parameters. The experiments will then create a broad base of experimental data for further validation of our analytical developments.

3.2 Background

During the past three decades many experiments have been performed to study the problem of mixed-mode fracture. Erdogan and Sih [2] performed experiments on plexiglas plates. Each plate had an inclined center crack and was subject to uniform tension. Williams and Ewing [4], and Finnie and Weiss [5] tested the same specimen configuration with different materials. Ewing, Swedlow and Williams [6] tested plexiglas panels with an inclined edge crack. They applied two types of loading: uniform tension, and pure bending. Ingraffea [7] tested plexiglass and rock plates with inclined cracks loaded in compression. Banks-Sills [1] tested the plexiglass specimen shown in Figure 2.1. Ingraffea [8], Arrea and Ingraffea [9], Iosipescu [10], Walrath

and Adams [11], Sullivan, Kao and Van Oene [12], Barnes, Kumosa and Hull [13], Wang, Goetz and Corten [14], Bocca, Carpintteri, and Valenti [15], Ballatore, and Carpinteri [16], and Bazant and Pfeiffer [17] tested the so-called Iosipescu shear specimen with different types of materials including rock, concrete, composites and polymers.

In most of the reported experiments, only the initial fracture initiation angle and/or failure load were measured. Furthermore, most of the data, such as initial angle of crack growth, was reported as an average value. This does not allow one to make any statistical analysis of previously reported test data. Because of this, and because of interest in the complete crack trajectory and the need for sufficient variability in geometry and material, many additional experiments had to be performed.

In the forthcoming sections, the specimen material and geometry selection is described, followed by a description of specimen preparation. The experimental setup and testing procedure are then described. This is followed by a section presenting some typical results.

3.3 Selection of Specimen Material and Geometry

3.3.1 Selection of Isotropic Material. The isotropic material selected for use is commercial plexiglas (cyro acrylic FF plexiglas MC) manufactured by Rohms Company. This material has been chosen because:

(i)　　It is a good approximation to a homogeneous, isotropic material.

(ii)　On the scale of the experiments to be performed, it behaves in a linear elastic manner and obeys principles of linear elastic fracture mechanics.

(iii) The material is unaffected by changes in humidity and temperature. This reduces considerably variability in our experimental results caused by unwanted environmental effects.

(iv)　It is easy to machine and to form natural cracks.

(v)　　It is transparent so that it is easy to track crack growth, and to detect accurately fracture initiation.

(vi)　It is affordable, so many specimens can be tested.

3.3.2 Selection and Preparation of Anisotropic Material. To study the effects of ratio and orientation of principal material toughnesses, it was necessary to find an affordable material, isotropic in stiffness, but anisotropic in toughness. After an extensive investigation of material science and polymer engineering literature [18,19,20], and consulting with several researchers at Cornell, it has been found that by hot-stretching plexiglas above its glass transition temperature (about 110 degree centigrade), the material can be made anisotropic in toughness while keeping the same isotropic elasticity properties. Furthermore, by hot-stretching the material to different strains

(from 0% to 150%) a material with varying toughness ratios (from 1 to About 2) can be obtaine 1.

To create the specimens for this project the plexiglas was hot-stretched at a temperature of $120^{\circ}C$ to an elongation of about 50%. The material was then cooled slowly at constant length. The cooling rate was approximately $2^{\circ}C$/minute.

3.3.3 Selection of Specimen Geometry. Figure 3.1 shows the type of specimen selected for testing. It consists of a simply supported, centrally loaded beam. The initial crack is placed away from the center of the beam to produce, under the given boundary conditions, mixed-mode crack initiation and curvilinear trajectory. This specimen geometry has been chosen to:

(i)   ensure plane strain conditions and a small process zone ahead of the crack tip compared to crack length and other characteristic dimensions of the specimen, based on principles of linear elastic fracture mechanics.

(ii) prevent out-of-plane buckling and minimize maximum load.

(iii) guarantee sufficiently large area for t.1e crack trajectory, and to enable variable geometry parameters.

(iv) ensure that the specimen may be easily prepared and loaded.

A similar specimen configuration was used by Jenq and Shah [21] to study mixed-mode fracture in concrete. Note that the
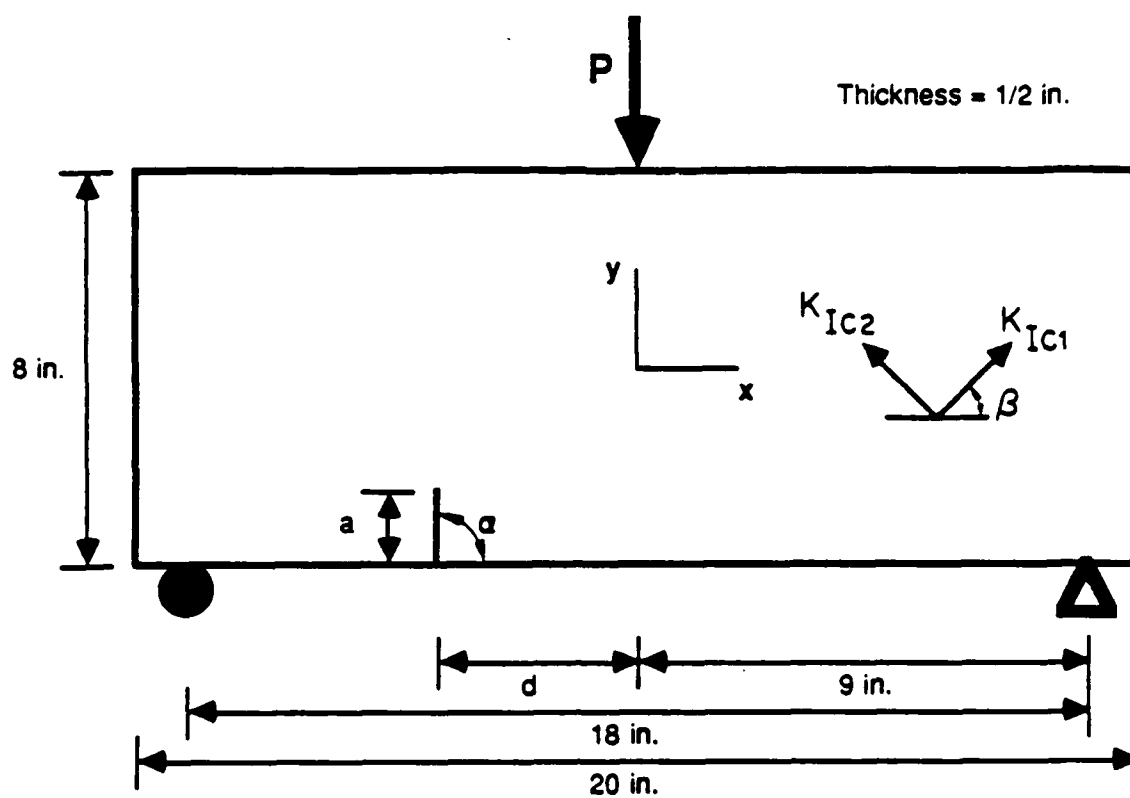
Figure 3.1 Configuration selected for testing

selected specimen is quite similar to the Iosipescu shear specimen. The reasons for not using the Iosipescu specimen are:

(i)   It contains two initial cracks symmetric to each other. In practice, one will always initiate before the other. This will make the specimen response asymmetric, and difficult to analyze. This was pointed out by Ingraffea and Panthaki [22].

(ii) the selected specimen is much easier to prepare and to load.

(iii) the selected specimen still allows mixed-mode fracture if the initial crack is placed away from the center of the beam.

3.4 Preparation of Specimen

Specimens have been made from plexiglas sheets with mechanical properties, provided by the manufacturer, shown in Table 3.1. However the key properties were determined directly from the material used in the tests.

After cutting the specimens, all edges were carefully machined to produce dimensional accuracy of +/- 1/32 inch. At the position of the starter crack, a notch was carefully made using an automatic bandsaw. The notch length is accurate to +/- 1/64 inch and orientation was accurate to +/- 1/4 degrees. At the end of the starter notch, a natural crack was formed by forcing a razor blade into the end of the notch.

Property	ASTM Method²	Units	Plexiglas MC
Mechanical Tensile Strength (¼" specimen- 0.2"/Minute) Maximum Elongation, Maximum Modulus of Elasticity	D638	psi % psi	10,000 4.5 450,000
Flexural Strength (Span depth ratio 16, 0.1"/Minute) Maximum Deflection, Maximum Modulus of Elasticity	D790	psi inches psi	15,000 0.6 450,000
Compressive Strength (0.05"/Minute) Maximum Modulus of Elasticity	D695	psi psi	16,000 430,000
Impact Strength Charpy Unnotched	D256	ft. lbs./ ½" x 1" section	7.0
Rockwell Hardness	D785	—	M-90°
Resistance to Stress Critical Crazing Stress Isopropyl Alcohol Toluene	ARTC Mod. of MIL-P-6997	psi psi	1,300 1,200

Table 3.1   Mechanical properties of plexiglas provided by Rhoms manufacturing company

Two small plexiglas pieces were then glued to the specimen at the two sides of the notch mouth. A clip gage, which was used to measure the crack-mouth-opening displacement (CMOD), was then attached to these pieces. This will be explained in more detail in the next two sections. Finally, a transparent graph paper was glued to one side of the specimen to record visually and approximately the location of the propagating crack tip during the test.

3.5 Experimental Setup

The experimental setup, shown schematically in Figure 3.2, consists of a new MTS load frame, a control microconsole, a data acquisition system with A/D and D/A converters, a microcomputer, and a microscope.

An MTS control microconsole is used for initial control of this closed loop system. It is used prior to testing to zero all the channels and then to transfer control to the computer program which will control testing. The data acquisition system contains both A/D and D/A converters plugged directly into the microcomputer. An interactive, menu-driven program was written to control the experiments.

Three channels are monitored during the experiments: load, displacement under the load, and crack-mouth-opening-displacement. The experiments were conducted under CMOD control to ensure slow crack growth. If tested under load control, crack growth would always be unstable and dynamic. On the other hand,

Data Aquisition
System

MTS 458.30 Control
Microconsole

Microcomputer
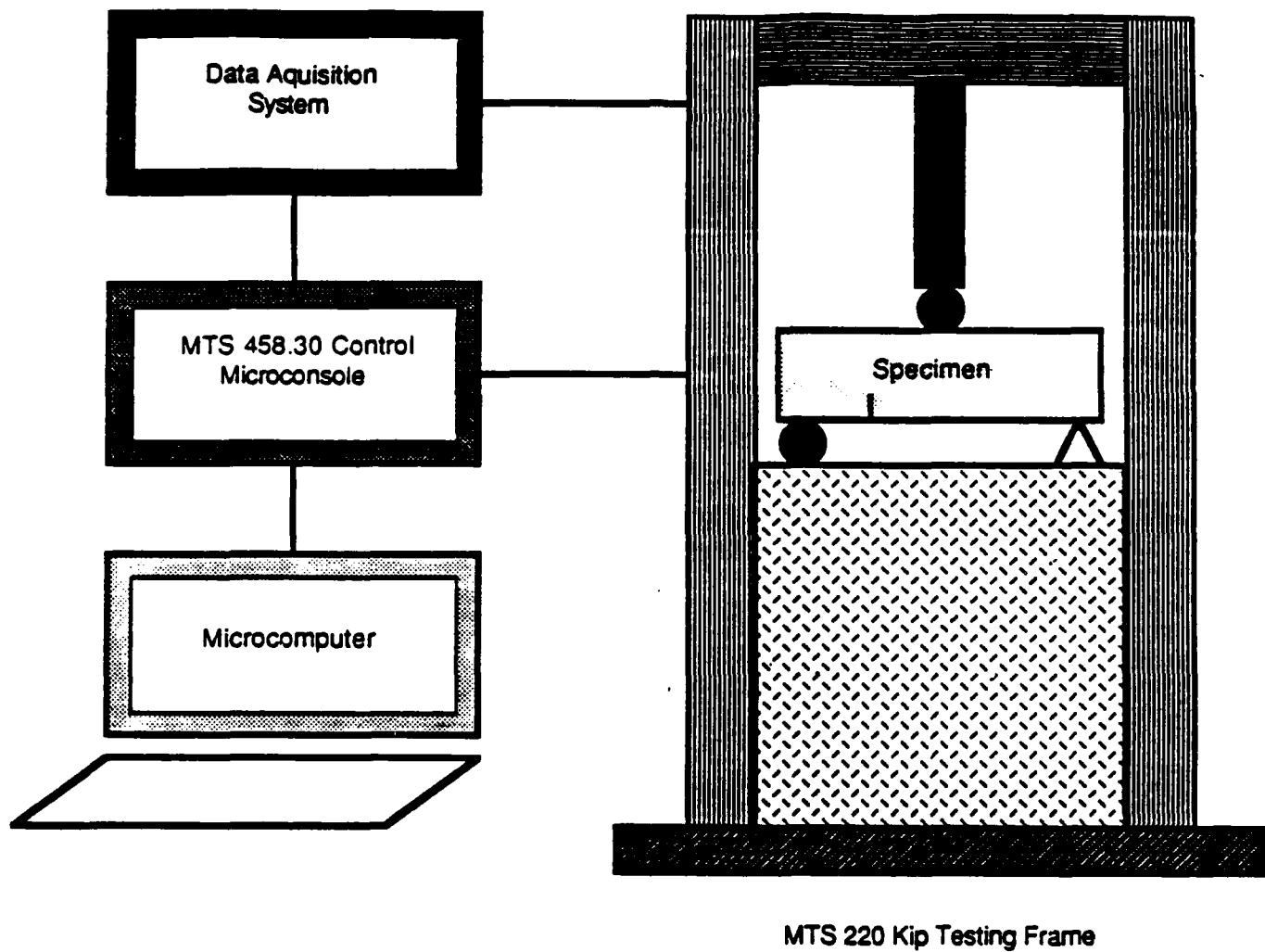
Specimen

MTS 220 Kip Testing Frame

Figure 3.2 Schematic description of experimental setup

if testing was performed under displacement control, then crack growth might or might not be stable and slow. This depends on length, inclination and location of the initial crack.

Clausing [23] confirms this result theoretically based on principles of linear elastic fracture mechanics. Figure 3.3 shows a simply supported beam with a center crack subject to two point loads. The figure reveals that there is a transition point from stability to instability when one decreases the initial crack length. The same conclusions were reached by Mai and Atkins [24,25]. Since their theoretical results were only valid for Mode I tests under displacement control, the applicability of this concept to the mixed-mode case was tested by performing a series of stability studies using the finite element method. It was observed, as predicted, that length, inclination and location of initial crack are the key parameters that control specimen stability. Under CMOD control, the selected configuration is unconditionally stable.

3.6 Test Procedure

Readings of load, displacement under the load, and CMOD were performed continuously. The CMOD was monitored with an MTS extensometer placed to measure the relative opening of the crack mouth. The extensometer was calibrated over the expected range of CMOD to a maximum error of about 0.25%. The load was monitored through a load-cell, mounted directly in the activation, with a capacity of 5 kips and calibrated to a maximum error of less than
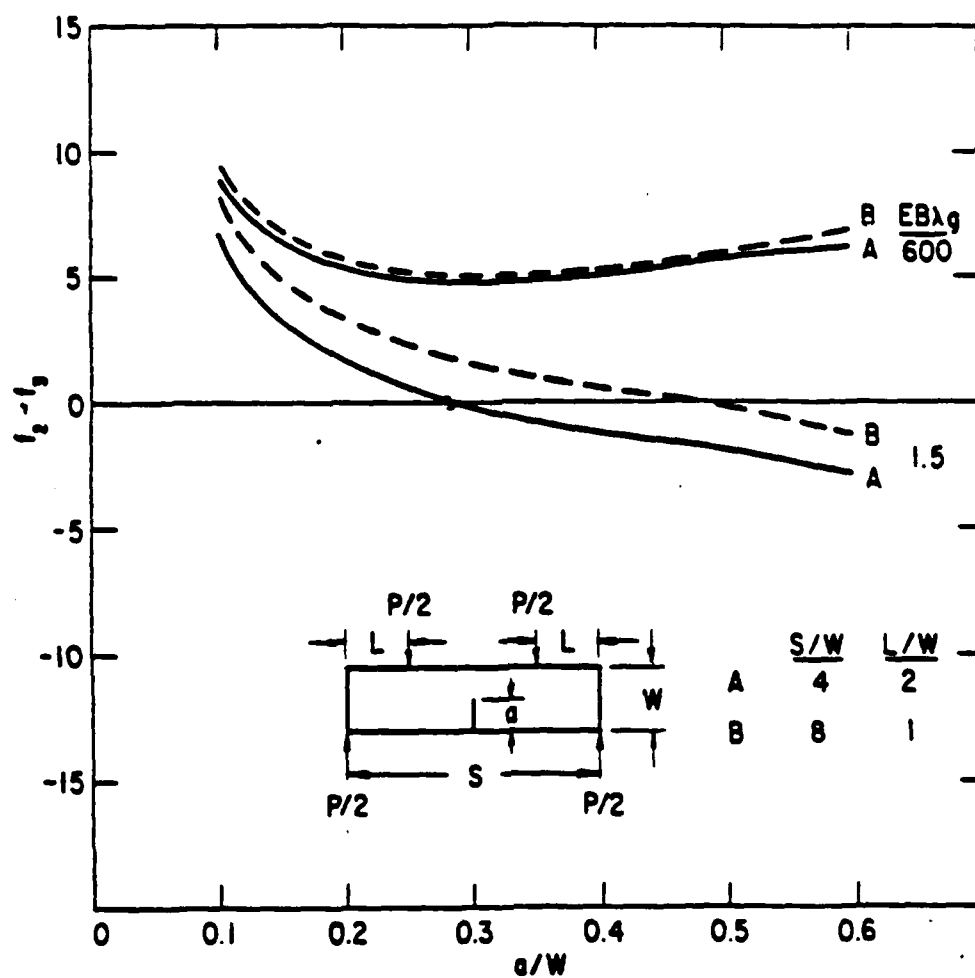
Figure 3.3 Stability parameter for bend specimens as function of ratio of initial
crack length to depth of beam. (From Clausing [23])

0.1% over this range. Displacement under the load was measured with an LVDT mounted within the load actuator. Although this LVDT has been calibrated to a maximum error of 0.25% over its 0.50 in range, its reading of beam displacement was relative since support settlements and load-line displacement is also included in its readings.

The specimen was loaded monotonically in CMOD control using very small increments. Prior to fracture initiation, load and CMOD increase proportionally in a linear fashion. The crack tip is observed with a traversing distance microscope to detect accurately start of fracture initiation. Load to fracture initiation was accurately measured by finding the points on the load-verus-CMOD curve at which departure from linearity commenced. After fracture initiation, load and displacement under the load adjusted themselves, i.e. increased or decreased, to keep the CMOD equal to the CMOD requested by the program. At fracture initiation, the crack propagated in a slow and stable manner until it stopped. The location of the new crack tip was then approximately recorded using transparent graph paper, but later accurately obtained from load versus-CMOD records using compliance calibration technique. This procedure was then repeated until the test was completed. Ingraffea [8], Ingraffea and Arrea [9] used the same testing procedure to test rock and concrete beams, respectively. Bocca, Carpinteri, and Valenti [15], and

Ballatore and Carpinteri [16] later used a similar experimental procedure.

3.7 Typical Results

3.7.1 Load, Displacement, and CMOD Records. A typical mixed-mode specimen (a=1 in,d=6 in), as shown in Figure 3.1, was tested under CMOD control. Its load-versus-CMOD and load-versus-load-line displacement curves are shown in Figures 3.4 and 3.5.

The load-versus-CMOD curve follows a straight line until the load reaches a critical value. As previously mentioned, this value corresponds to fracture initiation. The load-versus-displacement curve shows, however, a slightly nonlinear relation at small loads caused by local nonlinear deformation at load and reaction points. Upon further increase of load, the curve becomes linear up to fracture initiation. However, the predicted slope is always greater than the observed because of (i) nonlinear effects of supports and at loading point; and (ii) deformation in the loading train.

3.7.2 Crack Trajectory. Figure 3.6 shows an observed crack trajectory for a mixed-mode specimen. Following fracture initiation, the crack propagates along a curve that changes curvature in the upper part of the beam. It approaches a vertical direction toward the top of the beam and does not cross the load plane.

3.7.3 Observation of Fracture Surfaces. Figure 3.7 shows some characteristics of the fracture surfaces observed in the
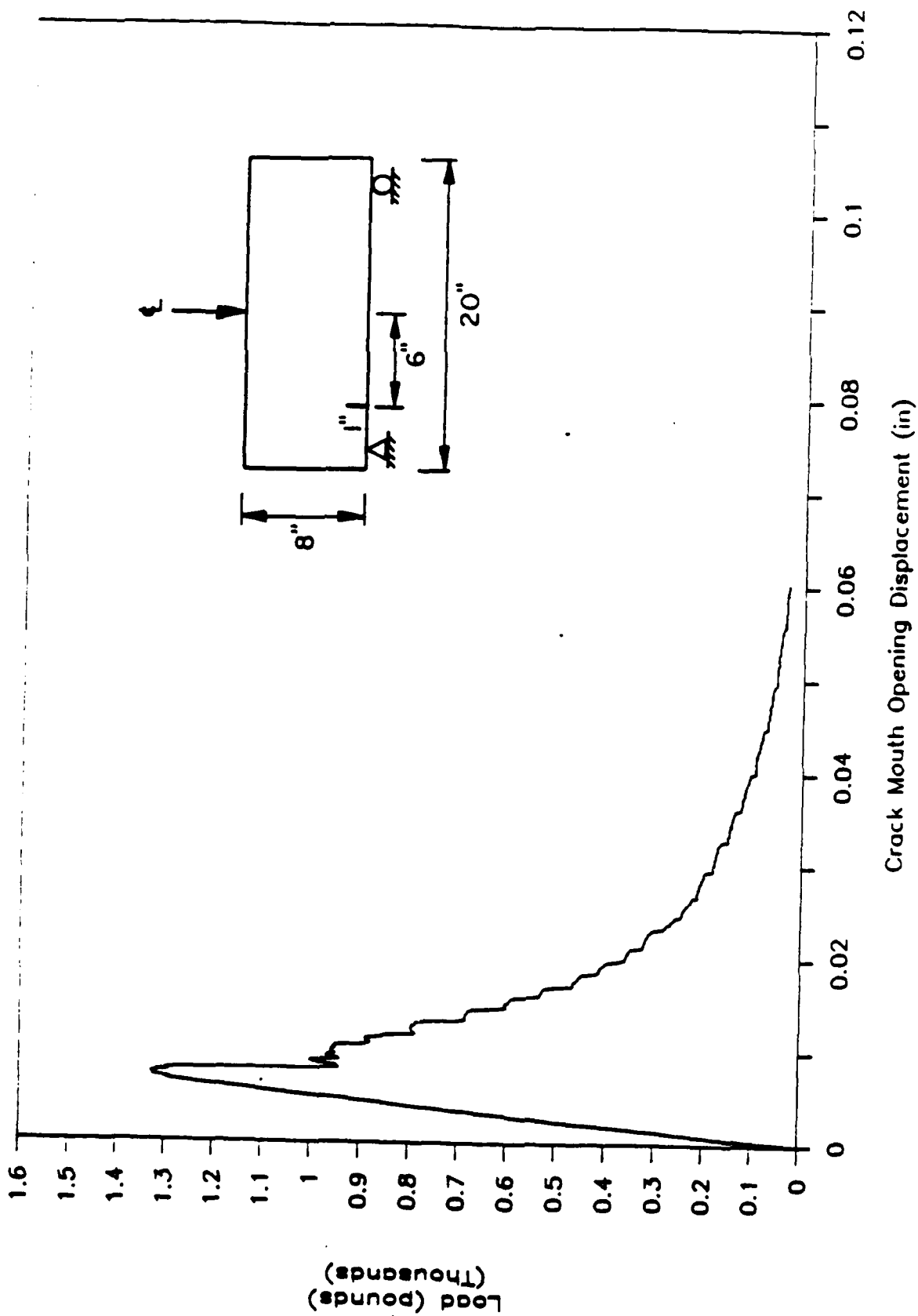
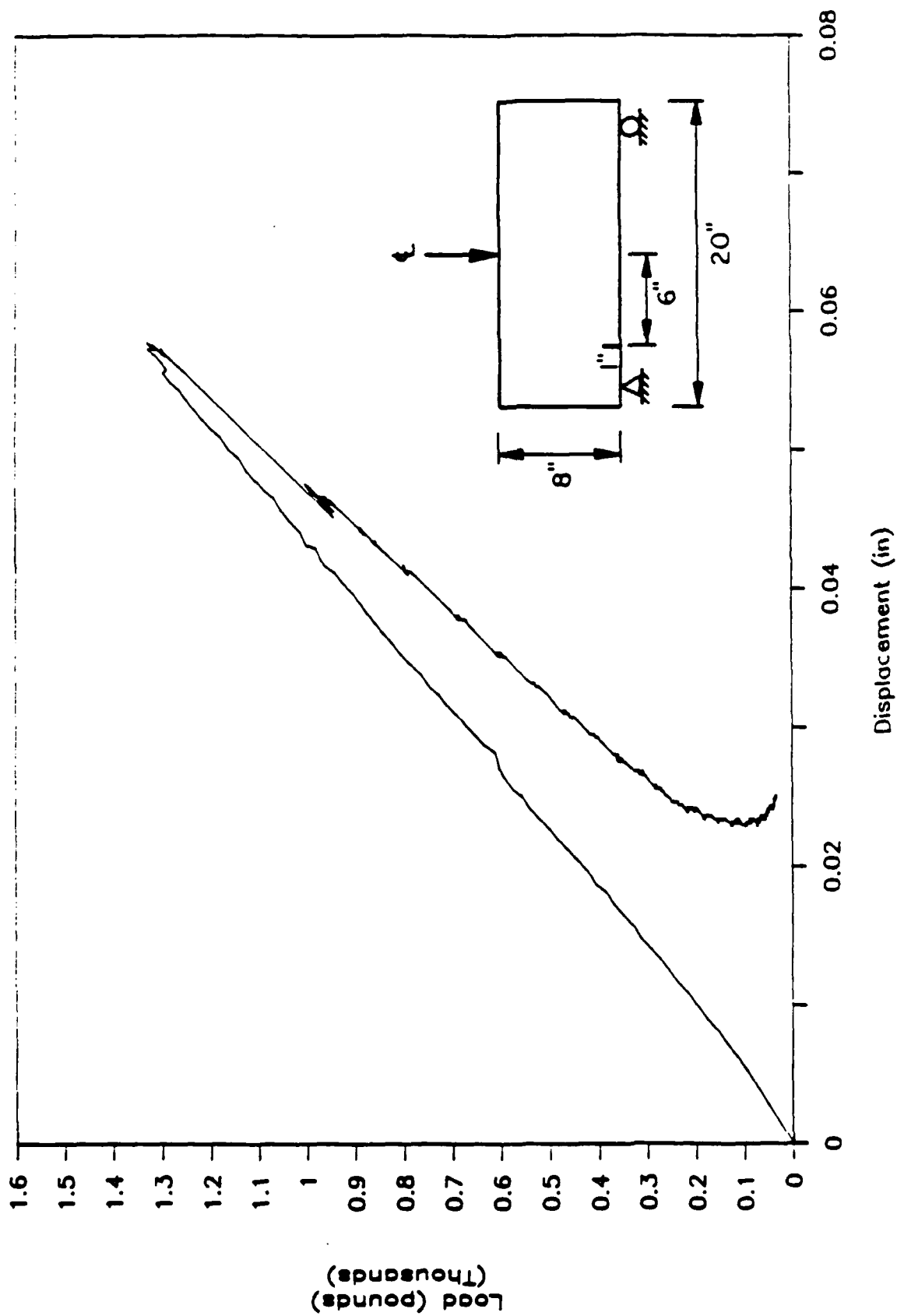Figure 3.4 Plot of measured load-versus-CMOD for a typical mixed-mode specimen (a = 1 inch, d = 6 inches)

Figure 3.5 Plot of measured load-versus-load-line-displacement for a typical
mixed-mode specimen (a = 1 inch, d = 6 inches)
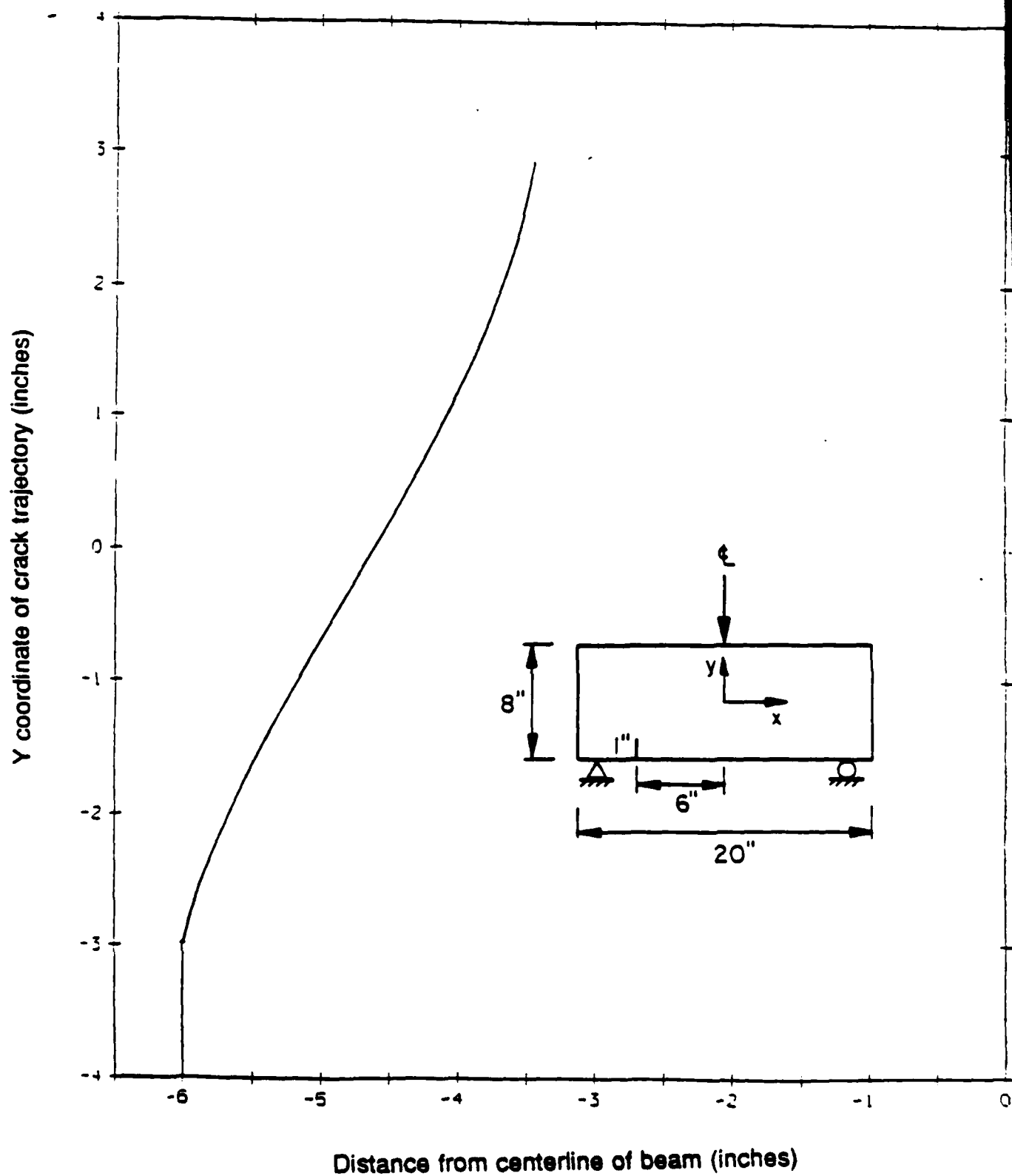
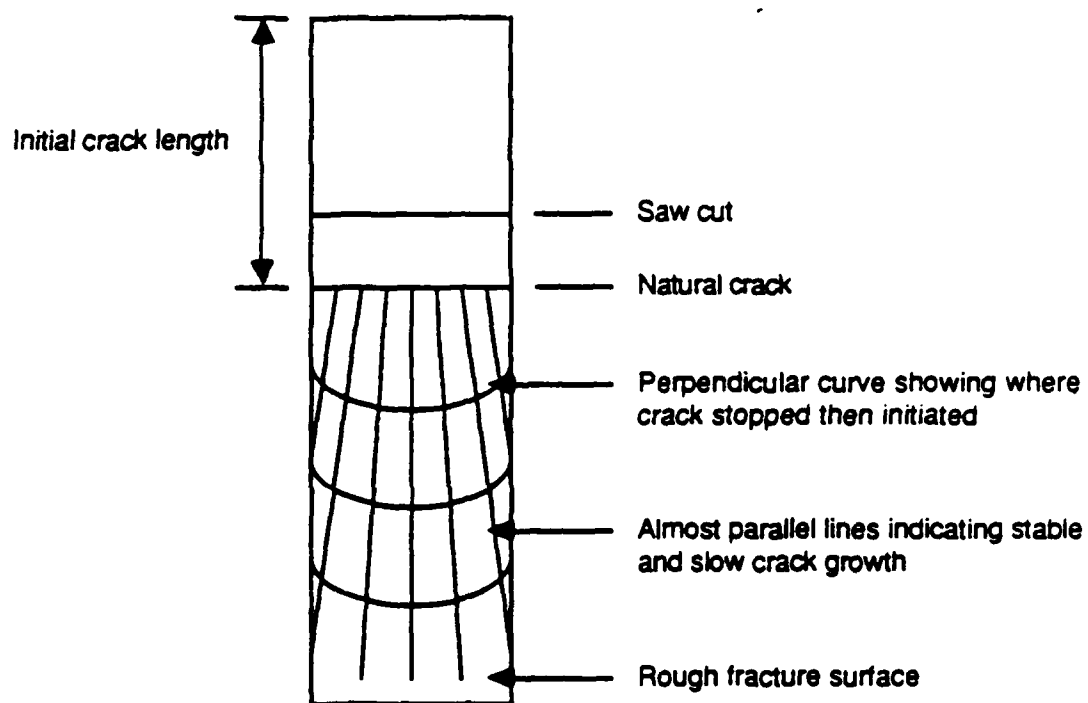Figure 3.6   Observed crack trajectory for a typical mixed-mode specimen (a = 1 inch, d = 6 inches)

Figure 3.7   Fracture surface observations (after Williams, Radon and Turner [27])

tests. The surface was rather rough with almost parallel mark-ings of lines in the direction of propagation, indicating stable and slow crack growth. The same observation was made by Williams, Radon and Turner [27]. The figure also shows a series of markings of curves that run roughly perpendicular to the crack trajectory. These curves indicate where the crack stopped and re-initiated. These curves provide, therefore, an accurate method to locate the crack tip at each step of propagation. In the future, this additional information will be used to verify crack length indirectly computed from compliance calibration.

3.8 Summary

The limited number of published data required that further experiments be performed to validate analytical developments for both isotropic and orthotropic materials. These experiments are investigating sensitivities of load to fracture initiation and crack trajectory due to length, inclination and location of initial crack, and ratio and orientation of principal material toughnesses. Their purpose is to create a uniform probabilistic distribution of these stochastic variables.

A mixed-mode specimen was carefully designed to ensure applicability of linear elastic fracture mechanics, ease of preparation and testing procedure and other criteria. CMOD control was used to ensure stable and slow crack growth. This is because the interest was not only the initial fracture initiation load but the entire fracture trajectory and load history.

Experimental results to date on isotropic plexiglas include records of load-versus-CMOD and load-versus-load-line displacement, as well as crack trajectories and observations of fracture surfaces. All of these results, and other material property measurements also performed, will be used in the following sections to validate both deterministic and probabilistic analytical formulations for isotropic materials.

Preliminary work completed on anisotropic materials includes:

(i)   Fabrication of orthotropic plexiglas using a special procedure to produce desireable ratio of principal toughnesses.

(ii)   Measurements of elastic properties and direct tensile strength.

(iii)   Measurements of fracture toughness in principal directions.

4.0 DETERMINISTIC FRACTURE VALIDATION

The probabilistic fracture mechanics code PROFRANC developed at Cornell is based on methods of reliability analysis and theories of deterministic linear elastic fracture mechanics. The code accounts for the uncertainty in loads, material properties, crack geometry and other uncertain parameters. The validation of PROFRANC requires the evaluation of fracture mechanics theories used in this code. This evaluation is performed as follows. An accurate finite element model of the model specimen was prepared. The models were calibrated to experimental measurements to minimize uncertainties in these parameters. An analysis was then performed, and predicted deterministic results were compared with actual measured results. These results include load, displacement, and crack mouth opening displacement records, fracture initiation load and angle, and crack trajectories.

4.1 Deterministic Fracture Analysis.

Four tested specimens with varying initial crack length (a=1,2,3,4 in) but the same crack location and inclination were selected for deterministic validation of the code (Figure 3.1). Values of geometrical and material parameters have been obtained from measurements of these specimens. Each analysis was based on average values of measured material properties and the observed values of geometry parameters include location, length and inclination of initial crack, length, depth and thickness of the

specimen. The material parameters include modulus of elasticity and fracture toughness.

The modulus of elasticity was obtained from the initial stiffness of observed load versus CMOD. The average value of the modulus of elasticity for the four selected specimens was 474,000 psi. The variation of observed modulus of elasticity about this value was 6%. The observed average modulus of elasticity is very close to the value of 450,000 psi provided by the manufacturer in Table 3.1.

The plane strain fracture toughness was obtained from a single edge notch bending fracture toughness test. The average value of fracture toughness was found to be 944 lb-in$^{-3/2}$. The variation about this value of measured fracture toughness was 1.8%.

PROFRANC running in a deterministic mode was used to predict fracture initiation loads, crack trajectories, and load-versus-CMOD and displacement. The output is consistent with experimental results. The analysis is based on the maximum circumferential stress theory. Several finite elements meshes of decreasing size have been used to insure computation accuracy.

4.2 Experimental Measurements and Deterministic Predictions

4.2.1 Load Versus CMOD Records. Figures 4.1 to 4.4 show plots of observed and predicted load-versus-CMOD for all four specimens. The agreement between experimental and predicted results is remarkable. The post-peak portion of both curves show
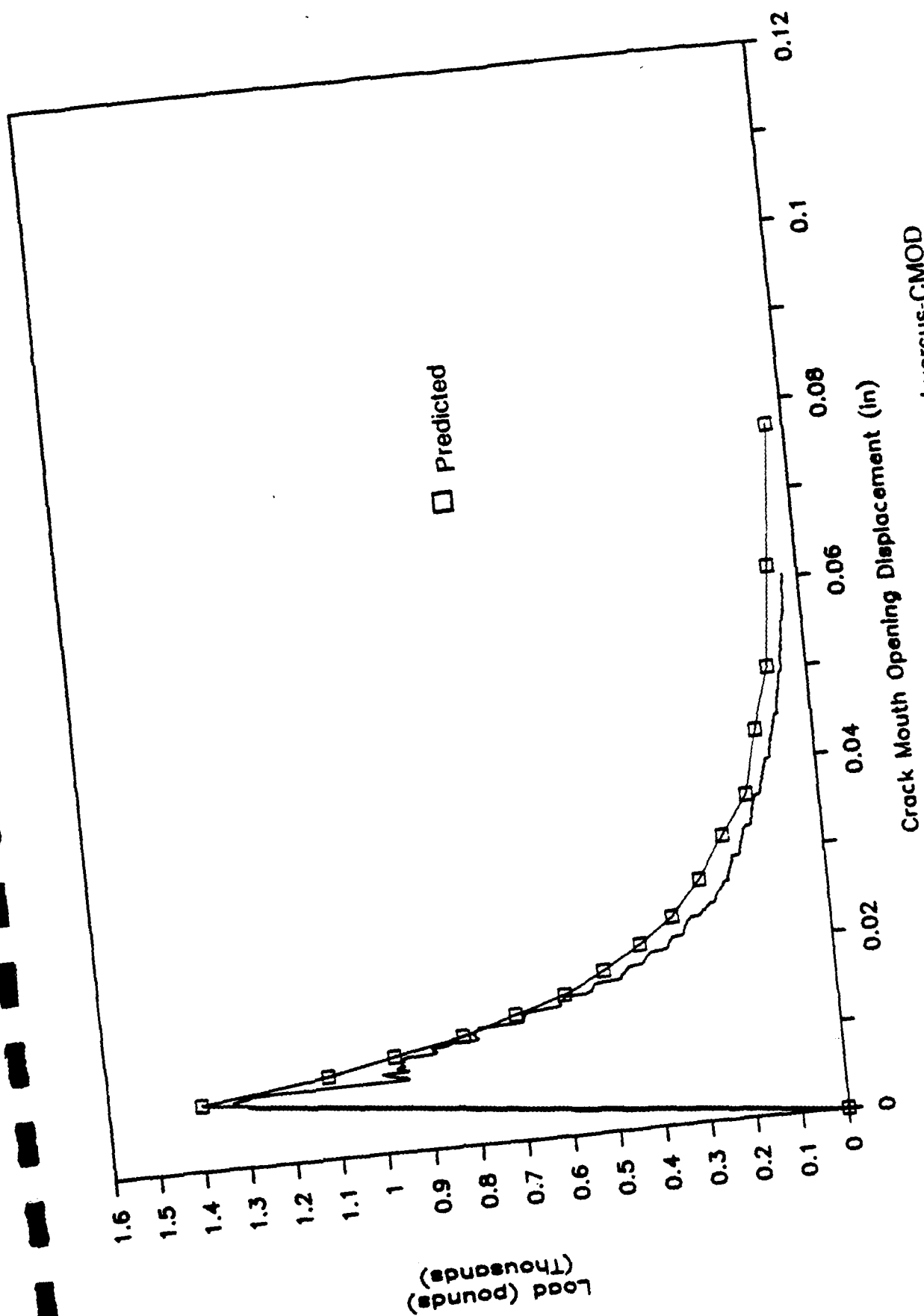
Figure 4.1 Plots of measured and predicted load-versus-CMOD
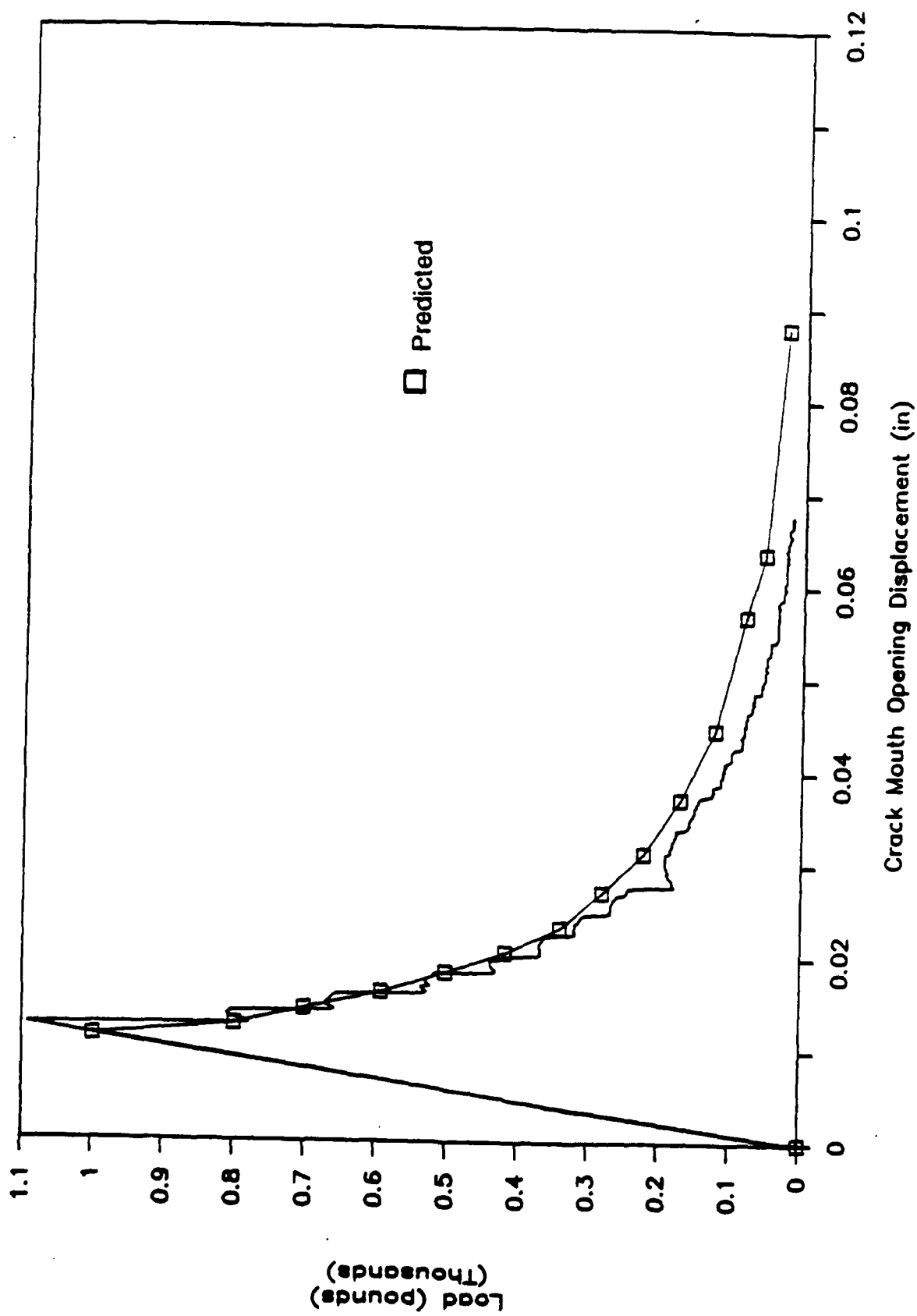for specimen #1 (a = 1 inch, d = 6 inches)

Figure 4.2 Plots of measured and predicted load-versus-CMOD
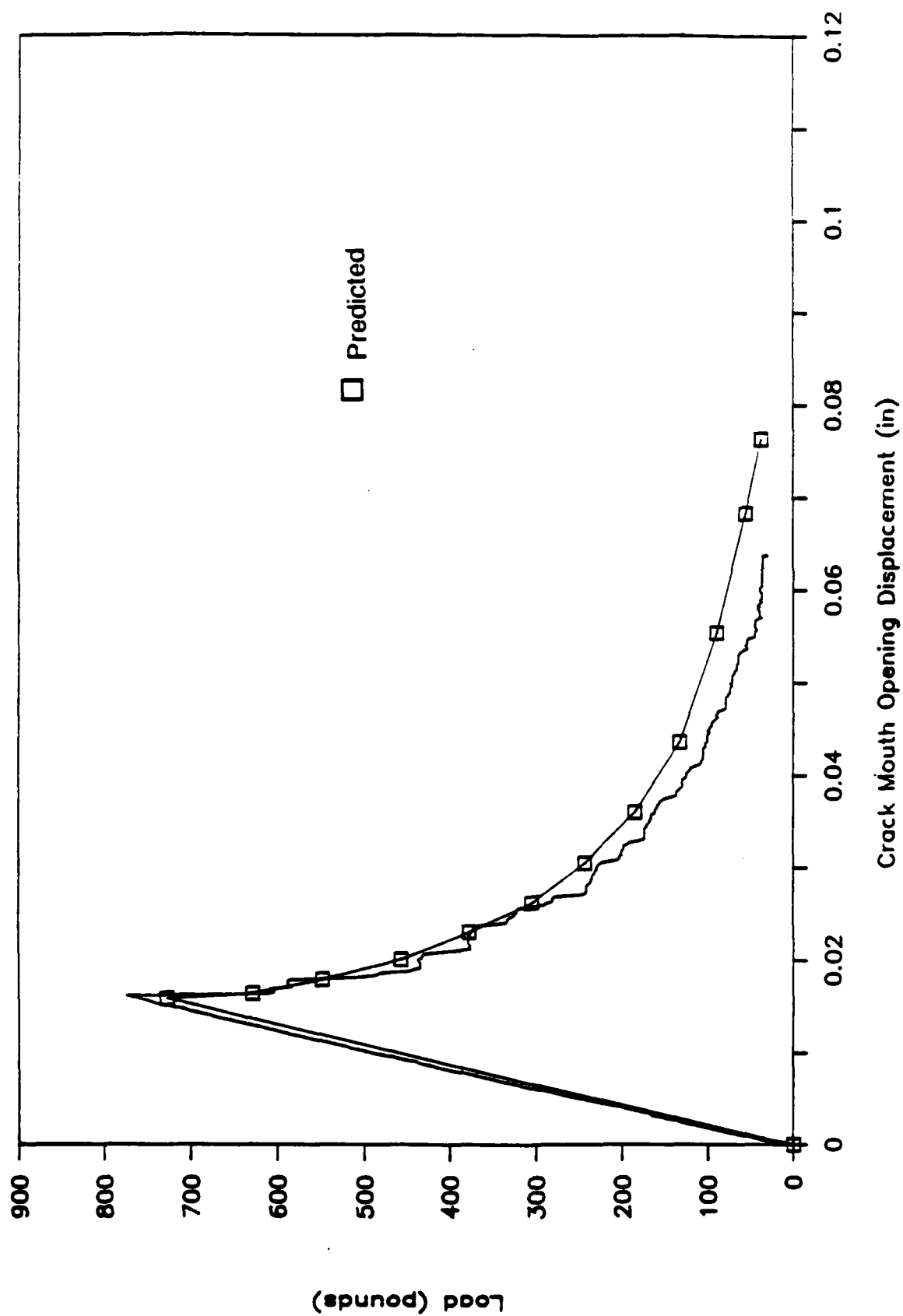for specimen #2 (a = 2 inches, d = 6 inches)

Figure 4.3 Plots of measured and predicted load-versus-CMOD
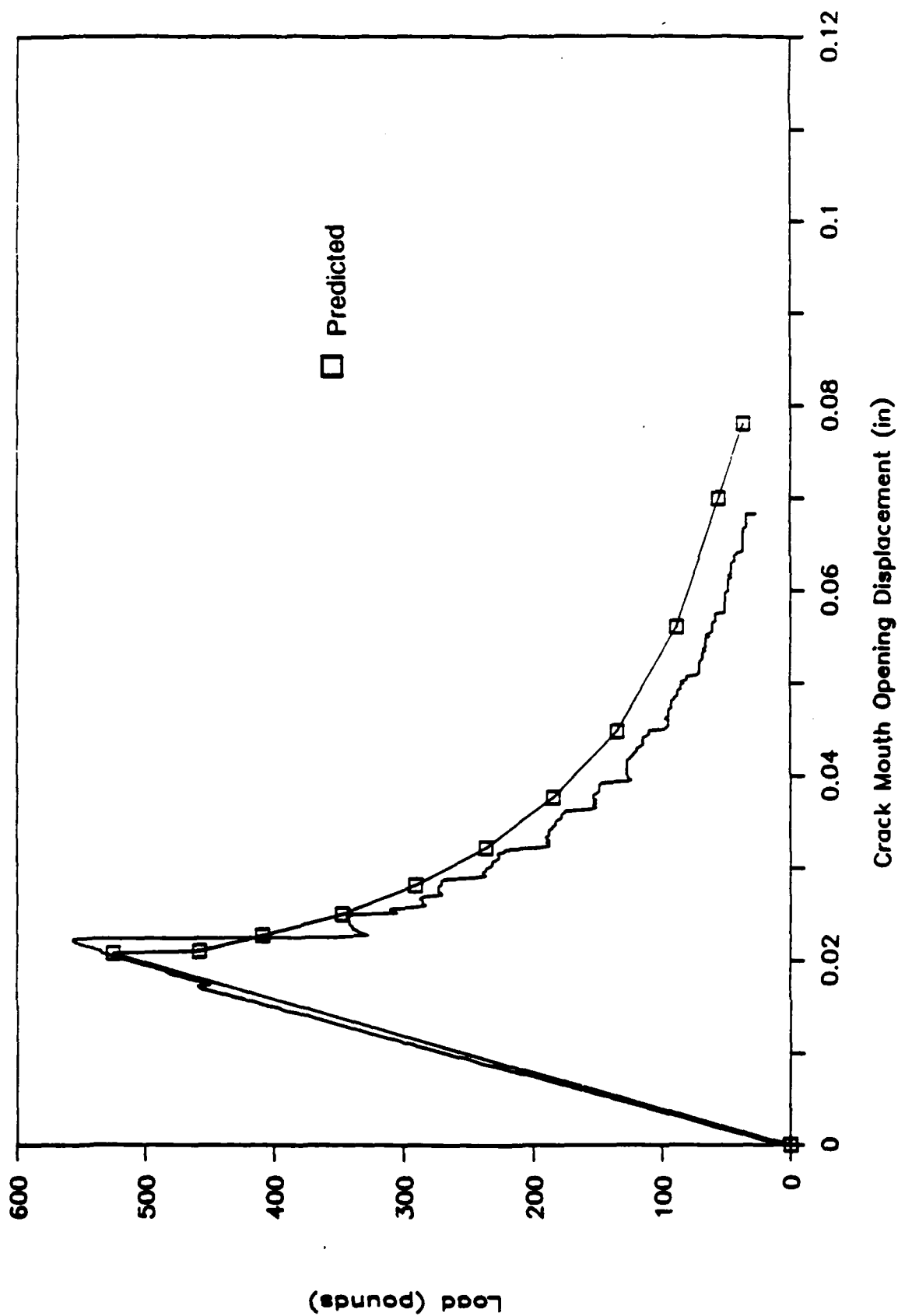for specimen #3 (a = 3 inches, d = 6 inches)

Figure 4.4 Plots of measured and predicted load-versus-CMOD
for specimen #4 (a = 4 inches, d = 6 inches)

also a very good agreement. This satisfactory remarkable per-
formance of PROFRANC was expected because plexiglas has a very
small process zone compared to specimen dimensions, so that
linear elastic fracture mechanics analysis is valid.

Figure 4.5 shows a plot of measured and predicted load-
displacement curves. Prediction curves are stiffer because (i)
nonlinear effects at supports and at loading point and (ii)
deformation of the loading table has not been included in the
numerical analysis.

Such a disagreement was not observed in Figure 4.1 to 4.4
because load versus CMOD measurement is not affected by either
nonlinear effects nor rigidity of the system.

4.2.2 Fracture Initiation Load. Table 4.1 shows measured
and predicted fracture initiation loads for all specimens. Both
the maximum circumferential stress theory and the minimum strain
energy density theory were used in predicting fracture initiation
loads.

Agreement between analysis and experiment is reasonable.
However, there are differences between predictions of various
fracture mechanics theories. These differences suggest another
source of uncertainty that is related to current understanding of
fracture phenomena. For example, fracture initiation loads pre-
dicted by the minimum strain energy density theory are higher
than those obtained by the maximum circumferential stress theory.
Differences increase with the ratio of mode II to mode I stress
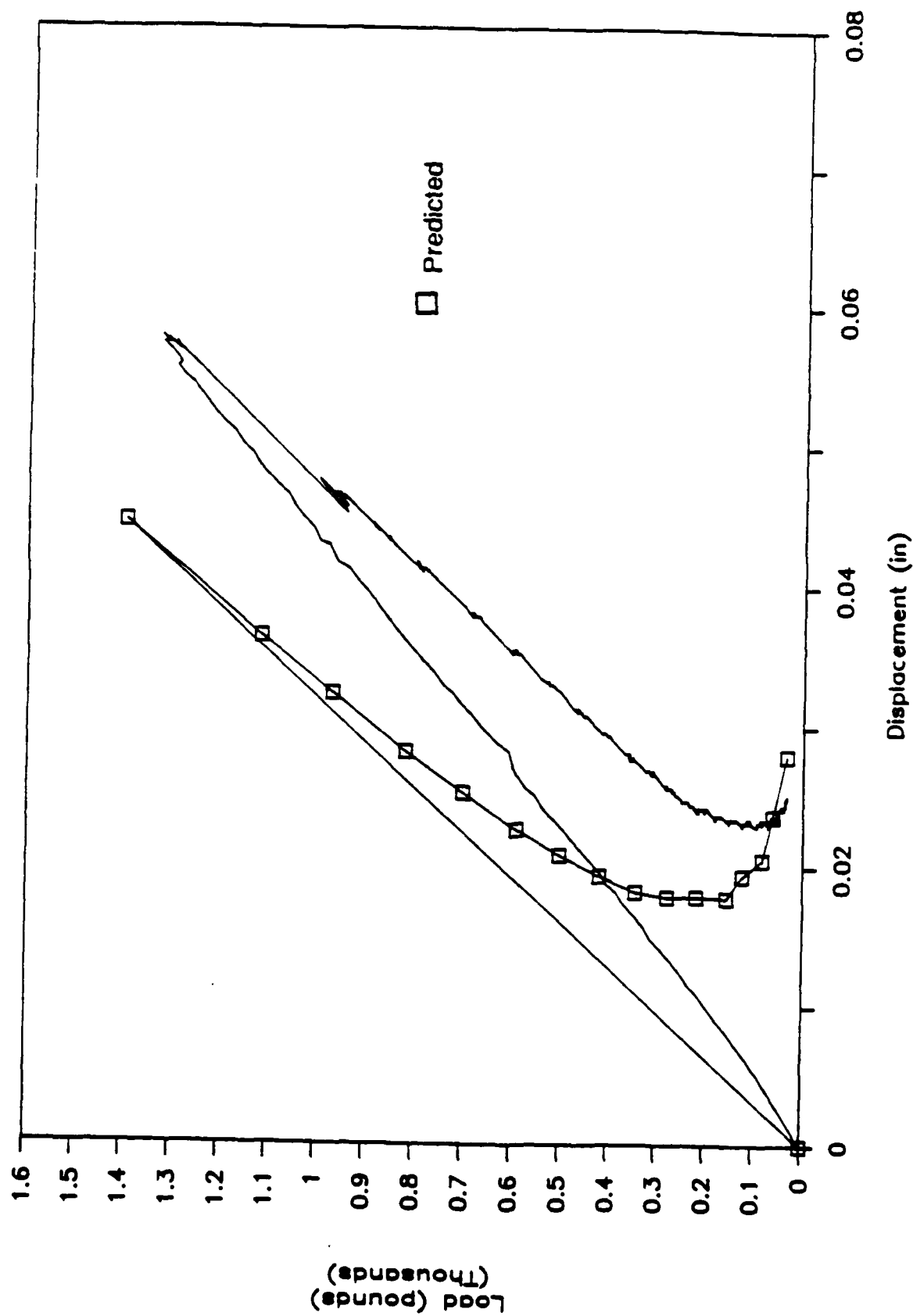intensity factors or crack length. A similar observation was

Figure 4.5 Plots of measured and predicted load-versus-load-line-displacement for specimen #1 (a = 1 inch, d = 6 inches)

Specimen number	Initial crack length (inches)	Measured (pounds)	Maximum circumferential stress theory (pounds)	Difference from Measured (%)	Minimum strain energy density theory (pounds)	Difference from measured (%)
1	1	1326	1399	5.5	1419	7.0
2	2	1091	1008	-7.6	1057	-3.1
3	3	774	723	-7.1	769	-0.6
4	4	534	524	-1.9	560	4.9

Table 4.1 Measured and predicted fracture initiation loads for $K_{Ic} = 944$ psi $\sqrt{in.}$

reported by Ewing, Swedlow and Williams [6] for plexiglas panels with an inclined initial edge crack in tension and pure bending.

4.2.3 Initial Fracture Initiation Angle. Fracture initiation angles were measured using an optical comparator, with a magnification of 10 and an accuracy of +/- 1/4 degree.

Table 4.2 shows a comparison between measured and predicted fracture initiation angles. Both the maximum circumferential stress theory and the minimum strain energy density theory were employed to predict the fracture initiation angle of each specimen.

The comparison indicates a reasonable agreement between experiment and predictions.

4.2.4. Crack Trajectory. Figures 4.6 to 4.9 show plots of observed and predicted crack trajectories for all four specimens. The predicted trajectories are in good agreement with actual trajectories. However, there is a consistent bias of the predicted trajectories toward the load point in all predicted plots. This is caused by differences between modeled and actual boundary conditions.

4.3 Summary

Results show that PROFRANC running in a deterministic mode provides an accurate technique for calculating load-CMOD curves, fracture initiation load, fracture initial angle, and crack trajectory. Therefore, proposed mechanical model and numerical

Specimen number	Initial crack length (inches)	Measured (degrees)	Maximum circumferential stress theory (degrees)	Difference from measured (%)	Minimum strain energy density theory (degrees)	Difference from measured (%)
1	1	15.25	13.76	-9.8	13.63	-10.6
2	2	26.00	25.80	-0.8	25.22	-3.0
3	3	30.25	29.83	-1.4	29.05	-4.0
4	4	34.25	31.09	-9.2	30.28	-11.6

Table 4.2 Measured and predicted fracture initiation angles
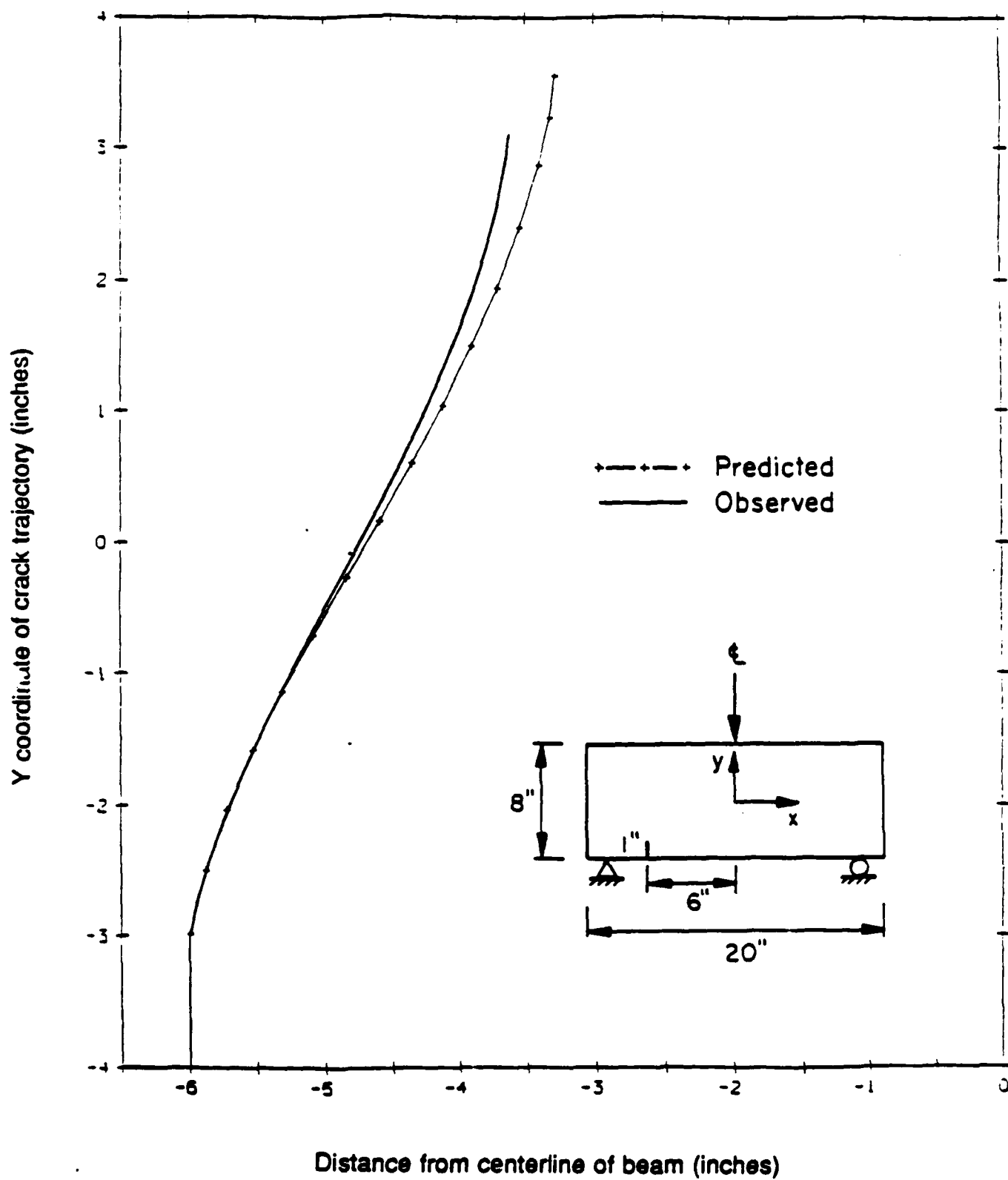
Figure 4.6 Plots of observed and predicted crack trajectories
for specimen #1 (a = 1 inch, d = 6 inches)
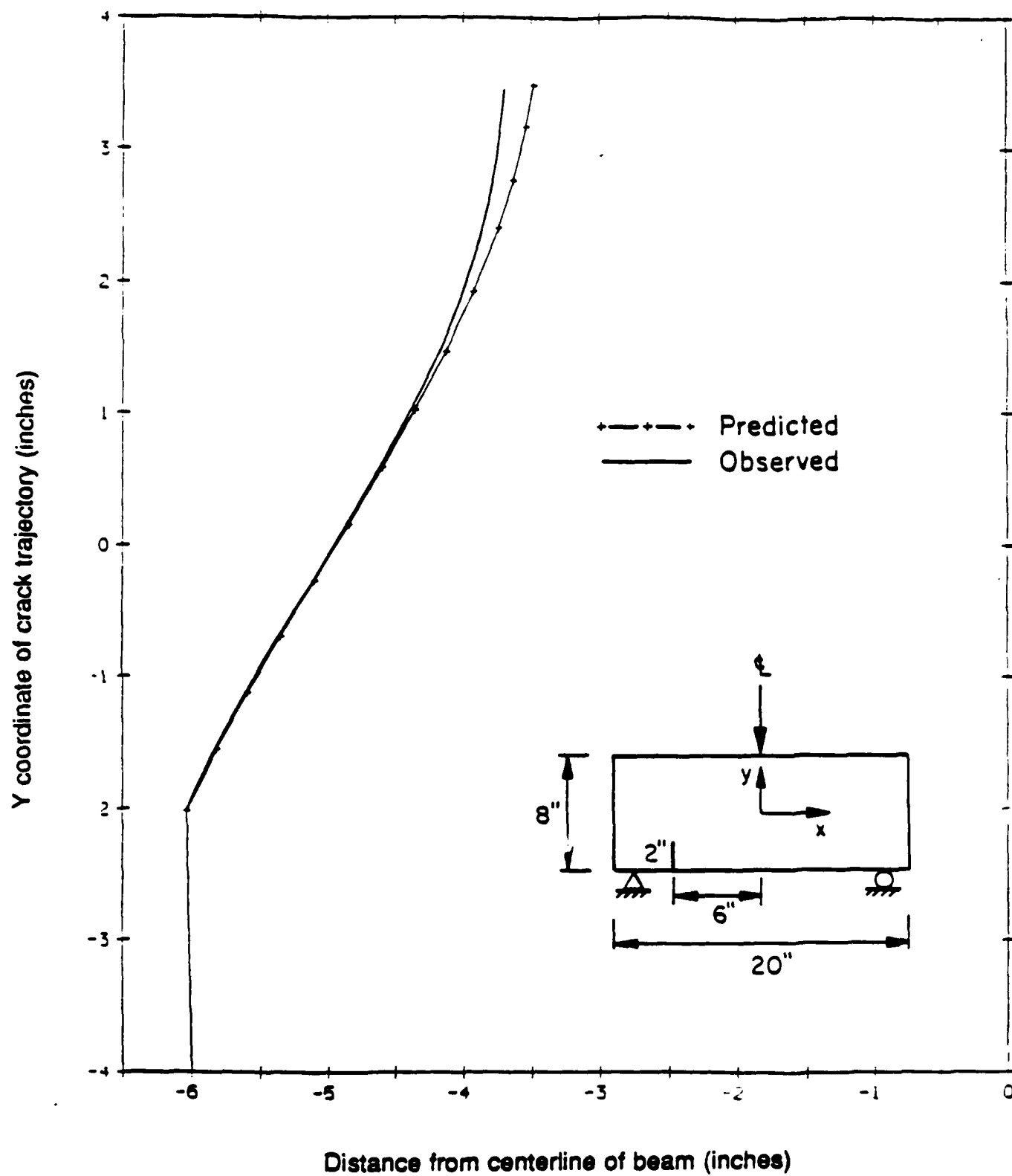
Figure 4.7 Plots of observed and predicted crack trajectories
for specimen #2 (a = 2 inches, d = 6 inches)
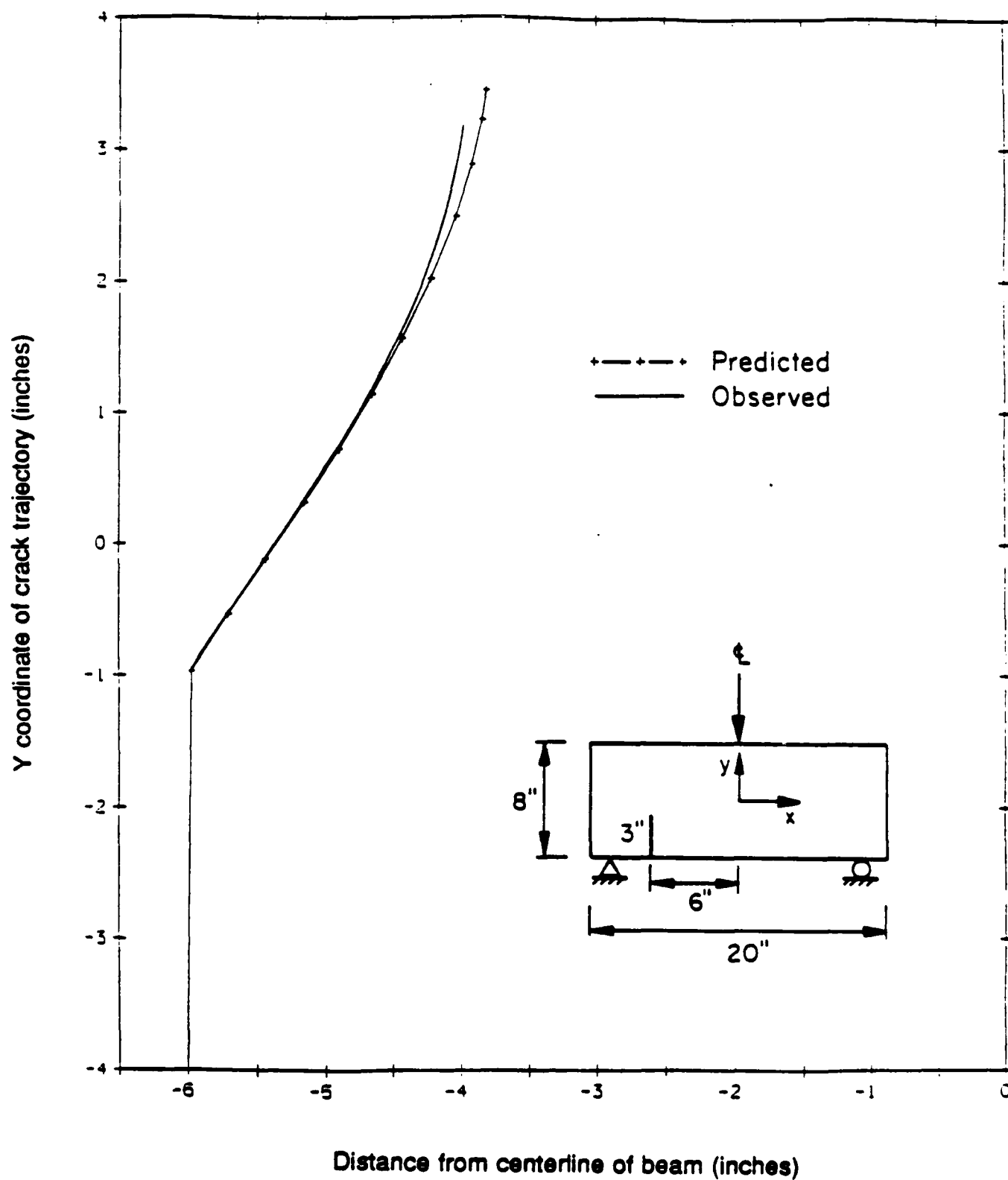
Figure 4.8 Plots of observed and predicted crack trajectories
for specimen #3 (a = 3 inches, d = 6 inches)
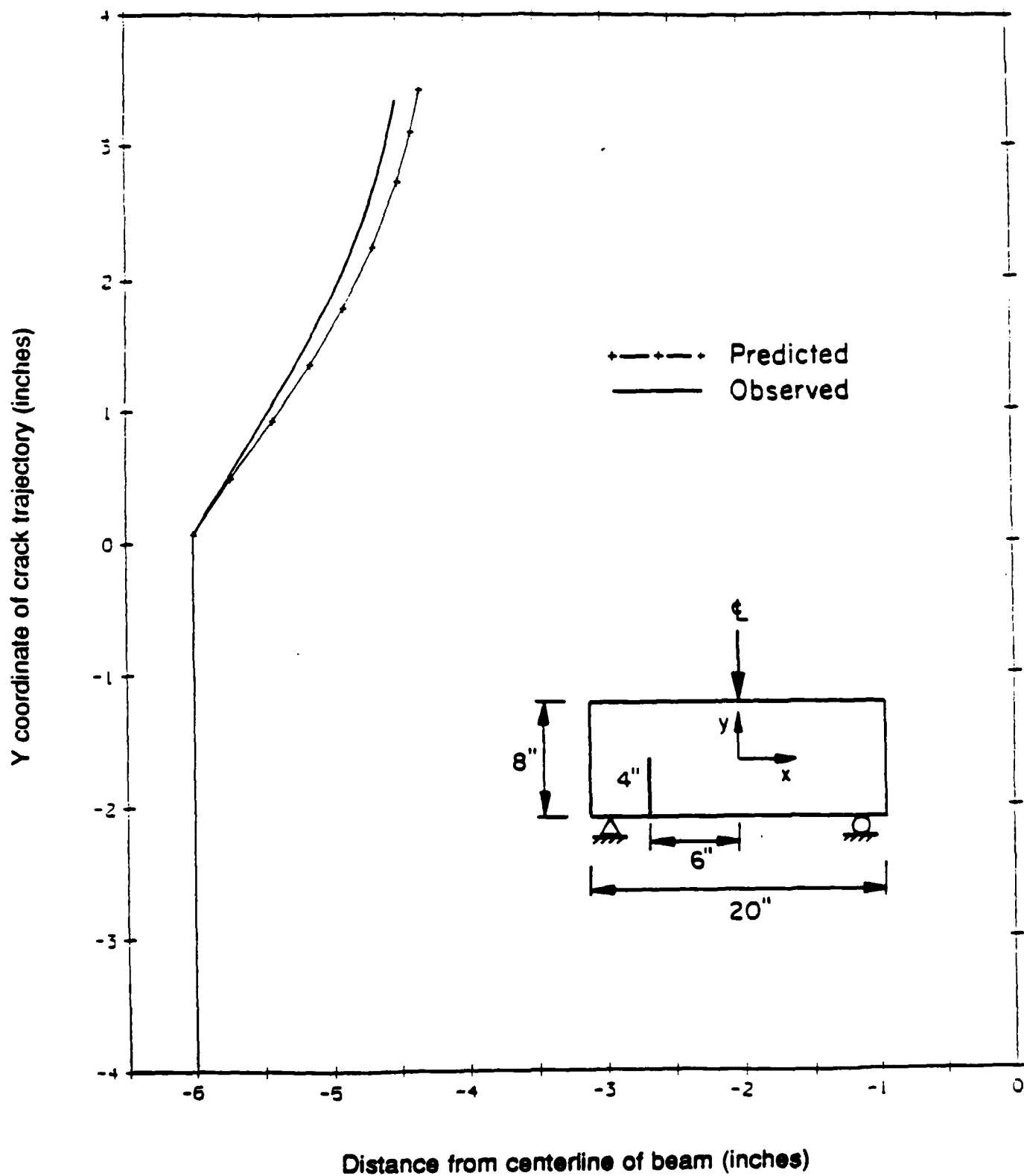
Figure 4.9 Plots of observed and predicted crack trajectories
for specimen #4 (a = 4 inches, d = 6 inches)

methods of analysis and sound. Their use in probabilistic fracture mechanics analysis is warranted.

5.0 EFFECTS OF HOLES ON MIXED-MODE FRACTURE

5.1 Introduction

The presence of holes in certain structures such as aircraft is sometimes a requirement set by the designer. The effects of holes on cracks present in a structure can be quite significant in that they can alter their trajectories. Holes in a structure can be an additional source of uncertainty.

This section describes crack trajectories obtained experimentally and predicted by PROFRANC (PRObabilistic FRacture ANalysis Code) for a structure of geometry shown in Fig. 5.1. The following sections describe testing procedures and analyses of these specimens. Comparisons are also given between crack trajectories of specimens with and without holes, and between observed and predicted results for those with holes. Finally, a discussion on sensitivity to initial conditions is presented.

5.2 Mixed-Mode Fracture Testing and Analysis of Specimens with Holes

5.2.1 Experimental Testing. Seven plexiglas specimens with holes were tested to study the effects of holes on mixed-mode crack trajectories. The overall dimensions were held constant, as were the number, size, and location of holes. The location, d, and length, a, of the starter crack were varied from specimen to specimen as shown typically for specimens 1 to 3 in Figures 5.2 through 5.4, respectively. The holes were drilled very slowly to reduce the likelihood of damage and residual stresses around them. The loading of the specimens proceeded in a manner
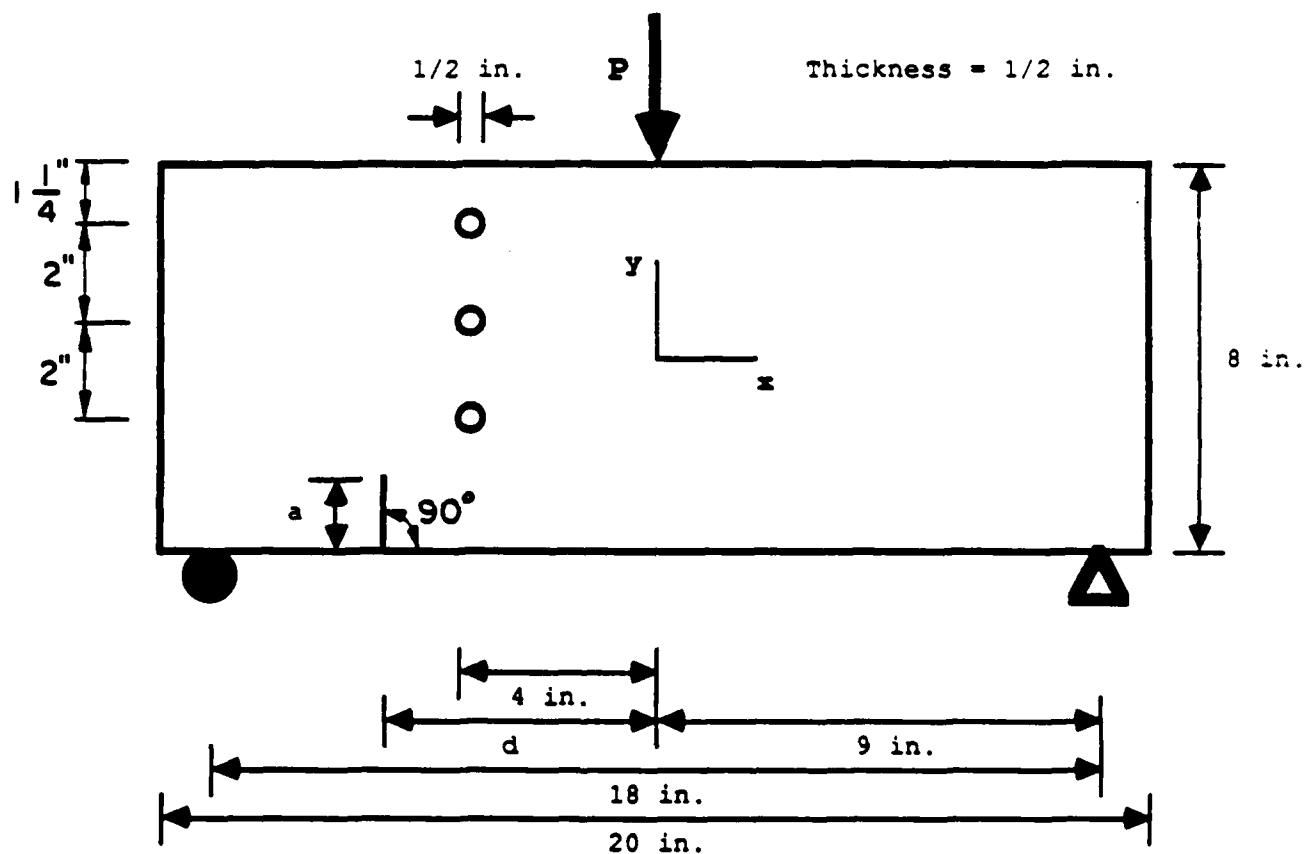
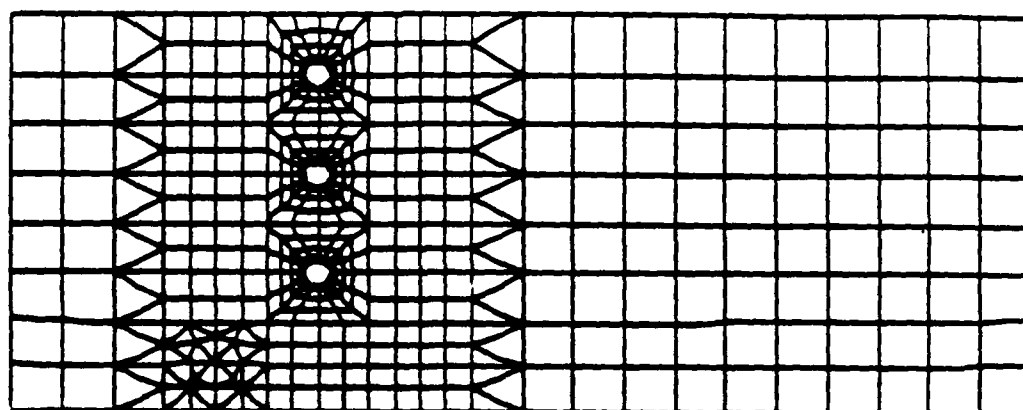Figure 5.1   Configuration of specimen with holes selected for testing

Figure 5.2 Finite element mesh of specimen #1 with holes
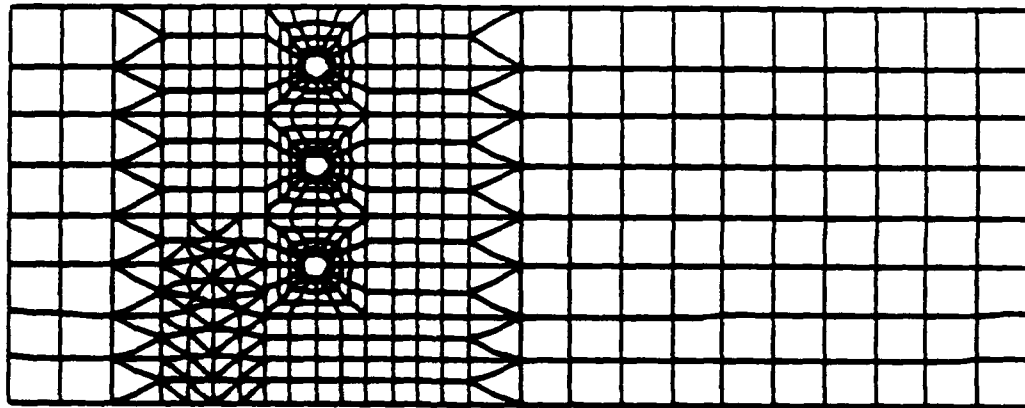(a = 1 inch   d = 6 inches)

Figure 5.3   Finite element mesh of specimen #2 with holes
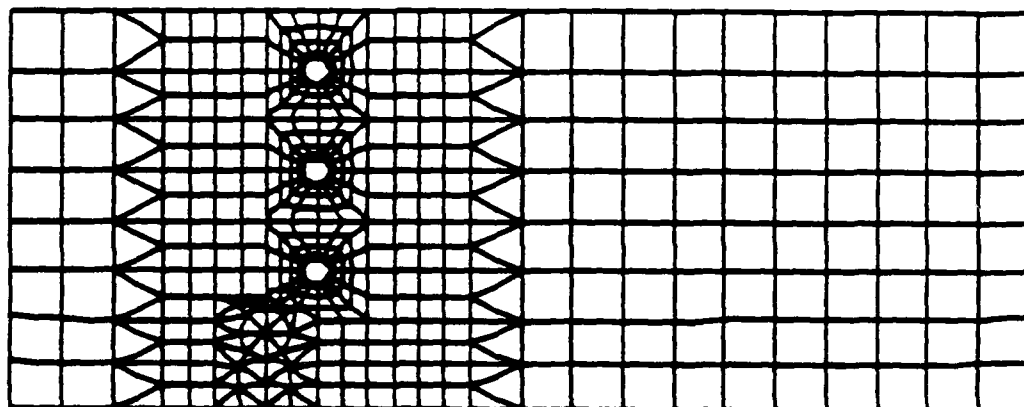(a = 2.5 inches, d = 6 inches)

Figure 5.4   Finite element mesh of specimen #3 with holes
(a = 1.5 inches, d = 5 inches)

identical to that previously described for specimens without holes.

5.2.2. Analysis of Specimens. Typical meshes used for PROFRANC predictions are shown in Figures 5.2 through 5.4. A new feature, automatic propagation, was implemented in PROFRANC to decrease user-induced bias in the simulations. With this feature, the entire simulation process is controlled by PROFRANC:

1) An analysis of the initial configuration is performed.

2) SIF's are computed.

3) Angle of propagation is computed using the $\sigma_{\theta\,\text{max}}$ theory.

4) The crack is extended in this direction by a constant pre-specified amount, here one-quarter of an inch.

5) Automatic remeshing is performed with local refinements around the crack tip.

6) A new analysis is performed, and

7) Steps 2 through 6 are repeated until the crack tip "approaches" a hole, or the user terminates the simulation because the length of the predicted crack exceeds that observed.

A current limitation in PROFRANC is that a crack cannot intersect a free surface, such as a hole, automatically. In the specimens simulated here, the predicted crack was propagated until it "approached" to within about 1/10 of a hole radius from the edge of a hole.

5.3 Effect of Holes on Mixed-Mode Crack Trajectories

5.3.1 Experimental Observations. To study the effects of holes on mixed-mode fracture, the crack trajectories obtained from specimens with and without holes were compared. Except for the holes, the specimens had nominally identical geometrical parameters. Figures 5.5 to 5.7 show comparison plots between observed crack trajectories of specimens 1, 2 and 3 with and without holes.

It is clear from these plots that the effect of any hole on a crack trajectory becomes significant when the crack approaches the hole. This is consistent with the Saint-Venant principle, which indicates that a hole begins to affect crack trajectory when the crack tip is at a distance of about one hole-diameter from the hole. Therefore, the hole-diameter can be a critical parameter. Note also that the fracture process may be arrested by a hole provided that it is in a particular location relative to what would have been the trajectory in the absence of a hole, although arrest does not always occur in a straightforward manner, as indicated in Figure 5.7.

If the hole is placed in front of the crack trajectory corresponding to a specimen without holes, then the crack might go straight into the hole. This is observed in the first specimen ($a = 1$ in, $d = 6$ in), as shown in Figure 5.5. If the hole, on the other hand, is placed slightly away from this crack path, the crack deviates from the trajectory of the specimen without holes
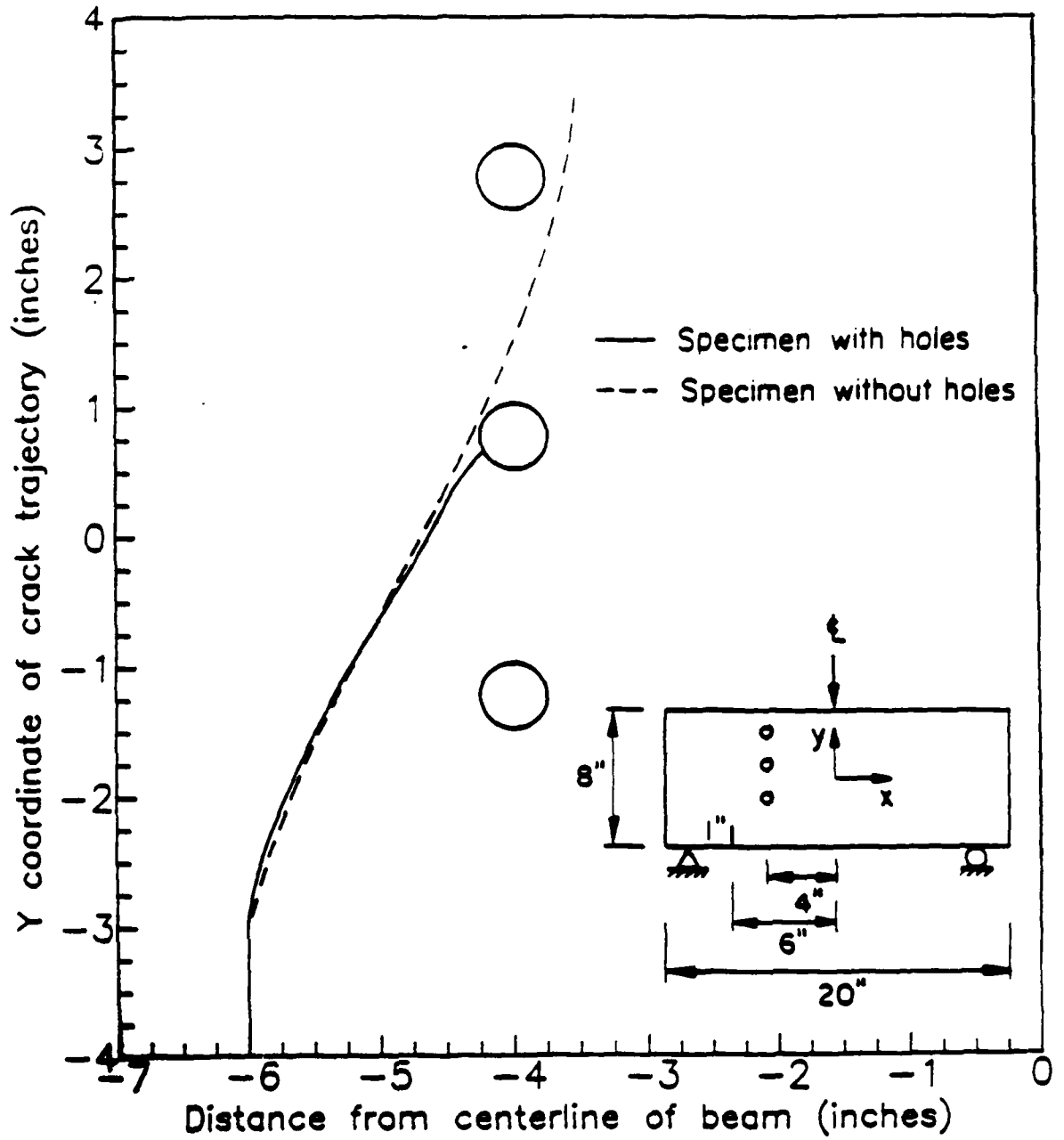
Figure 5.5 Plots of observed crack trajectories for specimen #1 with and without holes (a = 1 inch   d = 6 inches)
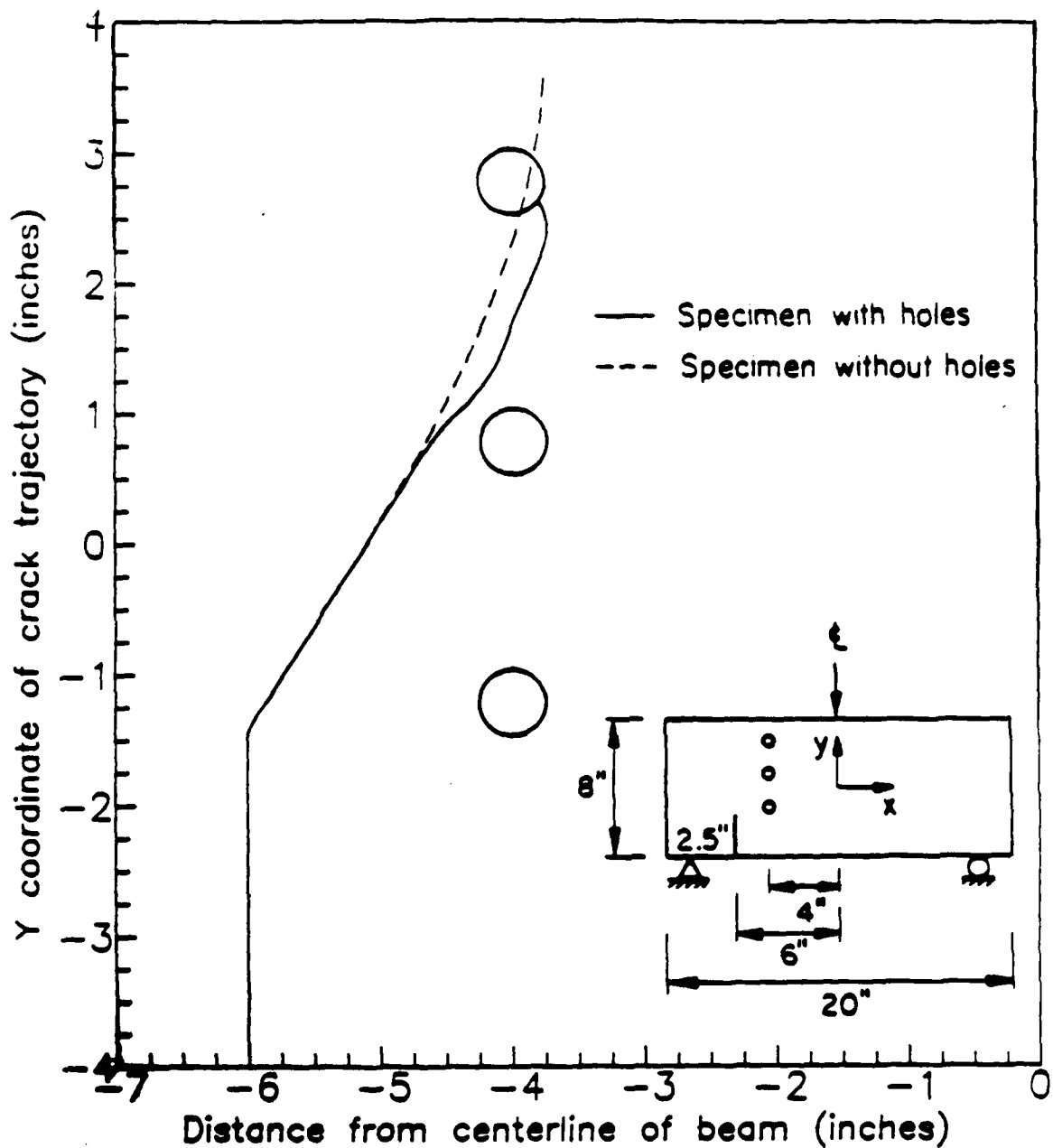
Figure 5.6   Plots of observed crack trajectories for specimen #2 with and without holes (a = 2.5 inches, d = 6 inches)
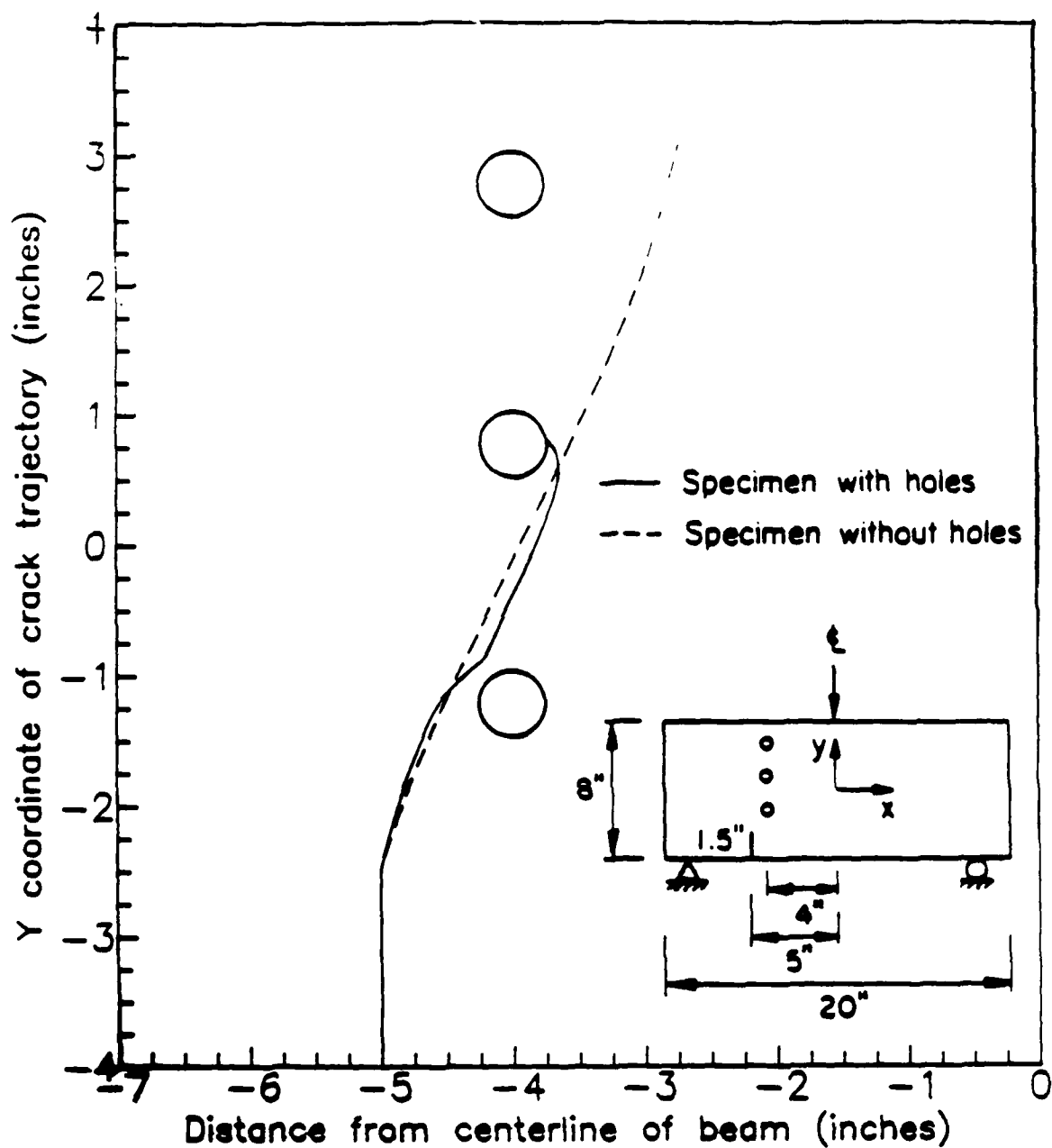
Figure 5.7   Plots of observed crack trajectories for specimen #3
with and without holes (a = 1.5 inches, d = 5 inches)

and is attracted toward the hole, as shown in Figure 5.6 as the crack approaches the middle hole.

5.3.2 Comparison of Observed and Predicted Trajectories

A deterministic analysis of each of the seven specimens with holes was performed using PROFRANC. A comparison between predicted and observed crack trajectories is shown in Figures 5.8 to 5.14.

In general deterministic predictions were in very good agreement with observations. PROFRANC predicted arrest in the correct hole in five of the six instances in which arrest occurred. Deviation from observed trajectory was, with one exception, always less than one-quarter inch, or a few percent of the current crack length.

The deterministic prediction failed on Specimen 3, Fig. 5.10, which had perhaps the most complex, and unexpected trajectory. PROFRANC failed to predict arrest into the loading side of the central hole, although influence of this and the lower hole on predicted trajectory are clearly evident.

5.4 Sensitivity to Initial Conditions

Specimens 3 through 7, Figures 5.10 through 5.14, comprise a test of sensitivity to initial conditions in that they span a relatively small range of initial crack locations. As the initial crack location moves farther from the load line, three distinct results are observed.
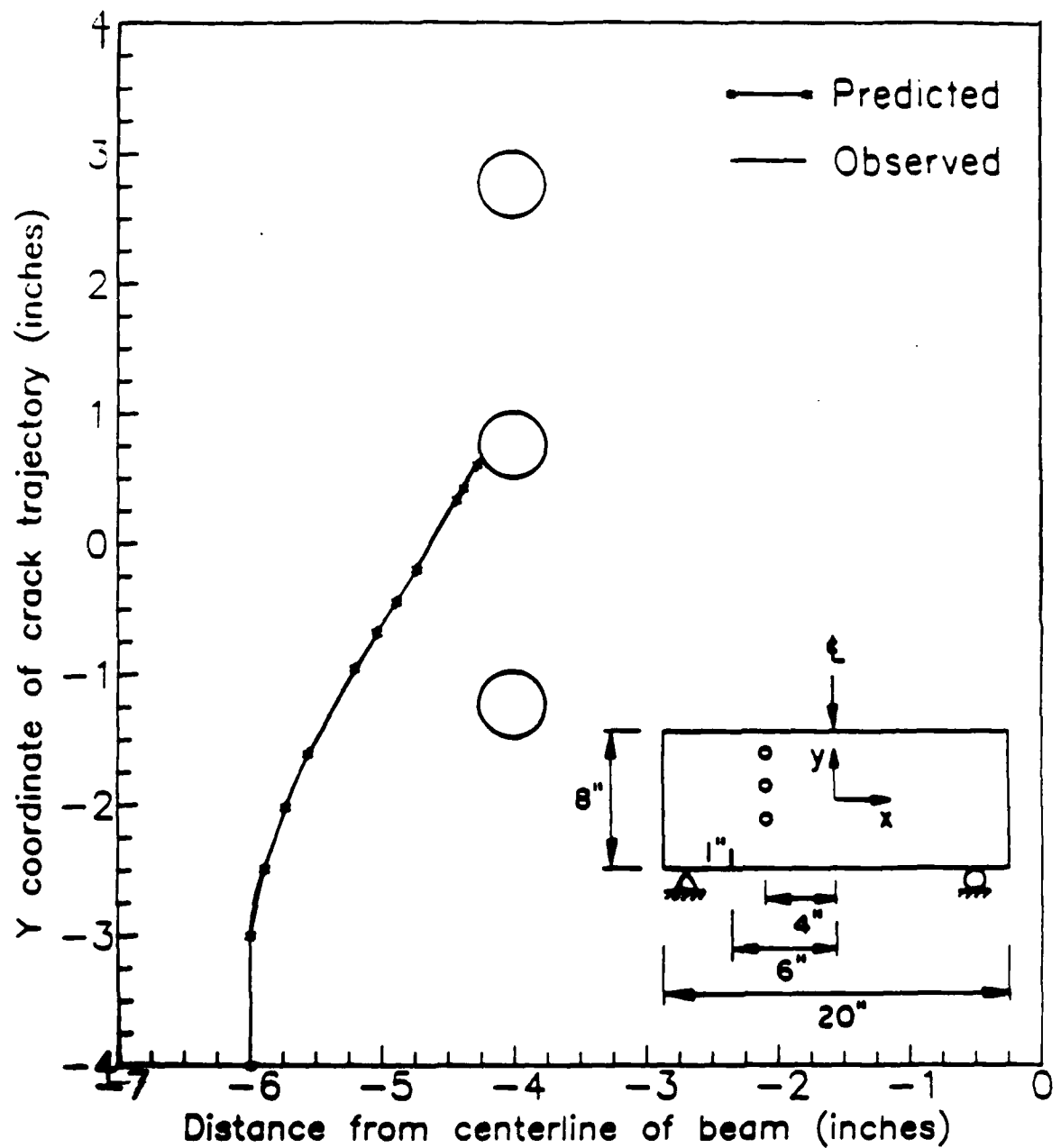
1. No arrest, specimen 4, Figure 5.11.

Figure 5.8   Plots of observed and predicted crack trajectories
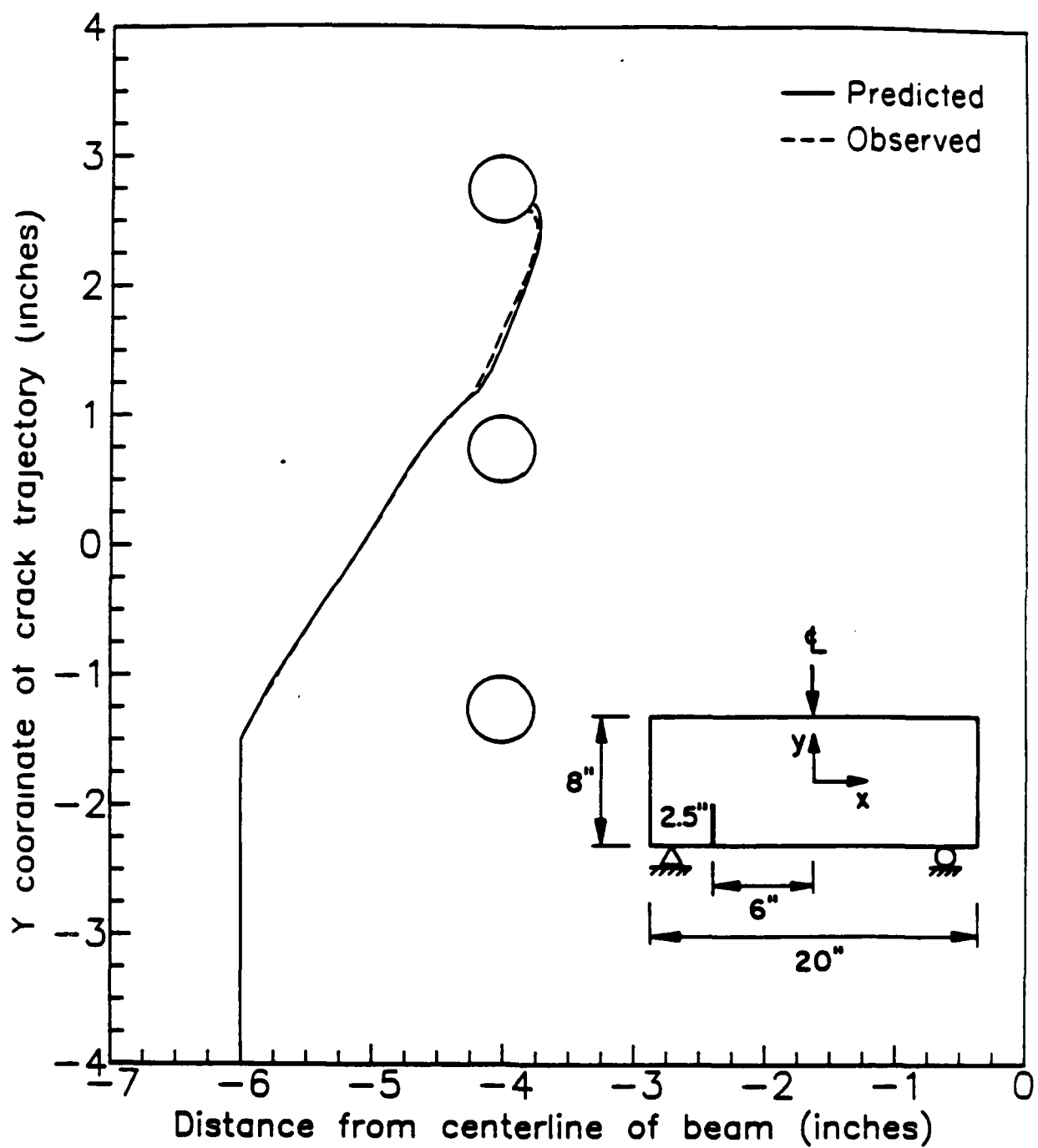for specimen #1 (a = 1 inch , d = 6 inches)

64

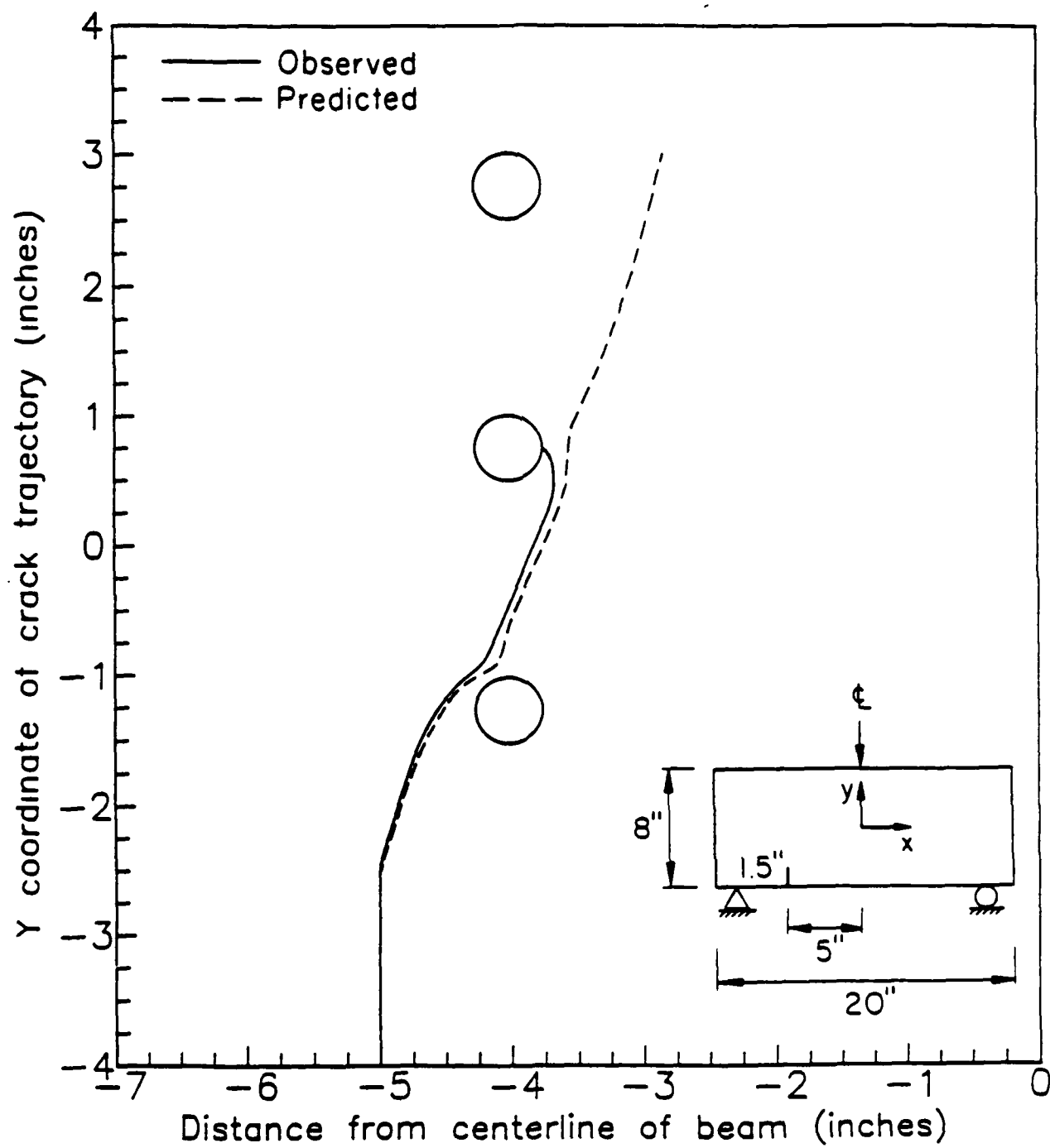Figure 5.9 Plots of observed and predicted crack trajectories (a = 2.5 in. d = 6 in.)

Figure 5.10 Plots of observed and predicted crack trajectories (a = 1.5 in. d = 5 in.)

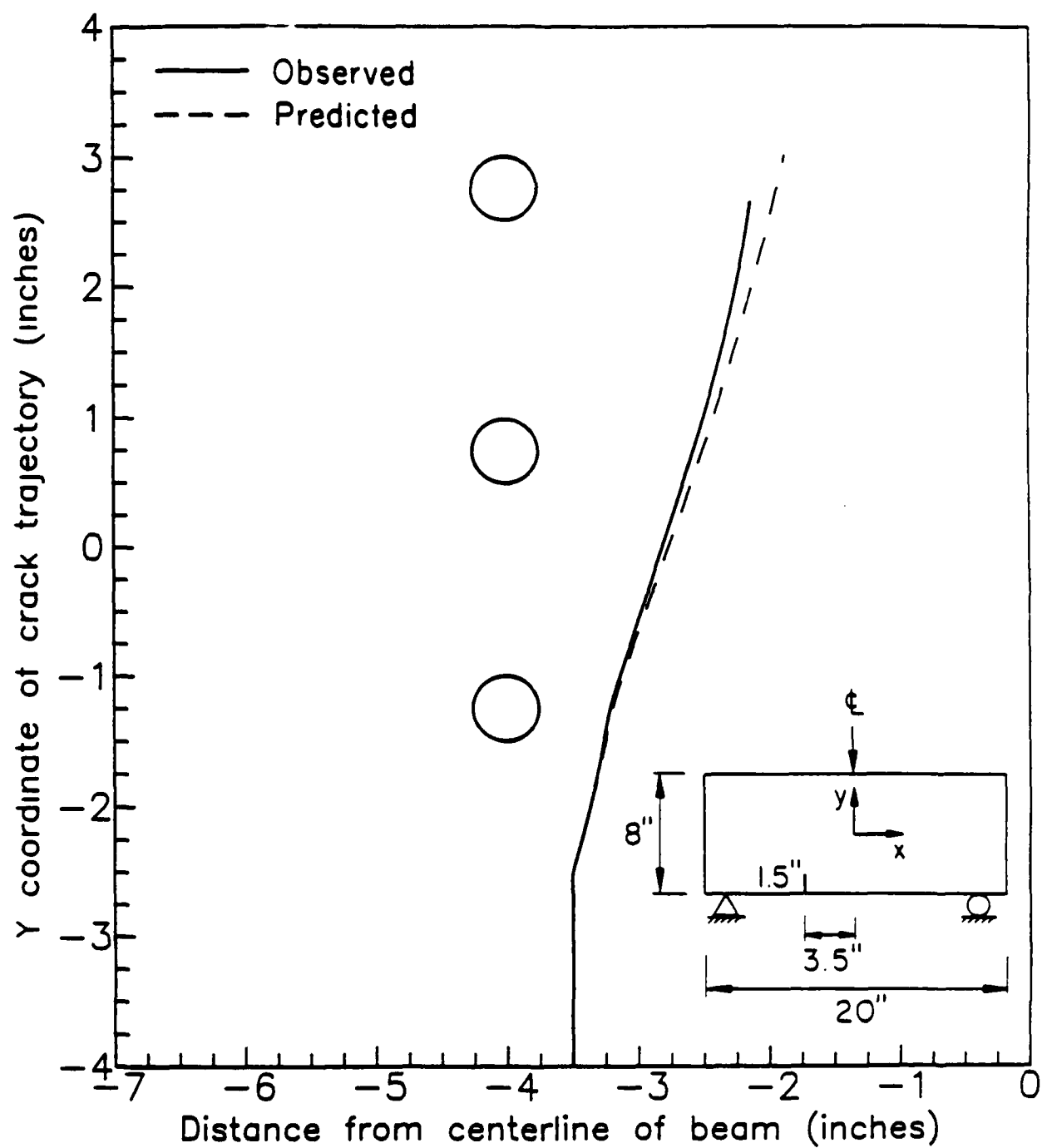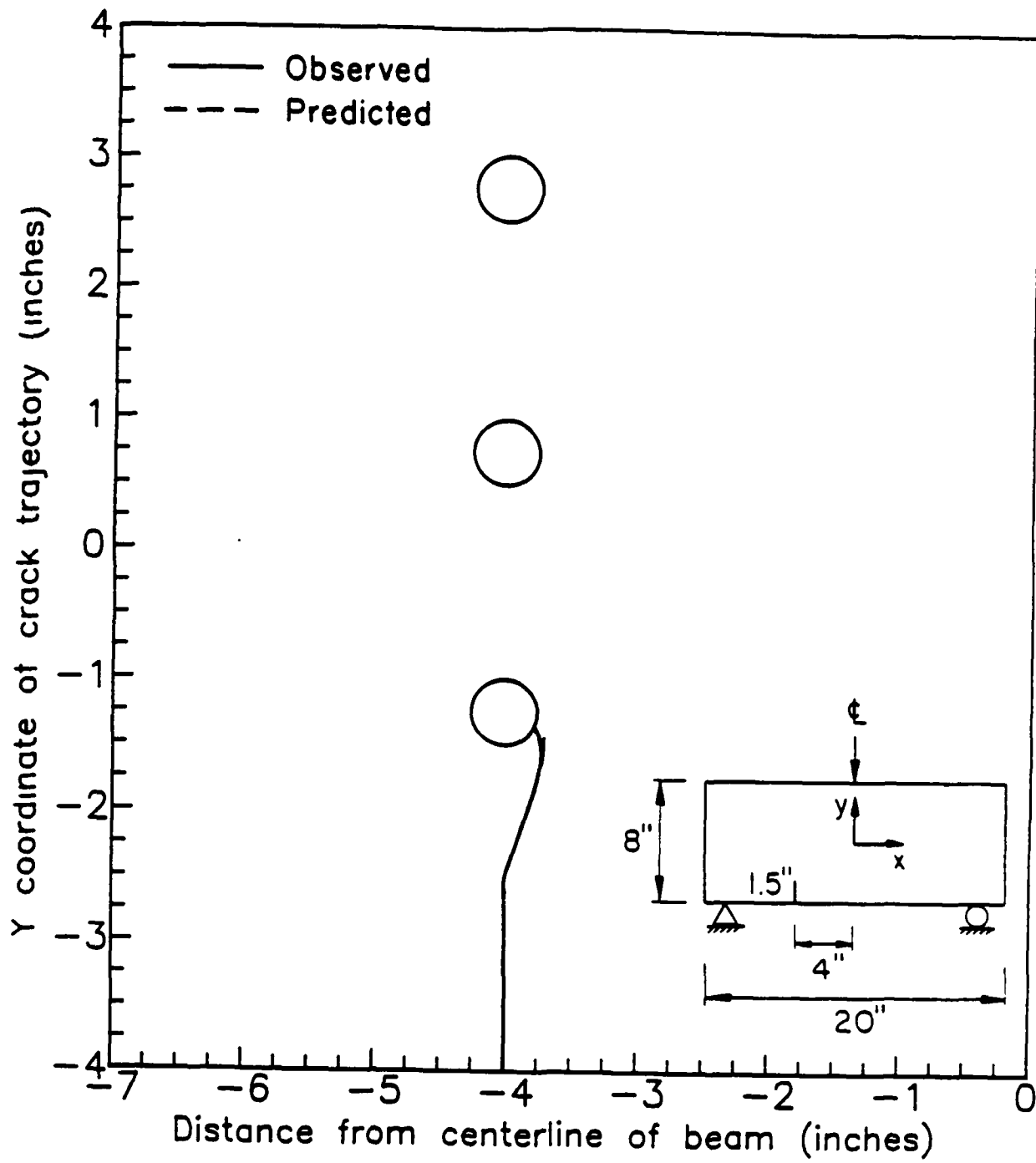Figure 5.11   Plots of observed and predicted crack trajectories (a = 1.5 in.
d = 3.5 in.)

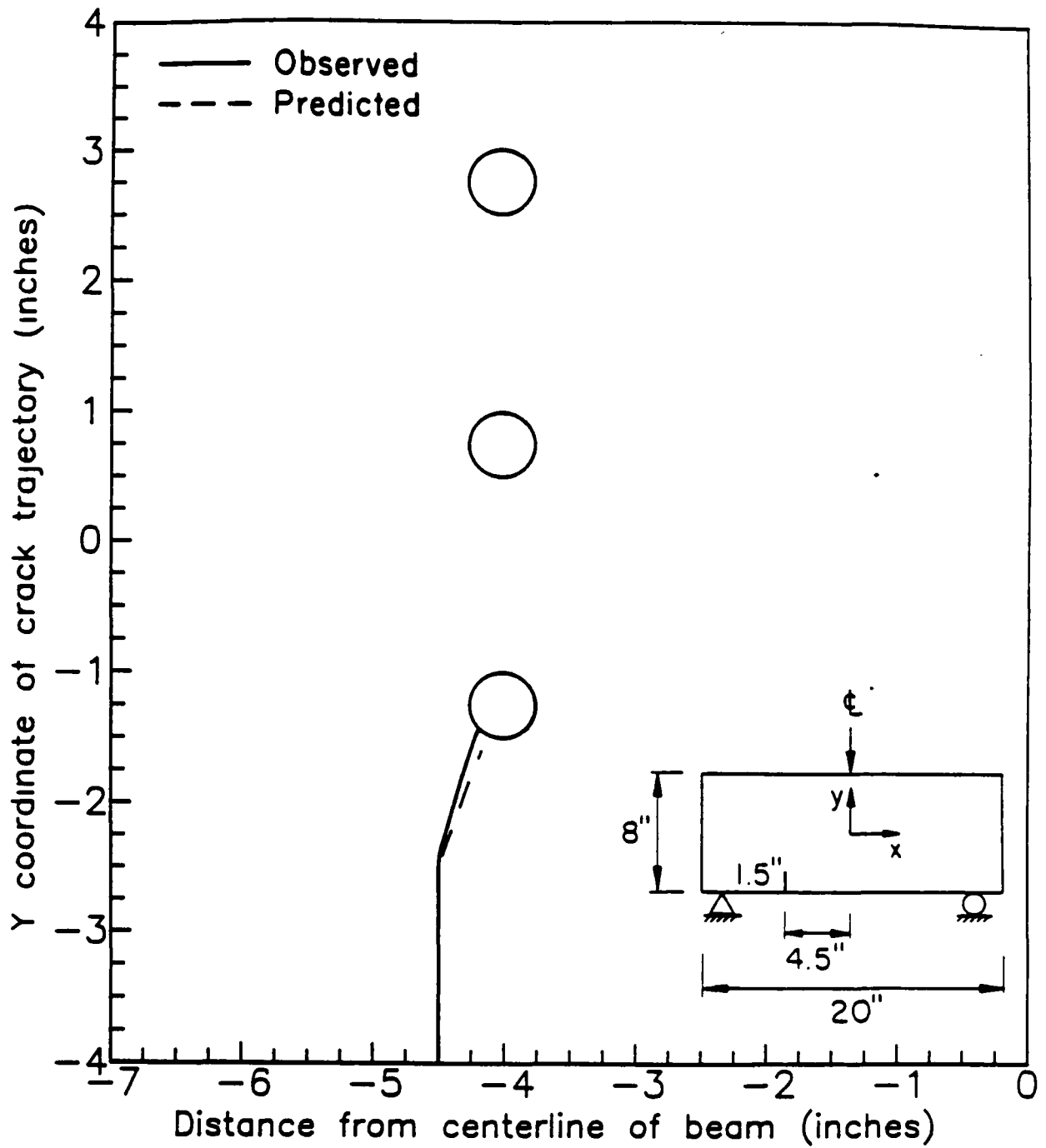Figure 5.12   Plots of observed and predicted crack trajectories (a = 1.5 in.
d = 4 in.)

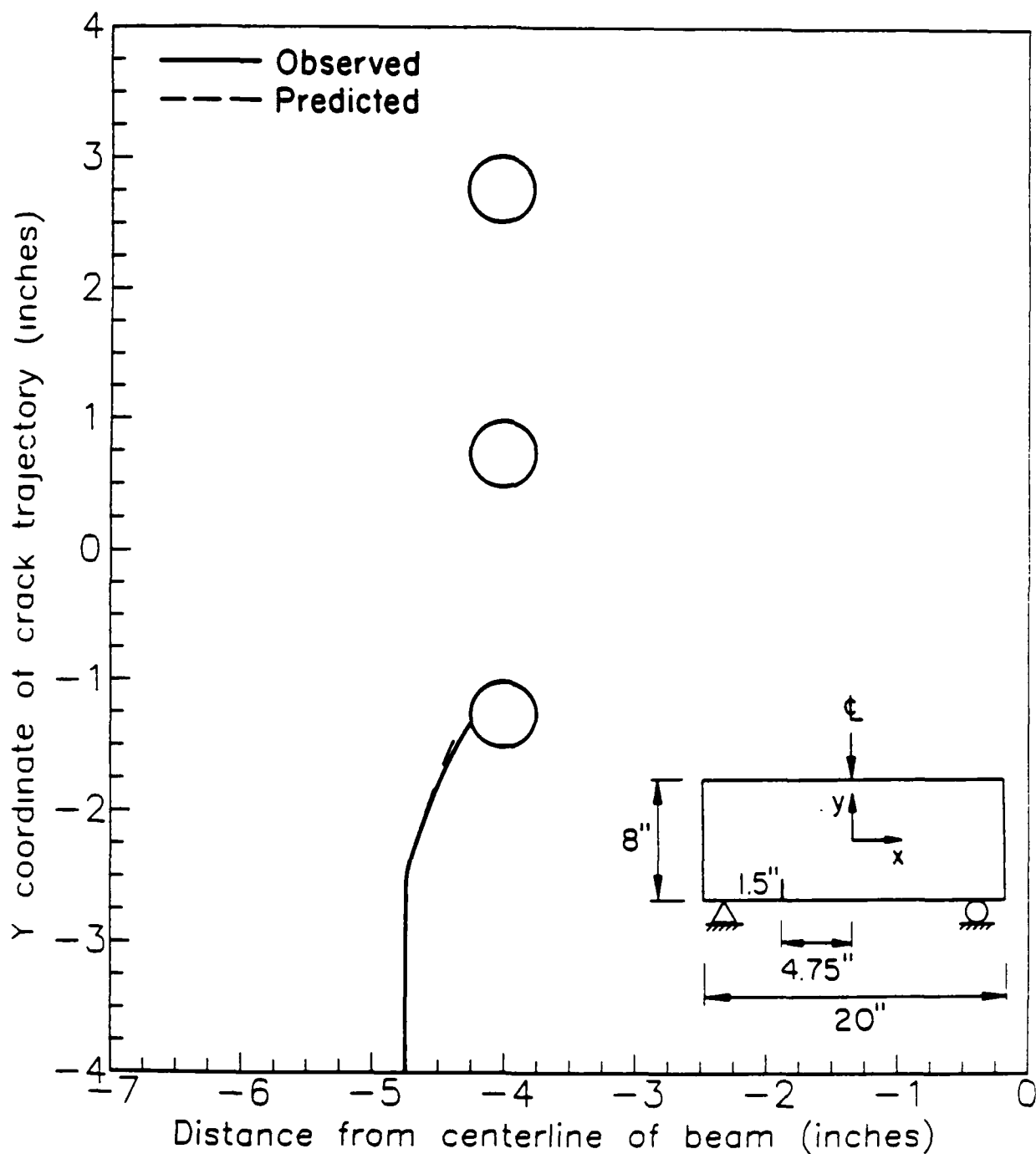Figure 5.13   Plots of observed and predicted crack trajectories (a = 1.5 in.
d = 4.5 in.)

Figure 5.14   Plots of observed and predicted crack trajectories (a = 1.5 in.
d = 4.75 in.)

2. Arrest in the lower hole, but at markedly different locations, Specimens 5, 6, and 7, Figures 5.12, 5.13, and 5.14.

3. Arrest on the loading side of the middle hole, Specimen 3, Figure 5.10.

Most interesting is the sensitivity shown in Specimens 3 and 7, Figures 5.10 and 5.14. The difference between these specimens was one-quarter inch in initial crack location. This represents less than 2 percent of the span of the beam. That is, an uncertainty of this small order in initial crack location can lead to the large difference in observed result. One could conjecture that an initial crack located between those in these specimens could produce a trajectory which does not arrest, like that predicted by PROFRANC for Specimen 3, Fig. 5.10.

Finally, there appears to be a corridor of stability accompanying the observed trajectories. As long as the prediction remains within this corridor, very good comparisons are obtained. If the prediction deviates from this corridor, divergence between observation and prediction occurs. It is obvious that the presence of holes narrows this corridor, and places much more stringent demands on accuracy in numerical modeling. The best evidence of this is Specimen 3, where a very small difference between observation and prediction as the early stages was sufficient, in the presence of the strong field gradients generated by the holes, to cause divergence.

6.0 PROBABILISTIC FRACTURE ANALYSIS

Sources of uncertainties in the experimental specimen studied in this report are:

(a) geometrical parameters:

(i) initial crack length, a

(ii) distance of crack initiation point from the load line, d.

(b) fracture toughness, K_{IC}

Probabilistic analyses are conducted in two phases. In phase 1, uncertainties in initial crack length and fracture toughness are examined. Phase 2 extends the studies of phase 1 by adding randomness in the distance d of the crack from the center of the beam. Initial crack length has been modeled as uniformly distributed over one to four inches, i.e. A ~ U(1, 4)in. K_{IC} has been measured experimentally from 15 samples. It has an average value of 944 lb-in$^{-3/2}$ and range (896,968) lb-in$^{-3/2}$. K_{IC} has been modeled as a Gaussian random variable with the above mean and same coefficient of variation as for results in Figs. 2.2 and 2.3, i.e. 7%. The distance, d, has been modeled as a uniform random variable with D ~ U(2, 6)in. In the following subsections the probability distributions of load to fracture initiation, P_0, and initial direction of extension, θ_0, predicted by the probabilistic model developed in [3], and implemented in PROFRANC, are compared with experimental studies for both the

phases. In phase 1, the predicted results have also been compared with simulation studies.

6.1 Fracture Initiation

The determination of probabilities of P_0 and θ_0 in PROFRANC involves several phases. First, the structure in Fig. 6.1 is discretized in finite elements involving singular elements at the crack tip. Second, analyses are conducted to determine stress intensity factors $\{k_1{}^i, k_2{}^i\}$ for several values of crack length a_i, $1 = 1, 2, \ldots n$ in the range of $(1, 4)$ in under unit load for phase 1. In case of phase 2, intensity factors $\{k_1{}^{ij}, k_2{}^{ij}\}$ are determined for several values of a_i in the above range and crack location d_j, $j = 1, 2 \ldots n$ in the range $(2, 6)$ in under unit load. Third, response surfaces $k_1 = k_1(a)$, $1 = 1, 2$, for phase 1 and $k_1 = k_1(a, d)$, $1 = 1, 2$ for phase 2 are calibrated to the resulting stress intensity factors $\{k_1{}^i, k_2{}^i\}$ and $\{k_1{}^{ij}, k_2{}^{ij}\}$ respectively. These surfaces give functional dependence between stress intensity factors and random variables $\{A\}$ and $\{A, D\}$ characterizing initial crack geometry. They are used to calculate the probabilities of P_0 and θ_0 based on the theories of linear elastic fracture mechanics.

According to the maximum circumferential tensile stress theory [2], the initial direction, θ_o of crack growth is the solution of the equation

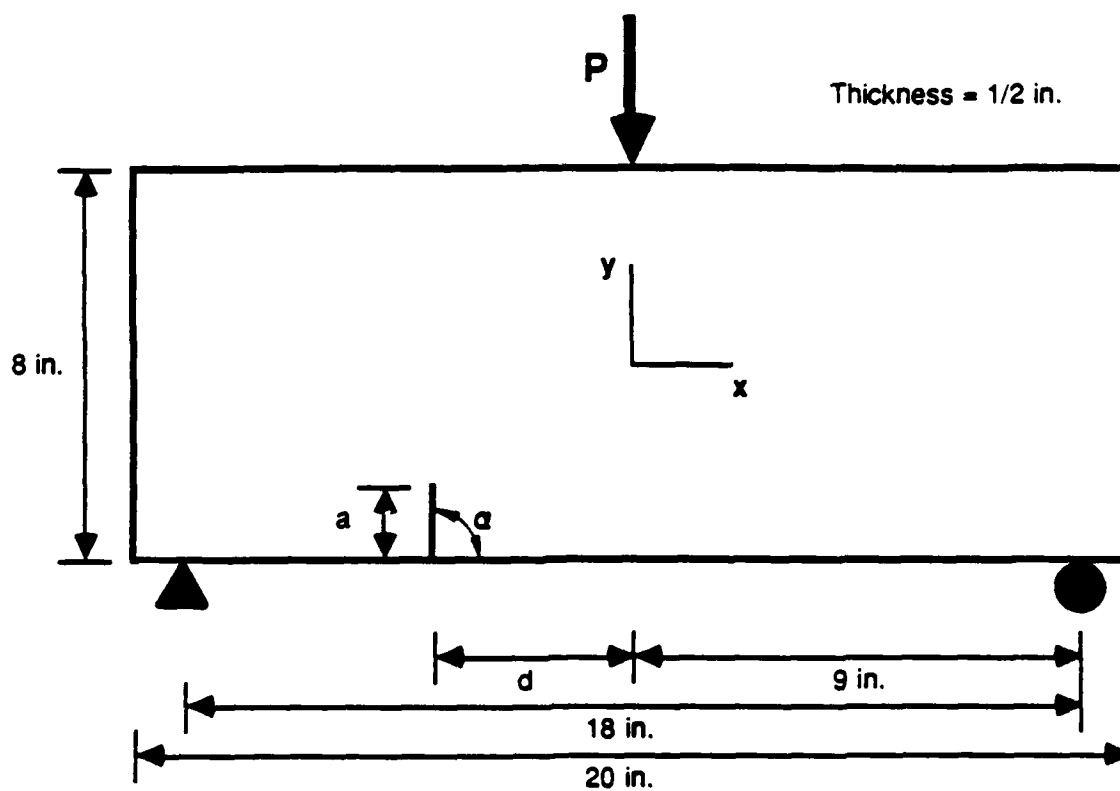$$K_I \sin\theta + K_{II} (3\cos(\theta) - 1) = \theta \tag{1}$$

or

Figure 6.1   Configuration of experimental specimen

$$X = K_I/K_{II} = (1 - 3 \cos(\theta))/\sin(\theta) \qquad (2)$$

Here θ_o is a random variable. The distribution of θ_o is obtained by using equation (2) and by computing the probability that θ_o is less than or equal to a given θ. PROFRANC has been employed to perform these computations.

According to the maximum circumferential tensile theory, the function

$$K_{I,eq}(K_I, K_{II}) = \cos(\theta/2) [K_I \cos^2 \theta - 1.5 K_{II} \sin (\theta)] \qquad (3)$$

is the mode I stress intensity factor along a given direction θ in a crack tip stress field where K_I and K_{II} are stress intensity factors. $K_{I,eq}$ is maximum when θ is the solution of Equation (1). For the structure under consideration K_I and K_{II} are stress intensities under unit load. Thus if P is the applied load, then the crack initiates when $P K_{I,eq} > K_{IC}$ and the load to fracture initiation, P_o, is given by $P_o = K_{IC}/K_{I,eq}$. Here P_o is random due to randomness in K_{IC} and crack geometry. The distribution of P_o has been obtained by PROFRANC using first and second order reliability algorithms in the space of random variables A and K_{IC} in phase 1 and in the space of A, D and K_{IC} in phase 2.

The theoretical distributions of θ_o and P_o predicted by PROFRANC have been compared with the results obtained from simulation and experiments in phase 1. Figures 6.2 and 6.3 show the distribution of θ_o compared with the values obtained from experiments and simulation studies respectively. The probabilistic
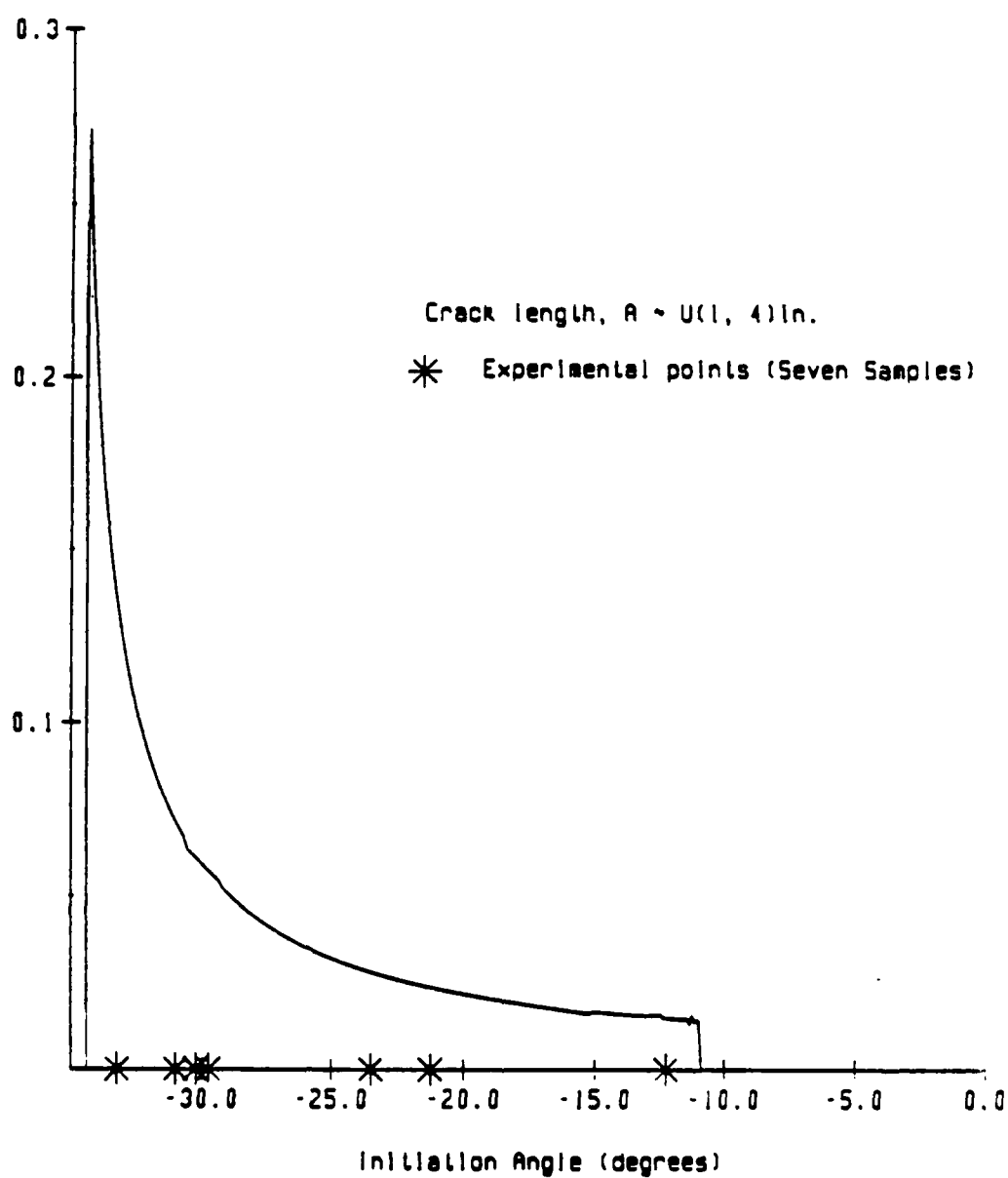
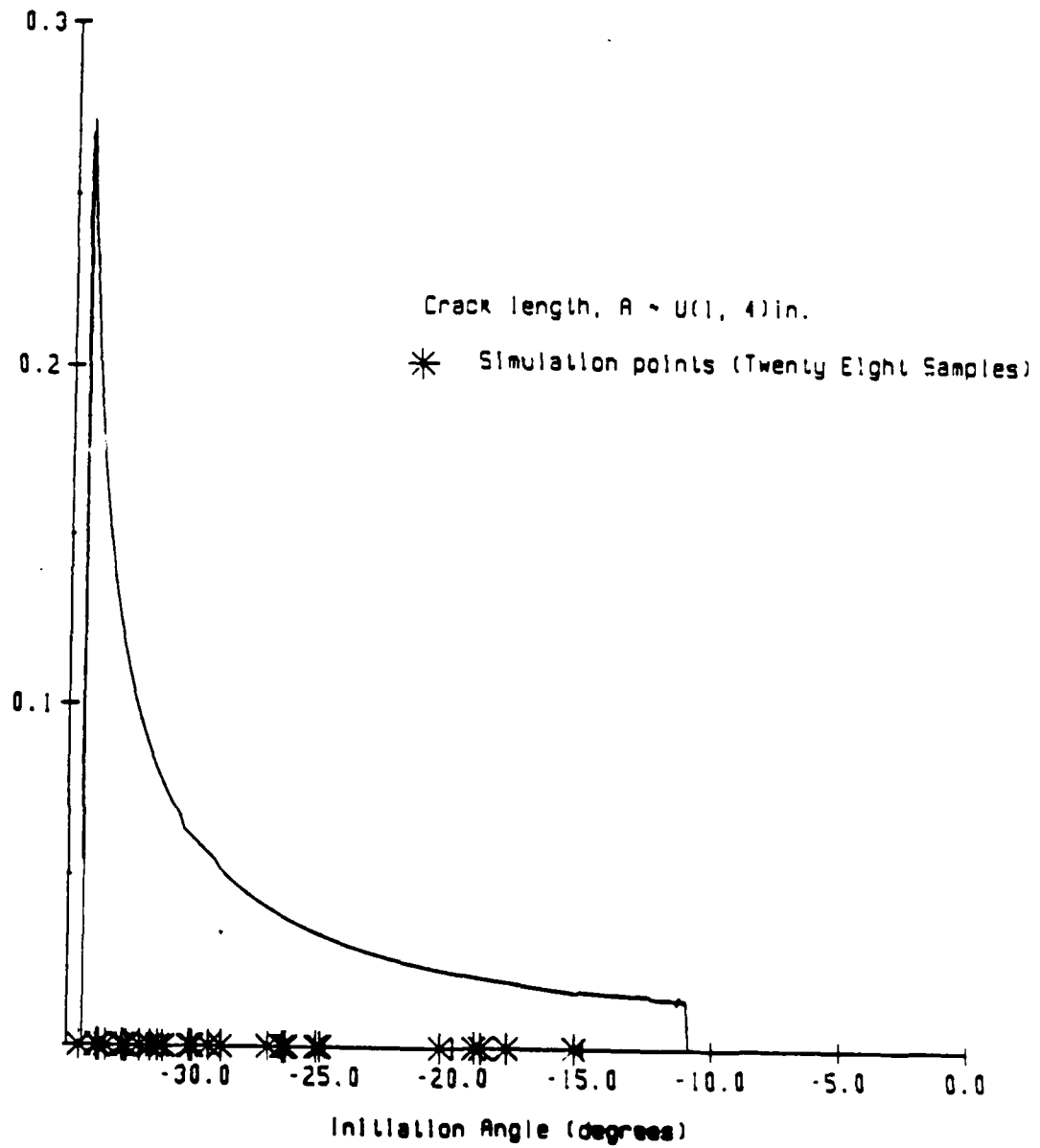Figure 6.2 Probability density curve of crack initiation angle

Figure 6.3   Probability density curve of crack initiation angle

model successfully embraces all the simulation and experimental values within the predicted range. The distribution of θ_o is highly skewed due to the nonlinearity in the relation between initiation angle and crack length shown in Figure 6.4.

Figures 6.5 and 6.6 show the distribution of P_o compared with results obtained from simulation and experiments. Again, good agreement between predicted range and simulation as well as experimental results is observed. The nonlinear relation between crack length and fracture initiation load (Figure 6.7) explains the skewness of the density curve of P_o.

Figure 6.8 shows probabilities of θ_0 predicted by PROFRANC for fixed crack length (A = 3 in) and uniformly distributed distance D in range (2, 6) in. The figure also shows experimental values of θ_0 for A = 3 in and D = 2, 3, 4, 5 and 6 in. The probabilistic model embraces most of the experimental values within the predicted range. Figure 6.9 shows the probability of θ_0 predicted by PROFRANC both A and D are random. From Figures 6.8 and 6.9, the uncertainty in the initial direction of crack extension increases when both A and D are random variables. This is consistent with physical anticipation.

Figure 6.10 shows the distribution of P_0 predicted by PROFRANC for D ~ U(2, 6) in, K_{IC} ~ N(944, 66) lb-in$^{-3/2}$ and A = 3 in and experimental values of P_0 for A = 3 in and D = 2, 3, 4, 5 and 6 in. The agreement between predicted range and experimental results is satisfactory. Figure 6.11 shows the distribution of
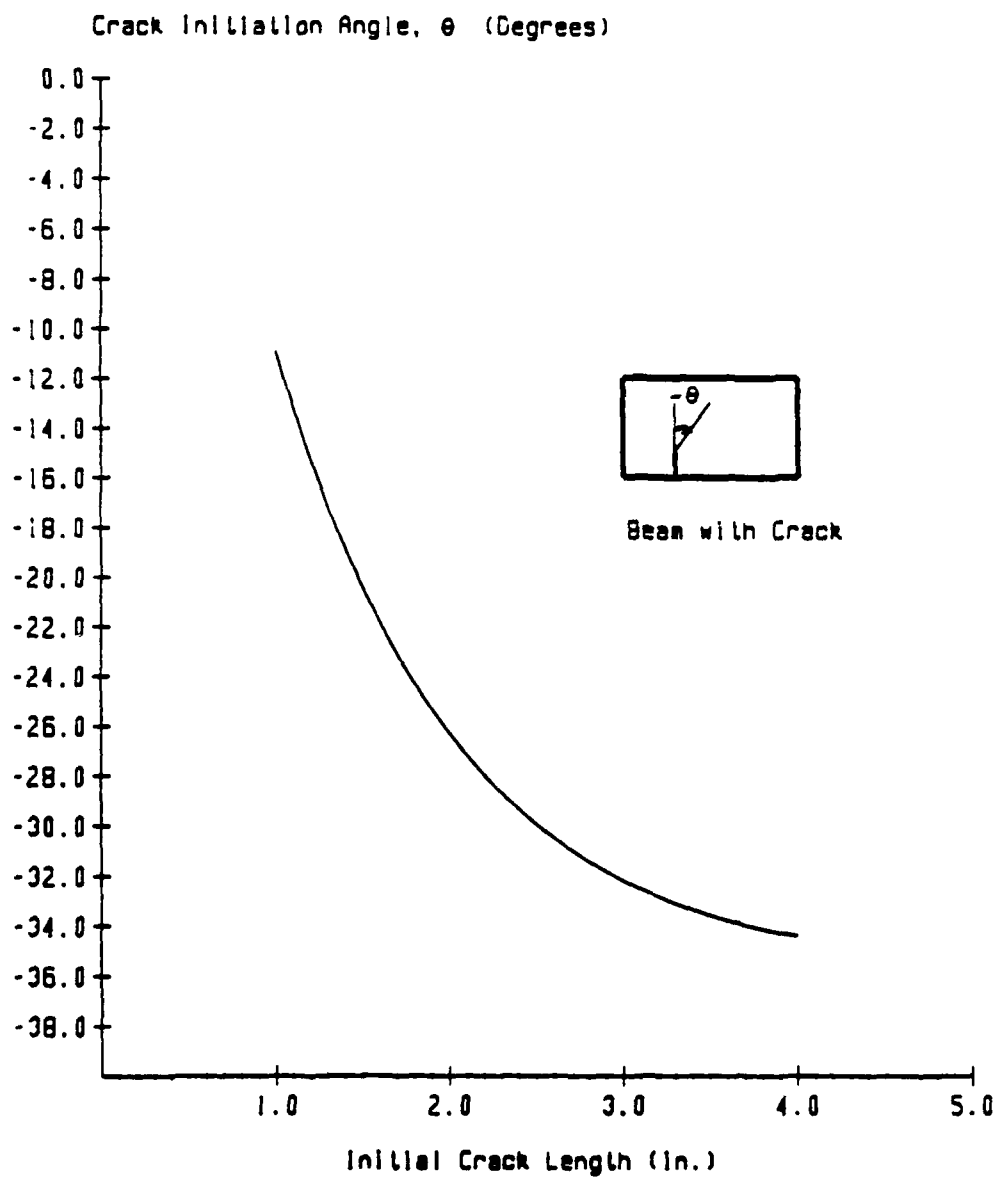
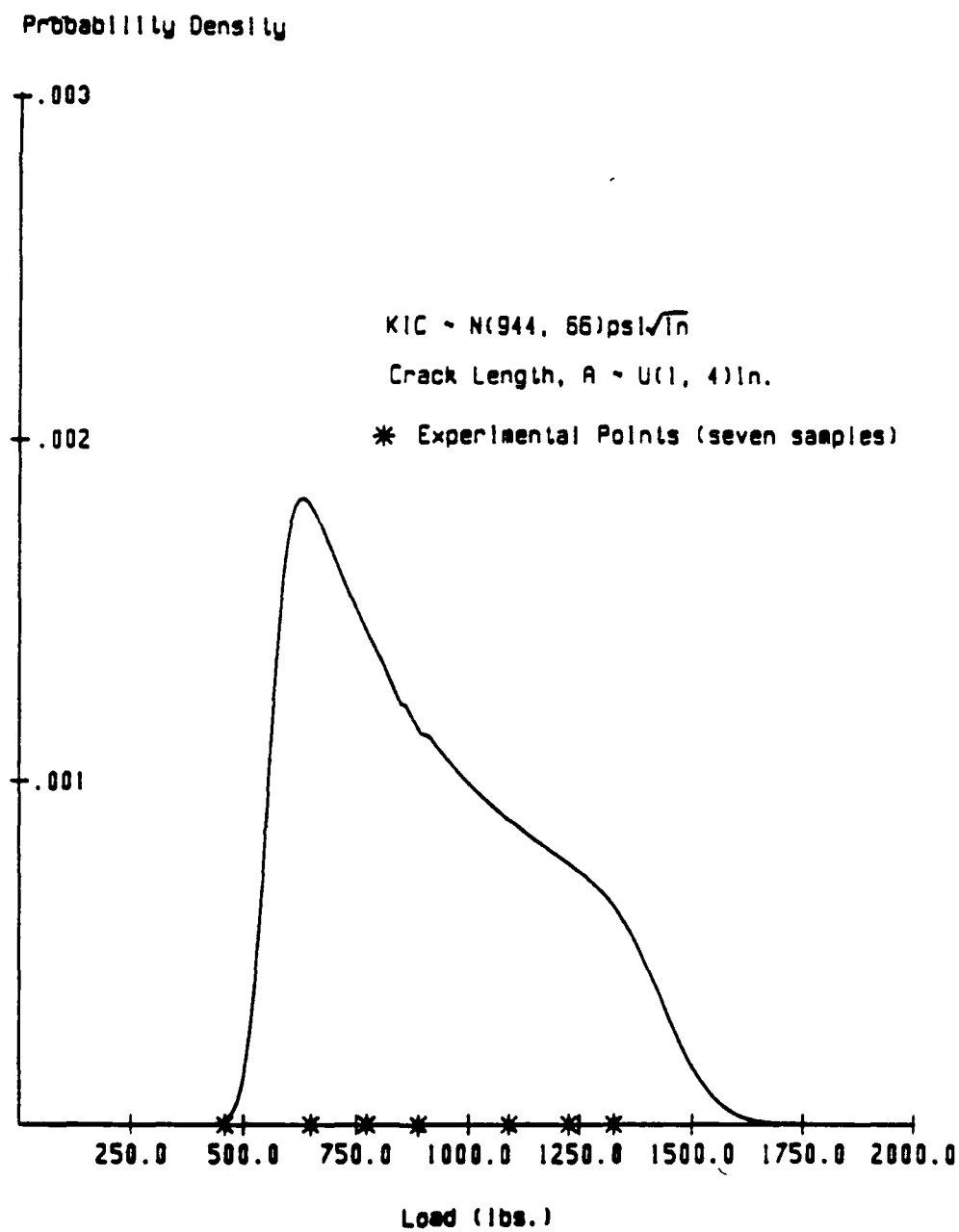Figure 6.4   Initial crack length versus direction of initiation

Probability Density

.003

KIC ~ N(944, 66)psi$\sqrt{\text{in}}$

Crack Length, A ~ U(1, 4)in.

✳ Experimental Points (seven samples)

.002

.001

250.0   500.0   750.0   1000.0   1250.0   1500.0   1750.0   2000.0

Load (lbs.)

Figure 6.5   Probability density curve of fracture initiation load

Probability Density

KIC ~ N(944, 66)psi√in

Crack Length, A ~ U(1, 4)in.

✳ Simulation Points (28 samples)

Load (lbs.)
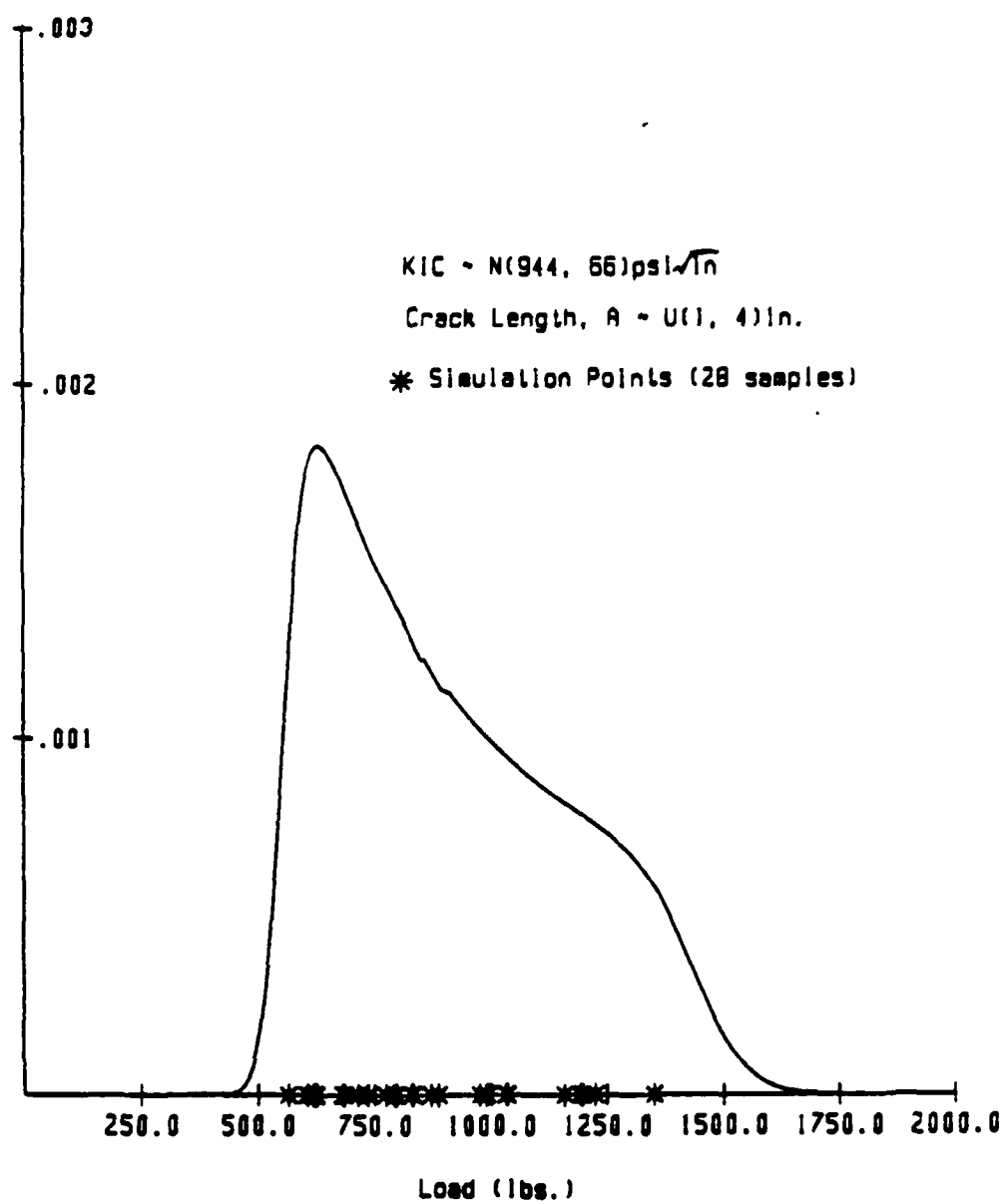
Figure 6.6   Probability density curve of fracture initiation load

Load to Fracture Initiation (lbs)
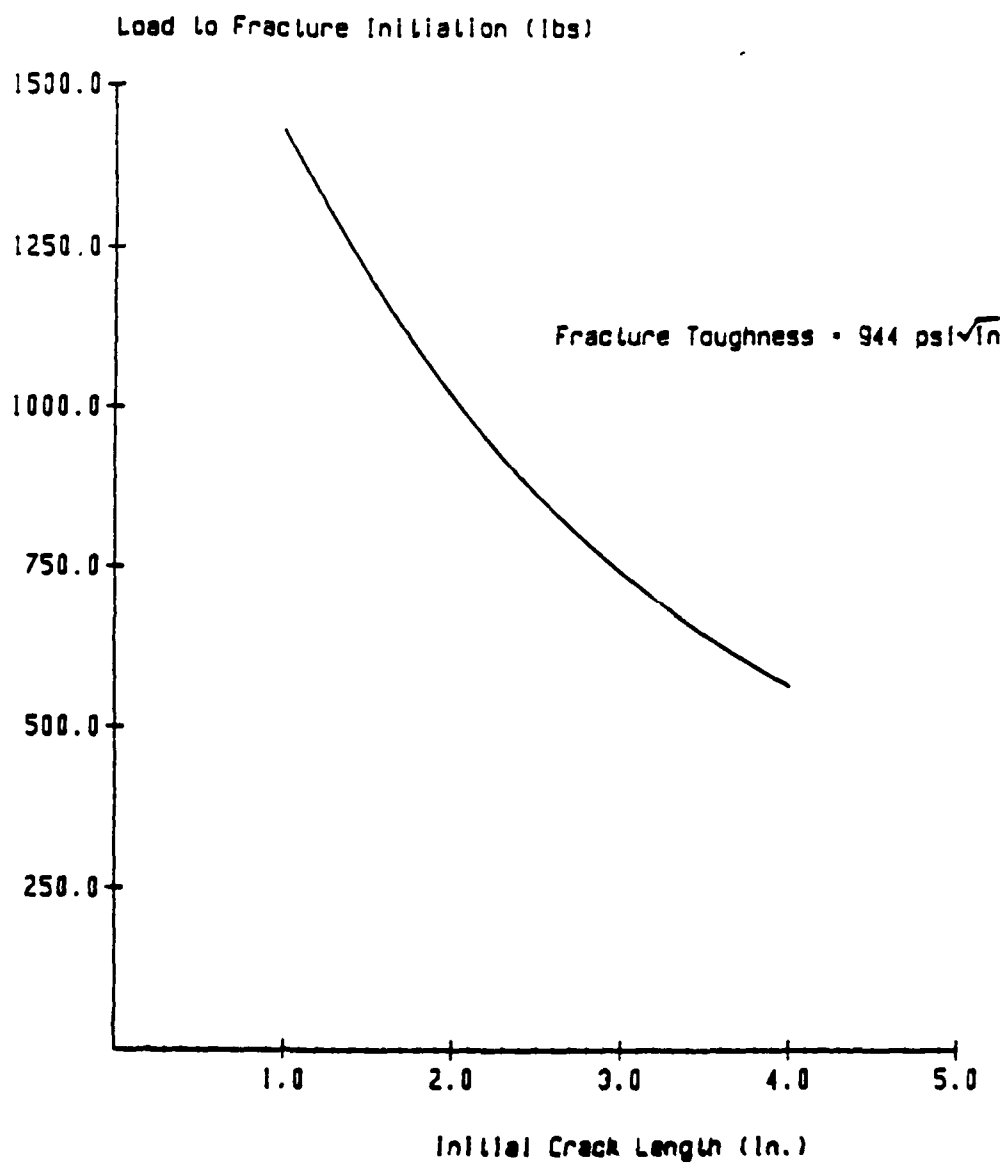
Figure 6.7   Initial crack length versus load to fracture initiation

Probability density

Distance of crack from beam center, D ~ U(2, 6)in.

Crack length, A = 3 in.

(From response surface over D and A)

＊ Experimental points (Five samples)

Initiation angle (degrees)
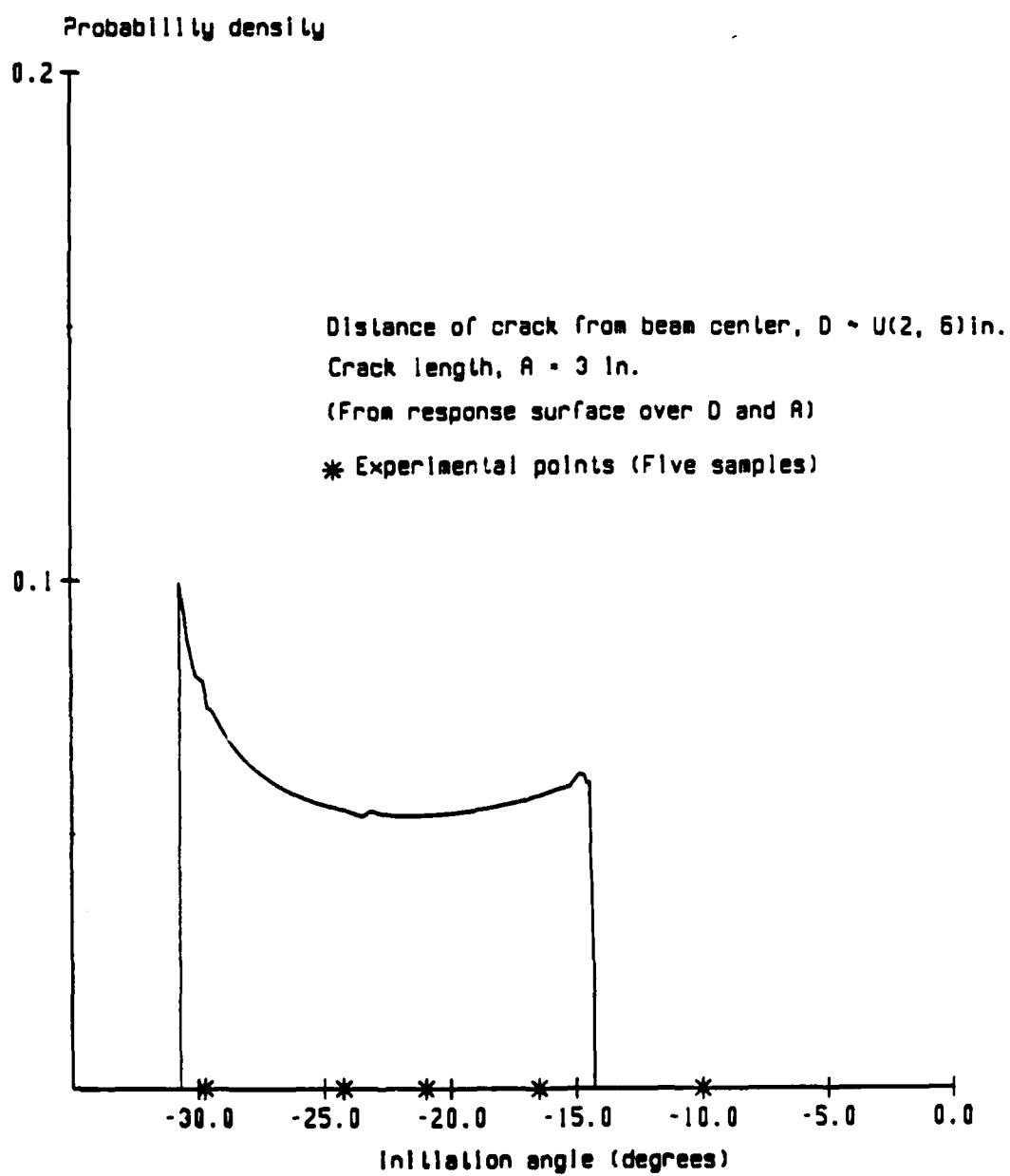
Figure 6.8   Probability density curve of crack initiation angle

Probability density

0.2

Distance of crack from beam center, D ~ U(2, 6)in.

Crack length, A ~ U(1, 4)in.
(From response surface over D and A)

0.1

-30.0   -25.0   -20.0   -15.0   -10.0   -5.0   0.0

Initiation angle (degrees)
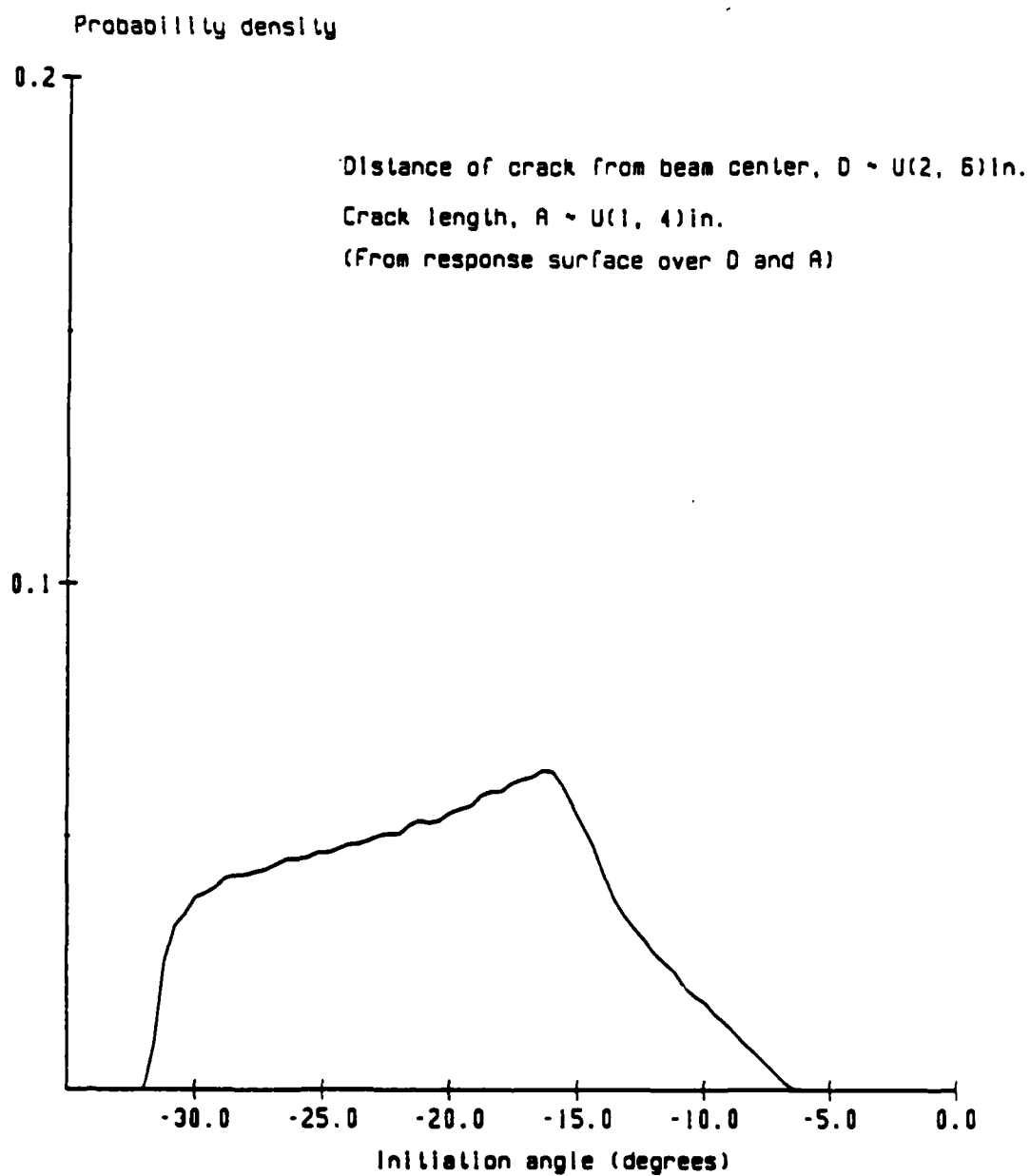
Figure 6.9   Probability density curve of crack initiation angle

Probability density

KIC ~ N(944, 66)psi√in

Crack length, A = 3 in.

Distance of crack from beam center, D ~ U(2, 6)in.
    (From response surface over D and A)

   * Experimental points (five samples)
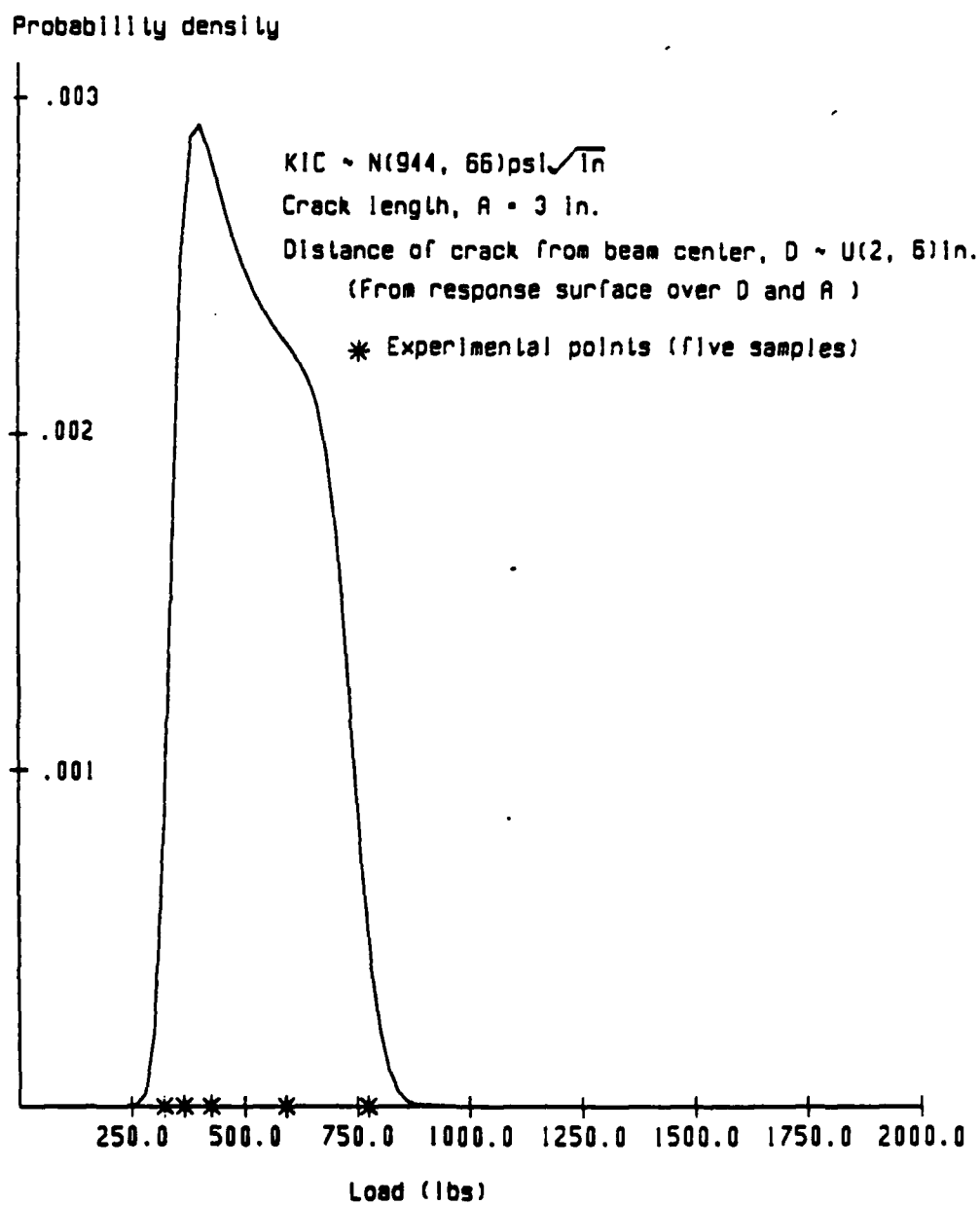
Load (lbs)

Figure 6.10   Probability density curve of fracture initiation load
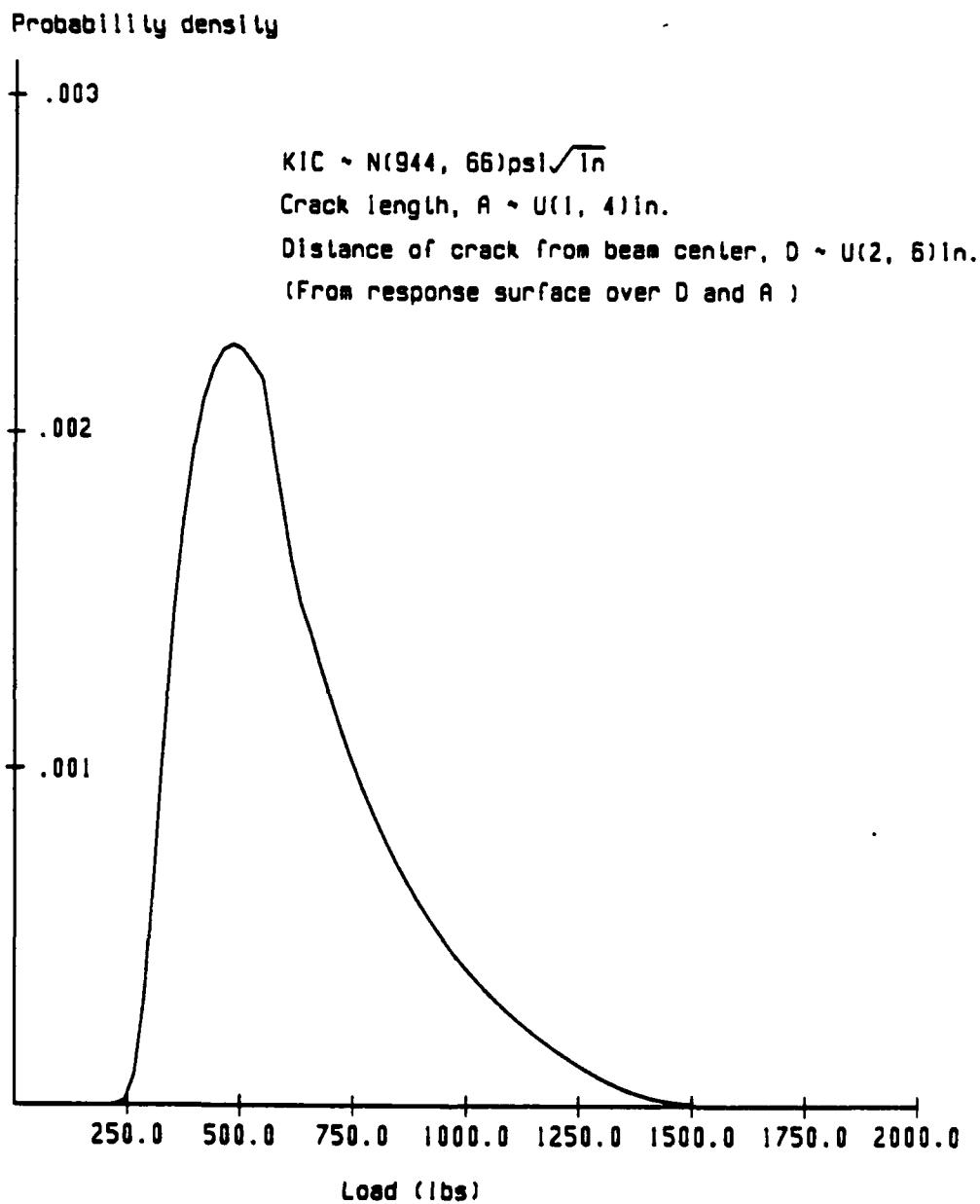
Probability density

Figure 6.11 Probability density curve of fracture initiation load

P_0 predicted by PROFRANC for $A \sim U(1, 4)$ in, $D \sim U(2, 6)$ in and $K_{Ic} \sim N(944, 66)$ lb-in-3/2.

6.2 Hypothesis Testing

The probability density curves obtained in phase 1 by PROFRANC for load to fracture initiation and initial direction of crack extension are quantitatively validated in this section by Kolmogorov-Smirnov test and Wilcoxon's test. These tests have been discussed in section 2 of the report. The results from Komogorov-Smirnov for load to fracture initiation and initial direction of crack extension are given in Tables (6.1) and 6.2) respectively. The corresponding results by Wilcoxon's test are given in Tables (6.3) and (6.4).

6.3 Crack Trajectory

Probabilistic study of trajectories is based on Monte Carlo simulation and response surface method in phase 1 and only response surface method in phase 2.

6.3.1 Monte Carlo Simulation

Twenty eight samples of initial crack lengths are generated for crack lengths uniformly distributed from 1 to 4 in for trajectory studies in phase 1. The distance of all crack initiation locations from the beam centerline was fixed at 6 in, (d = 6 in Figure 6.1). Using these samples, the structure has been analyzed by PROFRANC in automatic crack propagation mode. Thus twenty eight samples of crack trajectory was obtained.

Confidence Limit, γ	D_7^γ	Test Results
.01	.577	Accepted
.05	.486	Accepted
.1	.438	Accepted
.15	.405	Accepted
.2	.381	Accepted

$$D_{max} = .289$$

Table 6.1   Results of analyses by Kolmogorov-Smirnov Test for initial direction of crack extension. Random variable: Crack length, A ~ U(1,4)in.

Confidence Limit, γ	D_7^γ	Test Results
.01	.577	Accepted
.05	.486	Accepted
.1	.438	Accepted
.15	.405	Accepted
.2	.381	Accepted

$$D_{max} = .166$$

Table 6.2   Results of analyses by Kolmogorov-Smirnov Test for load to fracture initiation. Random variables: Crack length, A ~ U(1,4)in, K_{IC} ~ N(944, 66)psi-in$^{(1/2)}$

Confidence Limit, γ	$W_{7,7}^7$	Test Results
.001	29	Accepted
.005	32	Accepted
.01	34	Accepted
.025	36	Accepted
.05	39	Accepted
.1	41	Accepted

$$W = 60$$

Table 6.3   Results of analyses by Wilcoxon Test for initial direction of crack extension. Random variable: Crack length, A ~ U(1,4)in.

Confidence Limit, γ	$W_{7,7}^7$	Test Results
.001	29	Accepted
.005	32	Accepted
.01	34	Accepted
.025	36	Accepted
.05	39	Accepted
.1	41	Accepted

$$W = 55$$

Table 6.4   Results of analyses by Wilcoxon Test for load to fracture initiation. Random variables: Crack length, A ~ U(1,4)in, K_{IC} ~ N(944, 66)psi-in$^{(1/2)}$

Statistical analysis was performed using these samples. Figure 6.12 shows the sample trajectories.

Figure 6.13 shows the mean trajectory obtained by taking the mean of the y-ordinates of the sample trajectories at different vertical sections. The vertical sections at values of x greater than -4.2 inch intersects with fewer than 28 trajectories. This shifts the mean trajectory towards the right until it coincides with the trajectory corresponding to the lowest initial crack length. The figure also shows the trajectories one standard deviation away from the mean. These trajectories merge towards the mean trajectory as the vertical sections are taken at values of x higher than -4.2 inch.

Figure 6.14 shows the cumulative density curves of trajectories along horizontal sections at different values of y. The ordinates of these curves at x give the fraction of trajectories exceeding y at x. The spread of these density curves decreases as the horizontal section is raised. This is consistent with physical anticipation. In the limit as y approaches infinity all the trajectories should approach the load point. Thus at infinity, the density function would be a step function, located just to the left of the load point.

6.3.2 Response Surface

Phase 1

A response surface has been generated for crack trajectory from sample crack trajectories. The surface is given by the
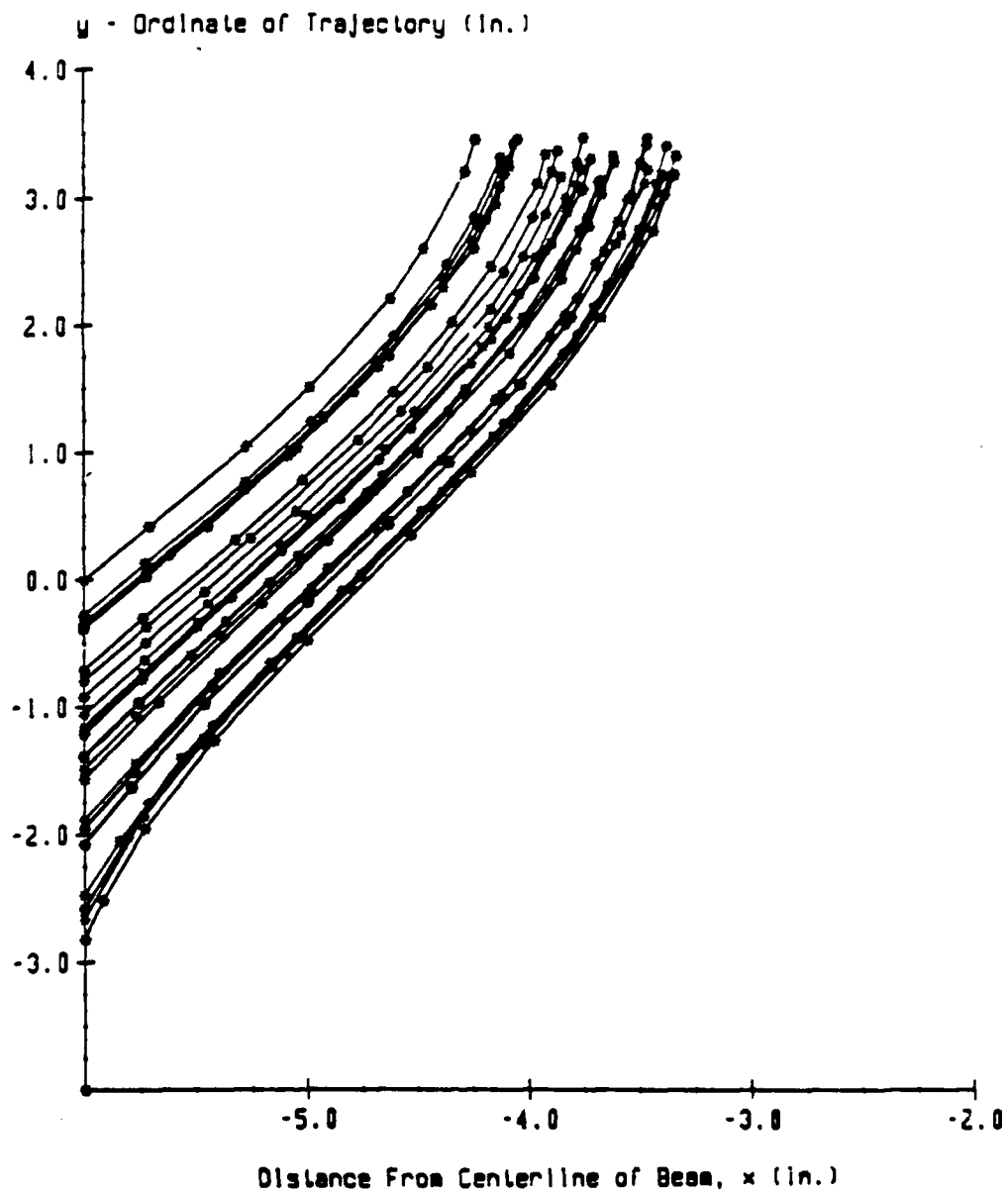
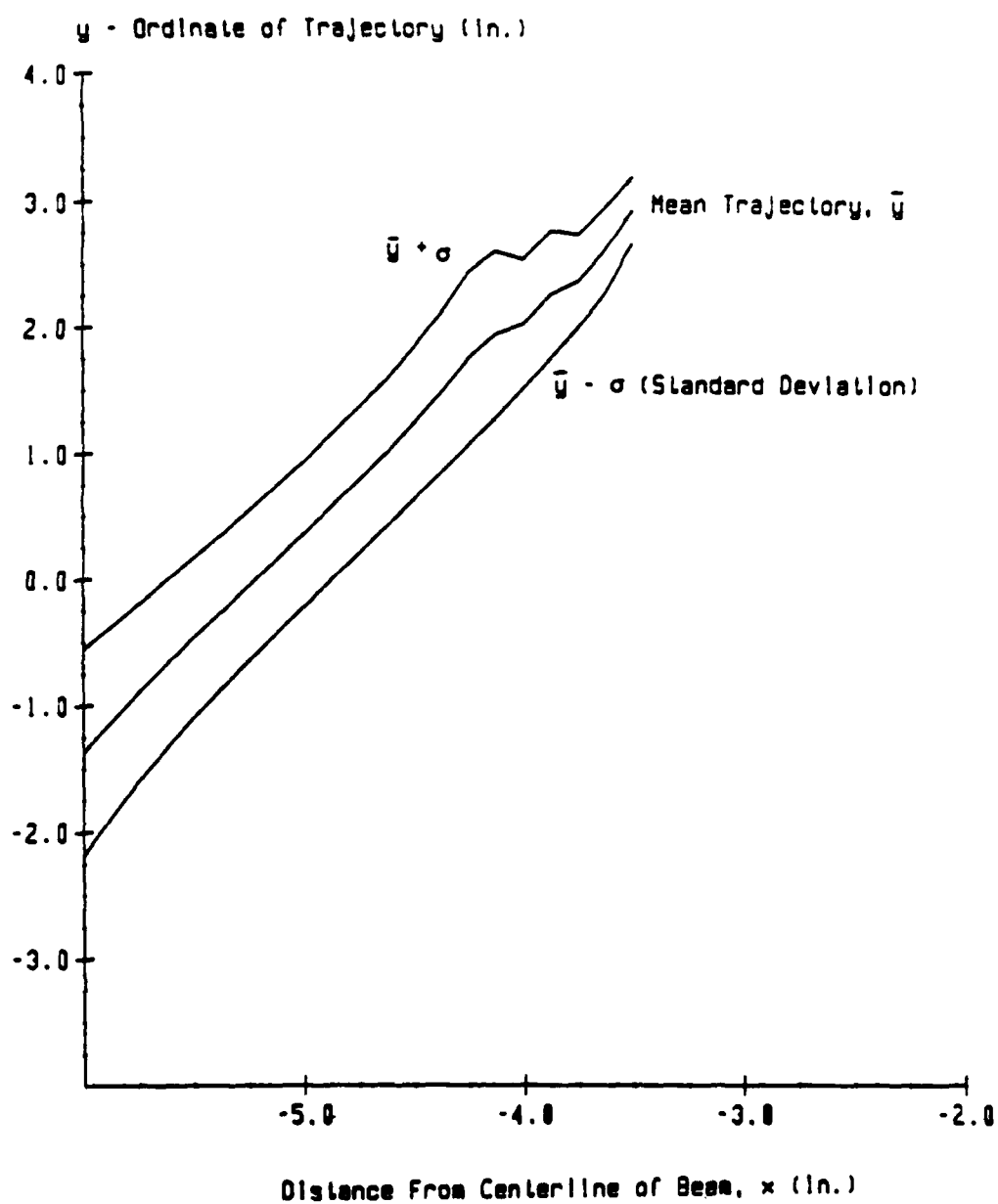Figure 6.12   Twenty-Eight samples of crack trajectory

Figure 6.13   Second moment characteristics of sample trajectories
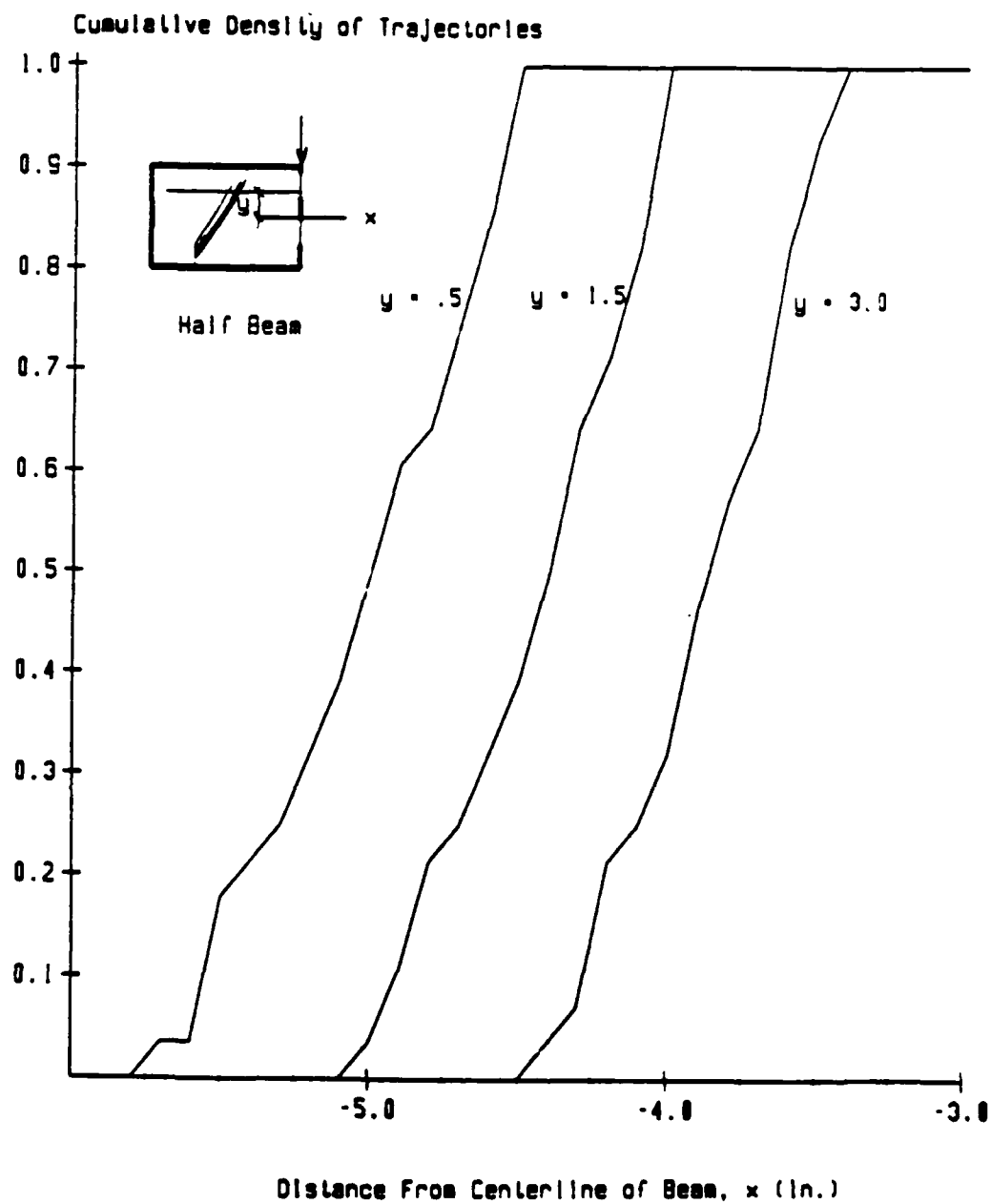
Figure 6.14   Cumulative distribution function curves of trajectories
along horizontal section

following function,

$$y(A, x) = 14.6 + 1.09A + 3.33x + .163A^2 + 15x^2 - .0315A^3 + .0404A^2x - .0037Ax^2 \qquad (4)$$

which defines the crack trajectory with respect to x for a given initial crack length, A. Figure 6.15 shows the trajectories obtained from Eq. (4) compared with experimental trajectories.

The response surface equation has been used to develop the evolution of the trajectory density with x (Figure 6.16). The density curves are skewed to the left. This is consistent with the fact that the trajectories corresponding to lower crack lengths tend to converge towards those corresponding to higher initial crack lengths (Figure 6.12). This is also observed from Figure 6.17 where the curves indicate the y-ordinates of trajectories at given values of x with increasing crack length. The slope of these curves increases with initial crack length. Since the initial crack length is uniformly distributed, the density curve of y becomes skewed towards its lower values. As x increases, the curves of Figure 6.17 become flatter and the skewness of the density curves of y in Figure 6.16 increases. We also observe that the ordinates of the density function in Figure 6.17 increase with x. This is due to the fact that these density curves account for those trajectories only which are within the boundary of the beam along a given vertical section. This increase in the ordinates of the density function with x is consistent with Figure 6.13 where the standard deviation of the
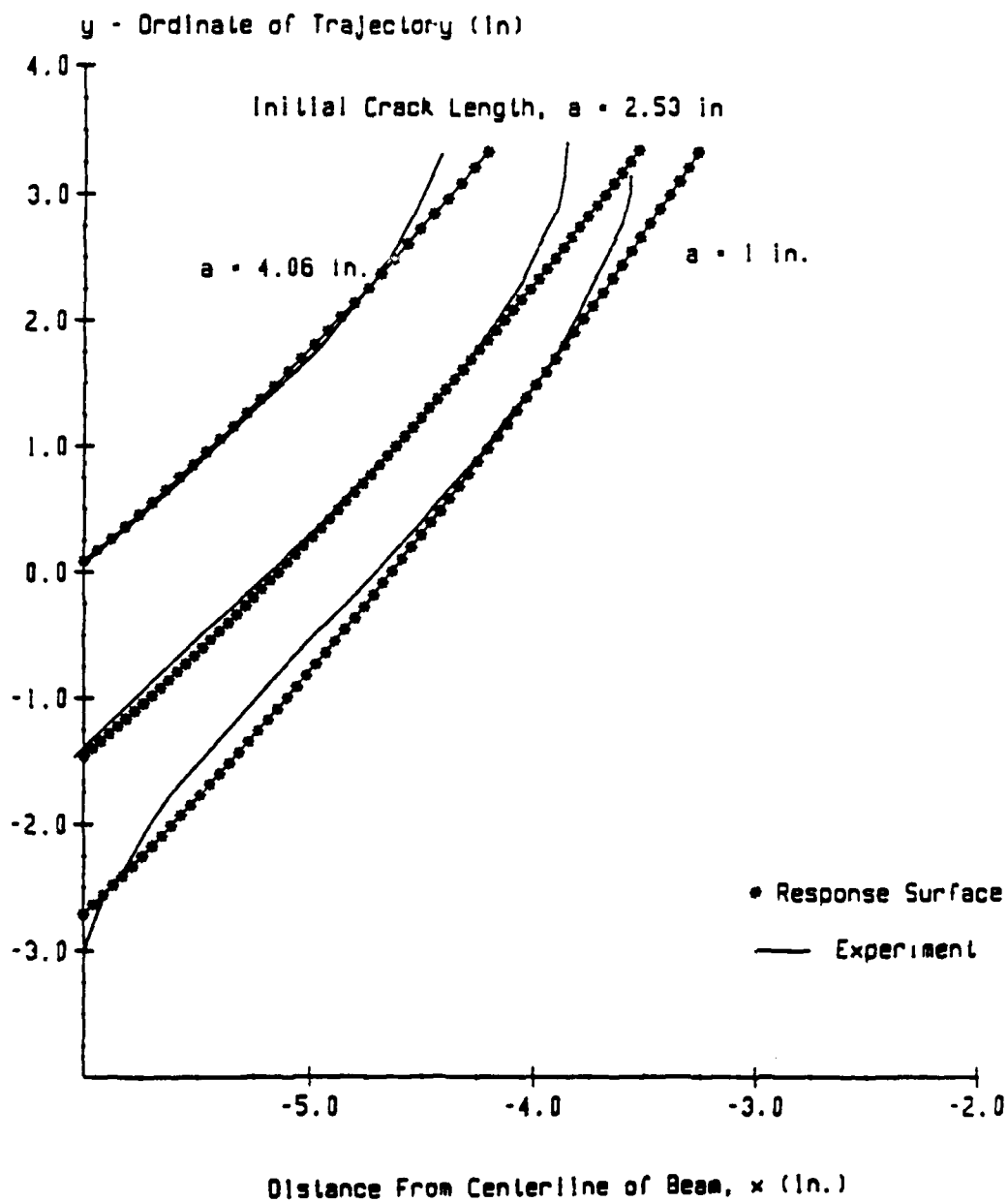
Figure 6.15 Comparison of trajectories from experiments and response surface predictions
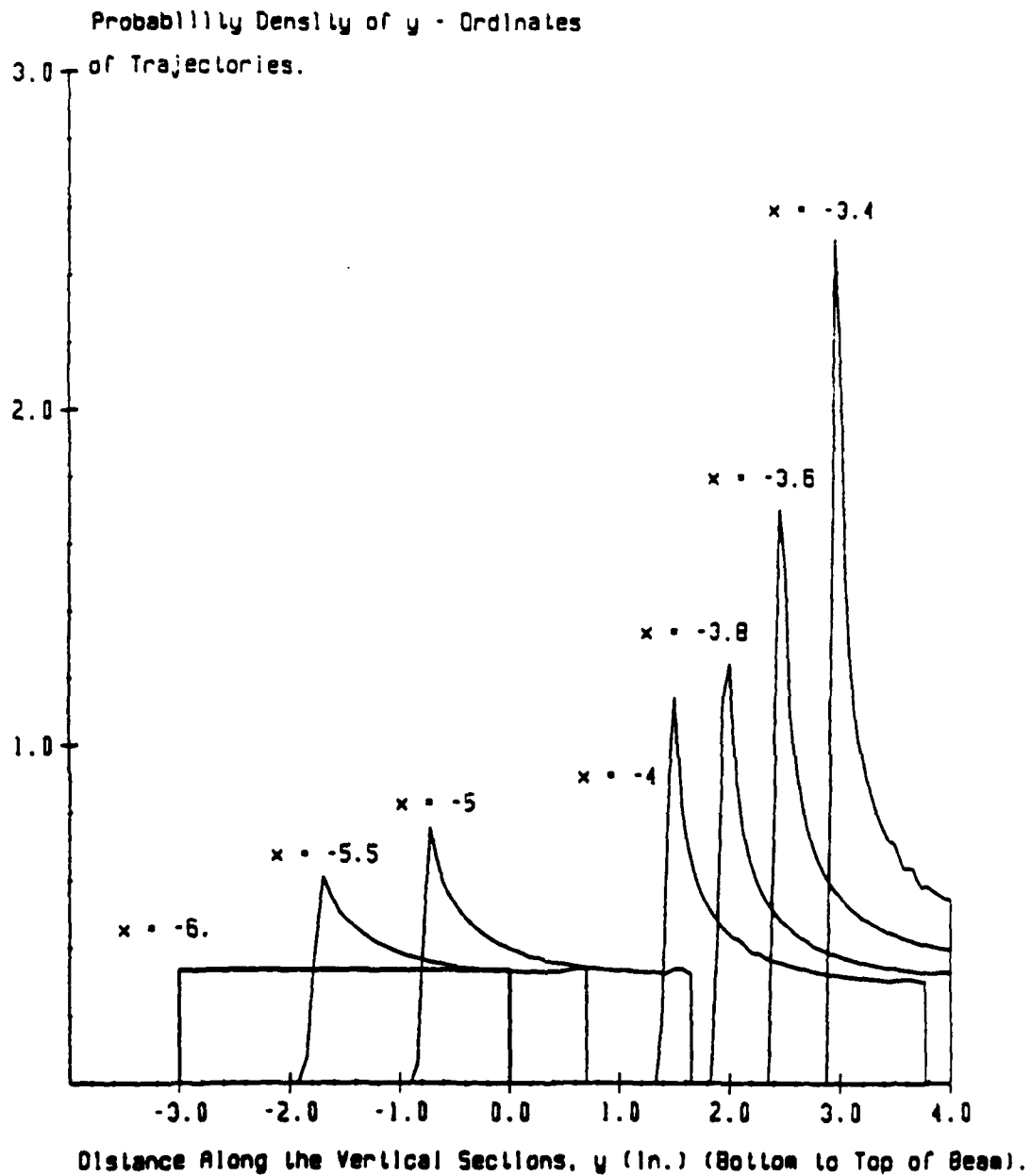
Figure 6.16   Probability density curves for Y-ordinates of crack trajectory at different vertical sections. (Response Surface Method)
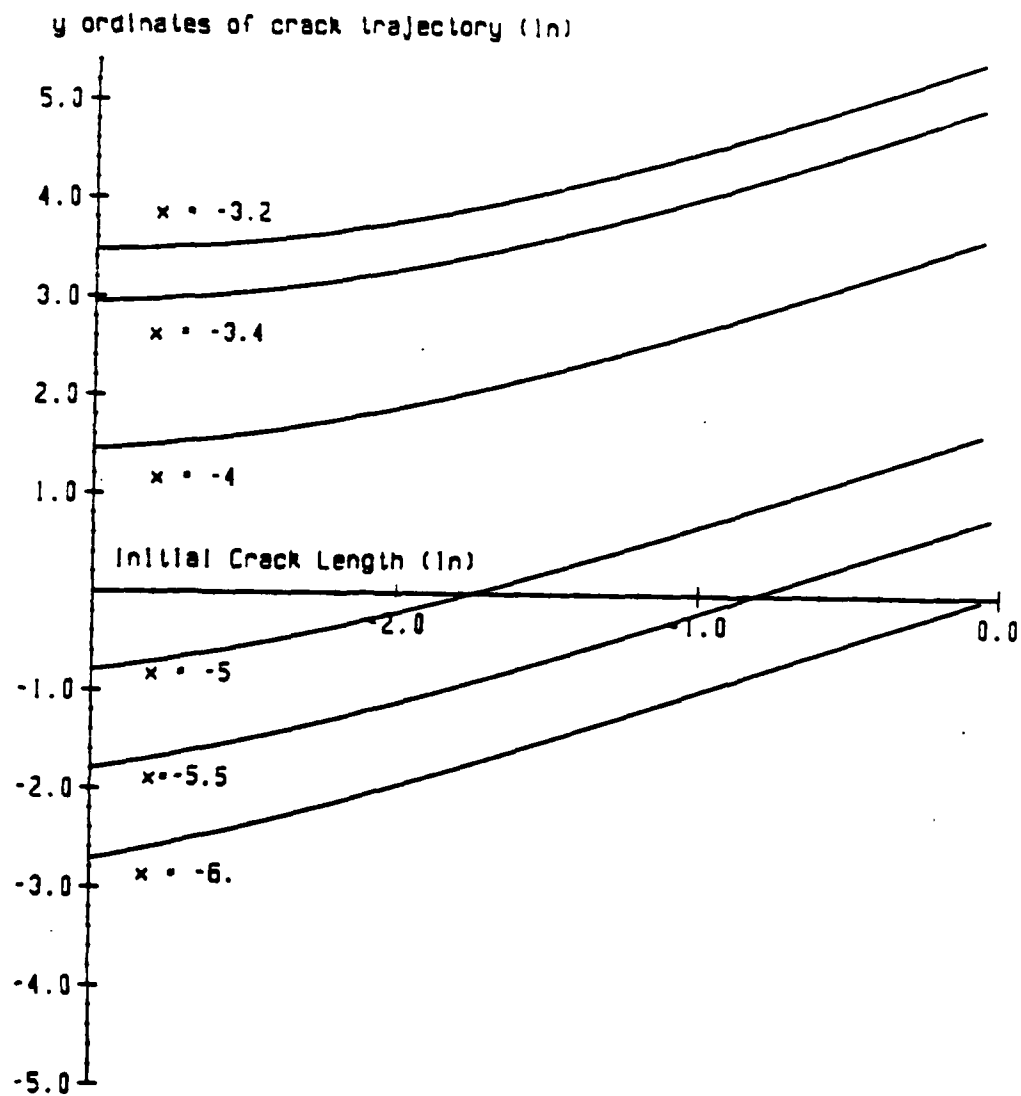
Figure 6.17   Y-ordinates of trajectories versus initial crack length at
            different values of x (from Response Surface Equation (4))

trajectories decreases with X shown by the curves one standard deviation away from the mean trajectory.

Phase 2

PROFRANC has been applied in an automatic crack propagation mode to determine crack trajectories for several values of crack length a_i, i = 1, 2, ... n, in range (1, 4)in and crack location d_j, j = 1,2, ... n, in range (2, 6)in. A response surface y = y(d,a,x) can be calibrated to the resulting crack trajectories. It depends on random variables {A, D} specifying the initial crack geometry and has the from

$$y(d, a, x) = 1.3833 + 4.4569d + 0.057a + 8.069x - 0.239d^2$$

$$\text{(5)}$$

$$+ 0.118a^2 + 1.296x^2 - 0.0115da - 0.043ax + 0.057xd +$$
$$0.087x^3$$

for given a and d. The system of coordinates xy is shown in Figure 6.1.

Figure 6.18 shows histograms of crack trajectories Y(D, A, x) for A ~ U(1, 4)in, D ~ U(2, 6)in and x = -5.5, -4, -2, -1 in. These histograms have been obtained from the response surface in Equation 5 and probabilistic characteristics of D and A by PROFRANC. They are normalized so that each of them has unit area. There is a significant difference between the shape of the histograms for various values of x. For example, the histogram for x = -5.5 in is skewed to the left, a behavior discussed in the previous report [31]. On the other hand, the histogram for x
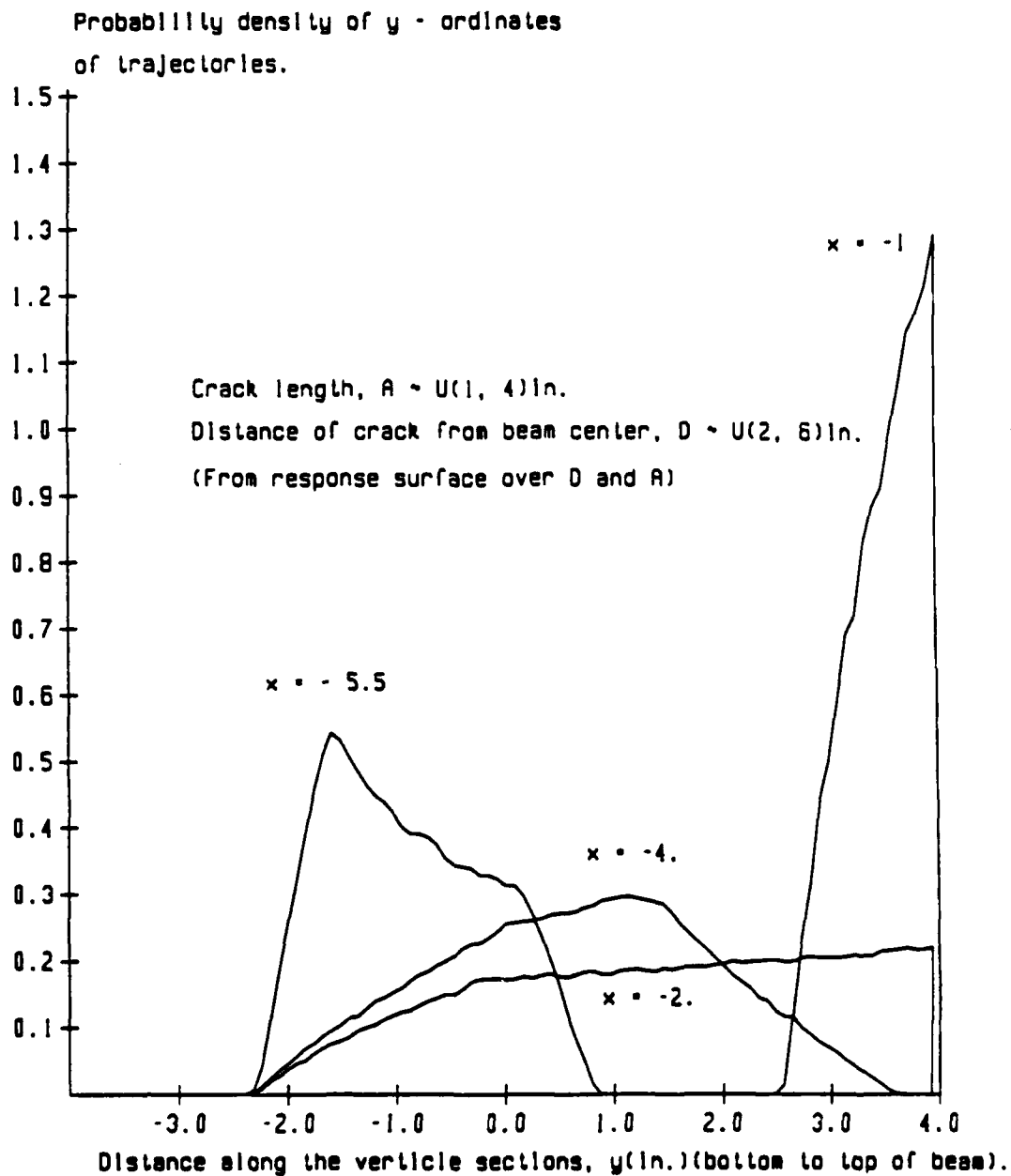
Figure 6.18   Probability density curves for y-ordinates of crack trajectory at different vertical sections (response surface method)

= -1.0 in shows a much smaller spread and is concentrated at higher values of y. This is consistent with experimental and analytical findings showing that differences between crack trajectories diminish as they approach the point of application of load.

6.4 Example Problem

Figure 6.19 shows a hypothetical version of the structure studied in this report. In this version a vertical crack arrester AB has been used in the structure at x = - 3.5 in. The important question that one needs to answer is the following:

"Suppose one knows the location of potential crack initiation and the distribution of possible initial crack lengths. What is the probability that the crack arrester will ever get an opportunity of serving its purpose?"

If the distribution of initial crack lengths is uniform over 1 in. to 4 in. and the crack initiates at 6 in. from the beam centerline then from Figure 6.14 it is obvious that the probability that the arrester will find a trajectory is zero. So the arrester will never serve its purpose. If the trajectory were placed at x = -5.0 in, it would capture trajectories due to any of the sample crack lengths and the probability that the arrester would arrest the crack would be unity. For arrester locations between x = -3.5 in and x = -5.0 in, a variable probability of effectiveness would be predicted. Note that these results depend upon the distribution of initial crack length.
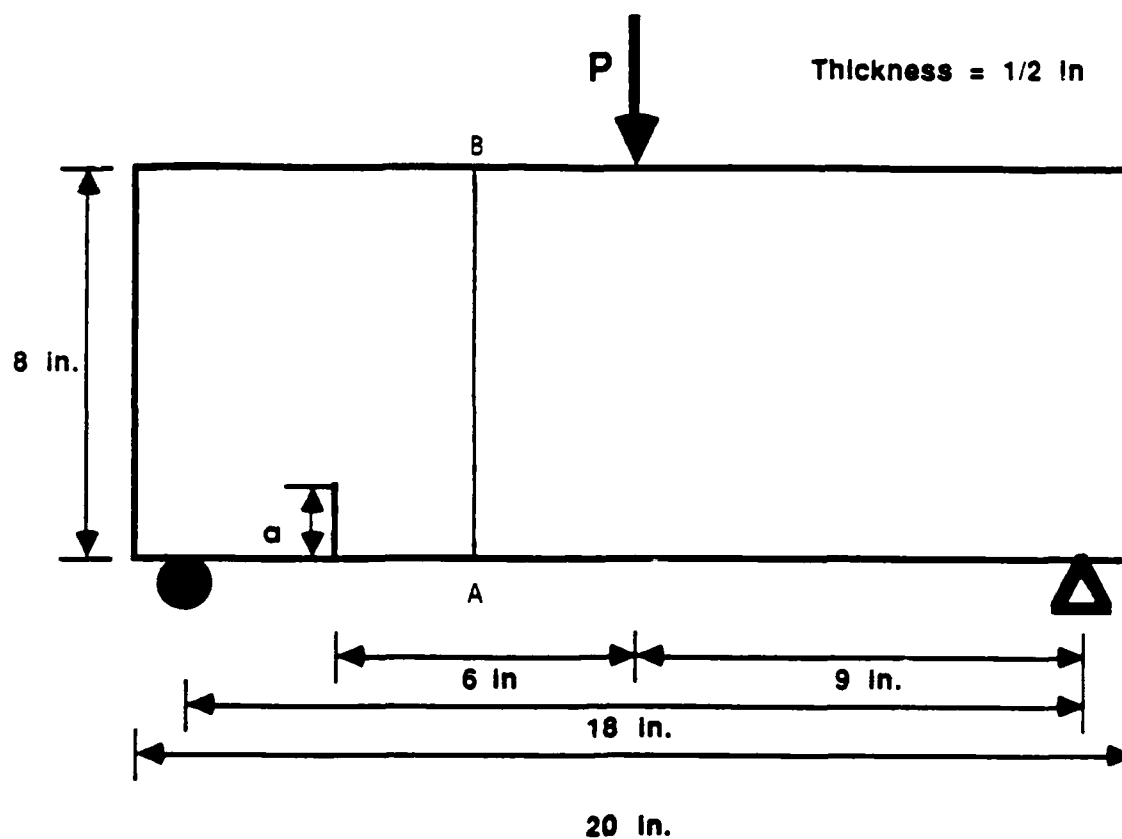
Figure 6.19   Beam with Crack Arrester, line A-B

6.5 Sensitivity of Crack Trajectories to Boundary Conditions

Sensitivity of crack trajectories to (a) location of load point and (b)support conditions has been studied. This study was undertaken to evaluate effects of differences between experiments and computer models. For example, the right support of the structure in Figure 6.1 was modeled for analysis as a roller. However this boundary condition cannot be reproduced in the laboratory exactly due to friction and local plastic deformations. A horizontal spring attached to the roller used in the analysis can be used to model these effects. The point of application of the load remains on a vertical line in the experiments but is drifting laterally in the computer model because it is associated with a node of the finite element mesh. PROFRANC has been applied to determine crack trajectories for A = 1.0 in, D = 6.0 in and several load locations c in the range (5, 7)in (Figure 6.20). A response surface, y = y(1,x), can then be calibrated to these trajectories, where 1 = d - c. It has the expression

$$y = 44.433 + 0.6431 + 25.195x - .023^2 +$$
$$+ 5.031x^2 + 0.1081x + 0.358x^3 \qquad (6)$$

and gives crack trajectories for any 1 in range (-1, 1)in.

Figure 6.21 shows probabilities of crack trajectories at different values of x for A = 1.0in, D = 6.0in and load location c modeled as a random variable uniformly distributed over range (5, 7)in. The narrow spread of these curves indicate that the
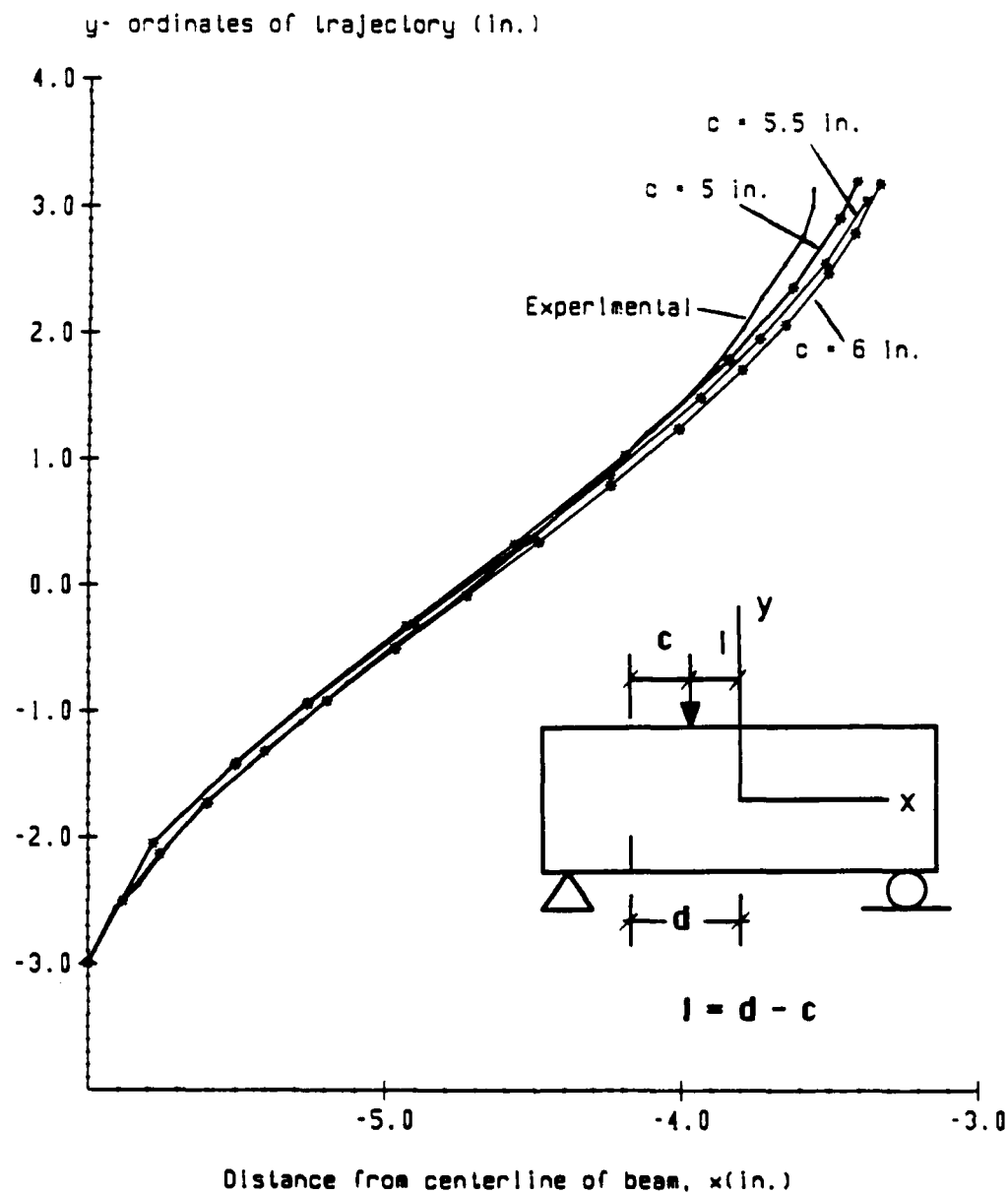
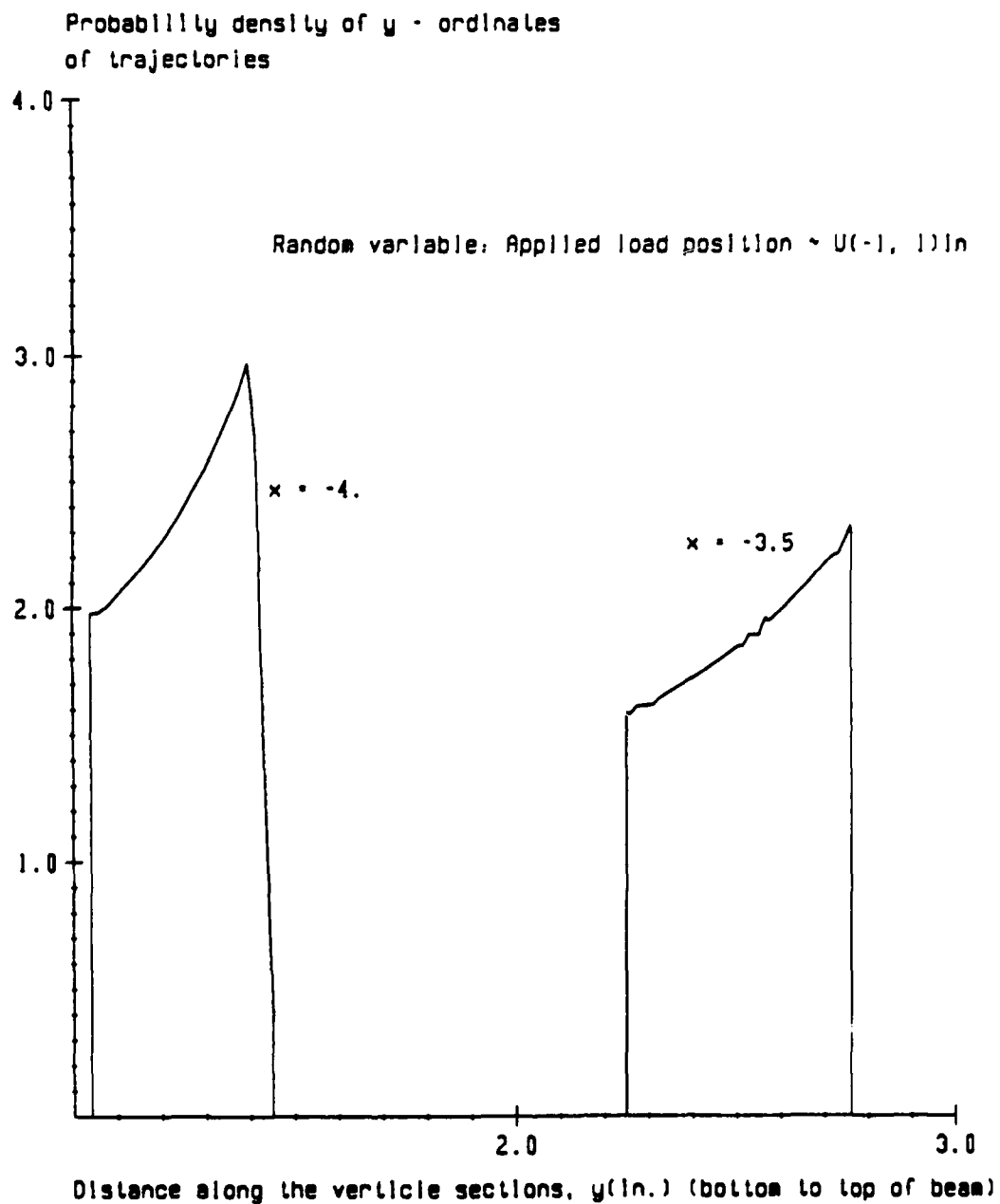Figure 6.20 Crack trajectories due to various locations of applied load

Figure 6.21   Probability density curves for y-ordinates of crack trajectory at different vertical sections (response surface method)

load position does not have a significant influence on the evolution of cracks for this structure.

Figure 6.22 shows the sensitivity of crack trajectory to the stiffness of a horizontal spring attached to the roller support of the beam for A = 1.0in and D = 6.0 in. Results show that the support stiffness has a limited effect on crack trajectory during the initial stage of propagation. However, as the crack evolves, the displacement at the roller increases rapidly and compression caused by the spring force becomes relevant and changes the stress field at the crack tip. This result in an increase of the ratio of mode II to mode I stress intensity which causes an increased deviation of predicted trajectories from experimental results.
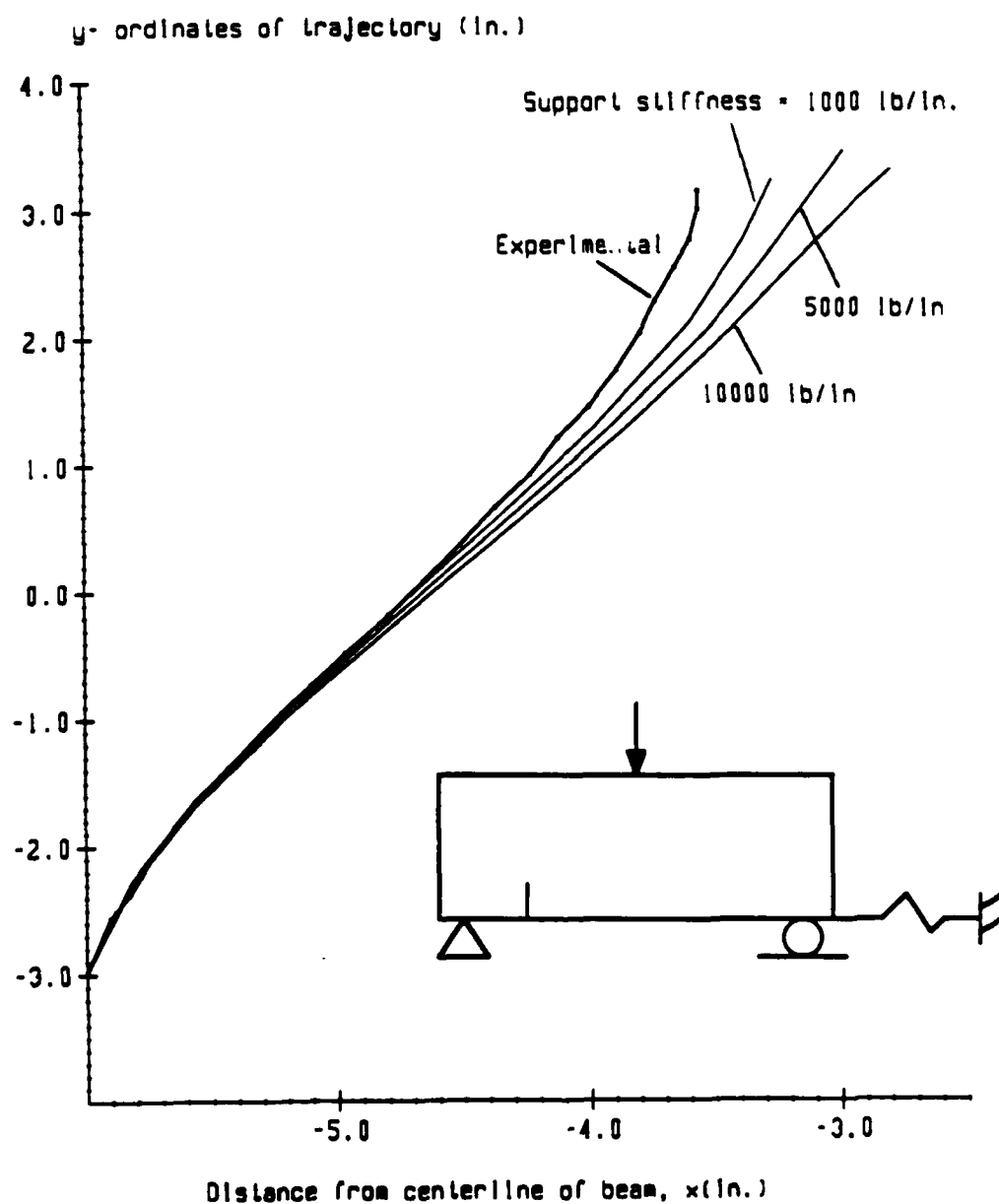
y- ordinates of trajectory (in.)

Figure 6.22 Crack trajectories due to various stiffness of the horizontal spring at the roller support

7.0 BIAS OF PREDICTED CRACK TRAJECTORIES

It has been observed that crack trajectories predicted by PROFRANC using the maximum circumferential tensile stress theory deviate from experiments. This deviation is not significant, but consistently predicts trajectories to the same side of those observed. A similar bias was reported by Williams and Ewing [4] for crack initiation angle. The results from the previous section appear to indicate that this bias is not due to systematic differences between the load line location or the frictional component of the reaction in experiments and the model. It may be caused by nonlinearities in the process zone which are inconsistent with the maximum tensile stress analysis based on the singular term of stress field at crack tip [32]. Inclusion of nonsingular terms in the stress field can significantly improve predictions of the maximum tensile stress theory [32]. Investigation into the cause of the bias in predicted trajectories is continuing.

8.0 CONCLUSIONS

A two-phase task was undertaken to validate PROFRANC. Phase one consisted in predicting deterministically the outcome of a subset of a larger number of experiments in which variability in geometry and material parameters was purposely minimized. The purpose of this phase was to verify that PROFRANC could predict nearly deterministic events accurately. This phase was shown to be highly successful.

This verification was based on experimental results which had to be obtained within this project due to a paucity of comprehensive mixed-mode fracture propagation data in the open literature.

In Phase two all currently available data involving inherent uncertainties in some material and geometrical parameters was assembled in a probabilistic framework and subsequently compared to the probabilistic predictions of PROFRANC qualitatively and quantitatively. These comparisons were shown to be very successful. The quantitiative comparison was performed by hypothesis testing, which is a mathematical rule deciding whether to except or reject PROFRANC predictions using experimental data.

Results to date show in particular that:

1. PROFRANC can predict deterministically load to fracture initiation, initial direction of crack extension, complete trajectory to failure, and various load-displacement relationships in arbitrary two-dimensional structures.

2. PROFRANC can accurately predict probabilistic character-
   istics of fracture phenomena for systems including
   uncertainties in geometrical and material parameters.
   This predictive capability includes not only means and
   variances of all relevant fracture-based responses, but
   also their full probabilistic descriptions. Two inde-
   pendent hypothesis tests namely, Kolmogorov-Smirnov and
   Wilcoxon tests, validated these descriptions.

3. It is possible to create a controlled, scientifically
   designed database for both deterministic and probabilis-
   tic response of two-dimensional mixed-mode fracture
   propagation. Such a database currently cannot be found
   in the open literature and has been critical in the
   validation of PROFRANC.

4. A previously unanticipated source of uncertainty was
   uncovered during the experiments and simulations:
   variability in supposed boundary conditions. This
   source of uncertainty has been shown to affect signi-
   ficantly trajectory of curvilinear fracture, and can
   have a profound effect on the reliability of fail-safe
   design of structures sensitive to such cracking.

9.0 REFERENCES

1. Bank-Sills, L. and Bortman, Y., "A Mixed-Mode Fracture Specimen: Analysis and Testing", I.J. Fracture, 30, (1986) 181-201.

2. Erdogan, F. and Sih, G.C., "On the Crack Extension in Plates Under Plane Loading and Transverse Shear", Trans. ASME. J. Basic Eng., 85D, (1963) 519-527.

3. Grigoriu, M. Saif, M.T.A., El-Borgi, S. and Ingraffea, A.R., "Mixed-Mode Fracture Initiation and Trajectory Prediction Under Random Stresses", Report 88-5, June 1988, School of Civil Engineering, Cornell University, Ithaca, New York.

4. Williams, J.G. and Ewing, P., "Fracture under Complex Stress -The Angled Crack Problem", I.J. Fracture, 8, (1972) 441-446.

5. Finnie, I. and Weiss, H.D., "Some Observations on Sih's Strain Energy Density Approach for Fracture Prediction", I.J.Fracture, 10, (1974) 136-138.

6. Ewing, P.D. Swedlow J.L., Williams J.G., "Further results on the Angled Crack Problem". I.J. Fracture, 1, (1976) 85-93.

7. Ingraffea, A. R., Heuze, F. E., "Finite Element Models for Rock Fracture Mechanics", International Journal for Numerical and Analytical Methods in Geomechanics, 4, (1980) 25-43.

8. Ingraffea, A.R., "Mixed-Mode Fracture Initiation in Indiana Limestone and Westerly Granite," Proc. 22nd U.S. Symposium on Rock Mechanics, Cambridge, MA, June 29-July 2, 1981, pp. 186-191.

9. Ingraffea, A.R. and Arrea, M., "Mixed-Mode Crack Propagation in Mortar and Concrete," Department of Structural Engineering Report 81-13, School of Civil and Environmental Engineering, Cornell University, Ithaca, N.Y., 1981.

10. Iosipescu, "New Accurate Procedure for Single Shear Testing of Metals", J. of Materials, 2, (1967) 537-566.

11. Adams, D.F. and Walroth, D.E., "Iosipescu Shear Properties of SMC Composite Materials", Composite Materials: Testing and Design (Sixth Conference) ASTM STP 787, I.M. Daniel, Ed., American Society for Testing and Materials, (1982), 19-33.

12. Sullivan, J.L., Kao, B.G. and Van Oene, H. "Shear Properties and a Stress Analysis Obtained from Vinyl-ester Iosipescu Specimens". Experimental Mechanics, September 1984, 223-231.

13. Barnes, J.A., Kumose, M. and Hull, D. "Theoretical and Experimental Evaluation of the Iosipescu Shear Test". Composite Science and Technology, v. 28, (1987) 251-268.

14. Wang, S.S., Goetz, D.P. and Corten, H.T. "Fracture of Random Short-Fiber SMC Composite under Shear Loading." I.J. Fracture, 26, (1984) 215-227.

15. Bocca, P. Carpinteri, A. and Valenti, S. "Size Effects in the Mixed-Mode Crack Propagation: Softening and Snap-Back Analysis". _Int. Conf. on Fracture and Damage of Concrete and Rock_, Vienna, July 4-6, (1988).

16. Ballatore, E. Carpinteri, A., Ferrara, G. and Melchiorri, G. "Mixed Mode Fracture Energy of Concrete". _Int. Conf. on Fracture and Damage of Concrete and Rock_, Vienna, July 4-6, (1988).

17. Bazant, Z. P. and Pfeiffer, P.A. "Shear Fracture Tests of Concrete." _Materials and Structures_, 19, (1986) 111-121.

18. Beardmore, P. and Rabinowitz, S. "Craze Formation and Growth in Anisotropic Polymers". _J.Materials Science_, 10, (1975) 1763-1770.

19. Farrar, N.R. and Kramer E.J. "Microstructure and Mechanics of Crazes in Oriented Polystyrene". _Polymer_, 22 (1981) 691-698.

20. Marshall, G.P. Coutts, L.H. and Williams J.G. "Temperature Effects in the Fracture of PMMA". _J. Materials Science_, 9,(1974) 1409-1419.

21. Jenq, Y.S. and Shah, S.P., "Mixed-Mode Fracture of Concrete". _I.J. Fracture_, 8,(1988) 123-149.

22. Ingraffea, A.R. and Panthaki, M.J., "Analysis of Shear Fracture Tests of Concrete Beams", _Finite Element Analysis of Reinforced Concrete Structures_, edited by C. Meyer and H. Okamura, ASCE Publishers, (1986) 151-173.

23. Clausing, D.P., "Crack Stability in Liner Elastic Fracture Mechanics", I.J. Fracture, 5, (1969) 211-227.

24. Mai, Y.W. and Atkins, A.G., "Crack Stability in Fracture Toughness Testing", J.Strain Analysis, 15 (1980) 63-74.

25. Atkins, A.G. and May, Y.W., Elastic and Plastic Fracture, published by Ellis Horwood limited (1985), Chapter 8, 638-703. 26. Marshall, G.P. and Williams, J.G. "The Correlation of Fracture Data for PMMA", J. of Material Science, 8 (1973) 138-140.

27. Williams, J.G., Radon, J.C. and Turner, C.E., "Designing Against Fracture in Brittle Plastics", Polymer Eng. and Science, April, (1968), 130-141.

28. Margolis, R.D. Dunlop, R.W. and Markovitz, H. "Fracture Toughness Testing of Glassy Plastics", Cracks and Fracture, ASTM STP 601, American Society for Testing and Materials, (1976), 391-408.

29. ASTM E399-83, "Standard Text Material for Plane-Strain Fracture Toughness of Metallic Materials". Annual Book of ASTM Standards, 1988.

30. Srawley, J. E., "Wide Range Stress Intensity Factor Expressions for ASTM E-399 Standard Fracture Toughness Specimens, Int. J. Fracture, 12, 1976, pp. 475-476.

31. Ingraffea, A. R., and Grigoriu, M., "Probabilistic Fracture Mechanics: A Validation of Predictive Capability," Report No. 89-11, School of Civil & Environmental Engineering, Cornell University, Ithaca, NY.

32. Palaniswamy, K., and Knauss, W. G., "On the Problem of Crack Extension in Brittle Solids Under General Loading," Mechanics Today, 4, Pergamon Press, 1978, pp. 87-148.

33. Martz, H. F., and Waller, R. A., "Bayesian Reliability Analysis, John Wiley and Sons, New York, 1982.

34. Bradley, J. V., Distribution Free Statistical Tests, Prentice Hall, Inc., Englewood Cliffs, New Jersey.

APPENDIX A

MEASUREMENT OF ELASTICITY MODULUS

A. 1 Introduction

An indirect technique was used to obtain an accurate measure of Young's modulus of elasticity. This technique uses data from the mixed-mode fracture tests and is superior to a standard tensile test. The following section explains the details of this technique.

A. 2 Description of Technique to Measure Young's Modulus

A series of deterministic analyses of four tested specimens with varying initial crack length of nominal value (a = 1, 2, 3, 4 in) but the same crack location and inclination was first performed (Figure A.1). Figures A.2 to A.5 show the finite element models for all four specimens. In each analysis, a value of unity was used for both Young's modulus and fracture toughness. Furthermore, each analysis was based on the measured values of geometry parameters, namely location, length and inclination of initial crack, length, depth and thickness of the specimen.

From each analysis the initial stiffness of the beam, defined as the ratio of applied load CMOD applied load, is computed. The actual initial stiffness is measured from the observed load-versus-CMOD. This corresponds to the slope of the load-versus-CMOD curve prior to fracture initiation. The ratio of observed stiffness to
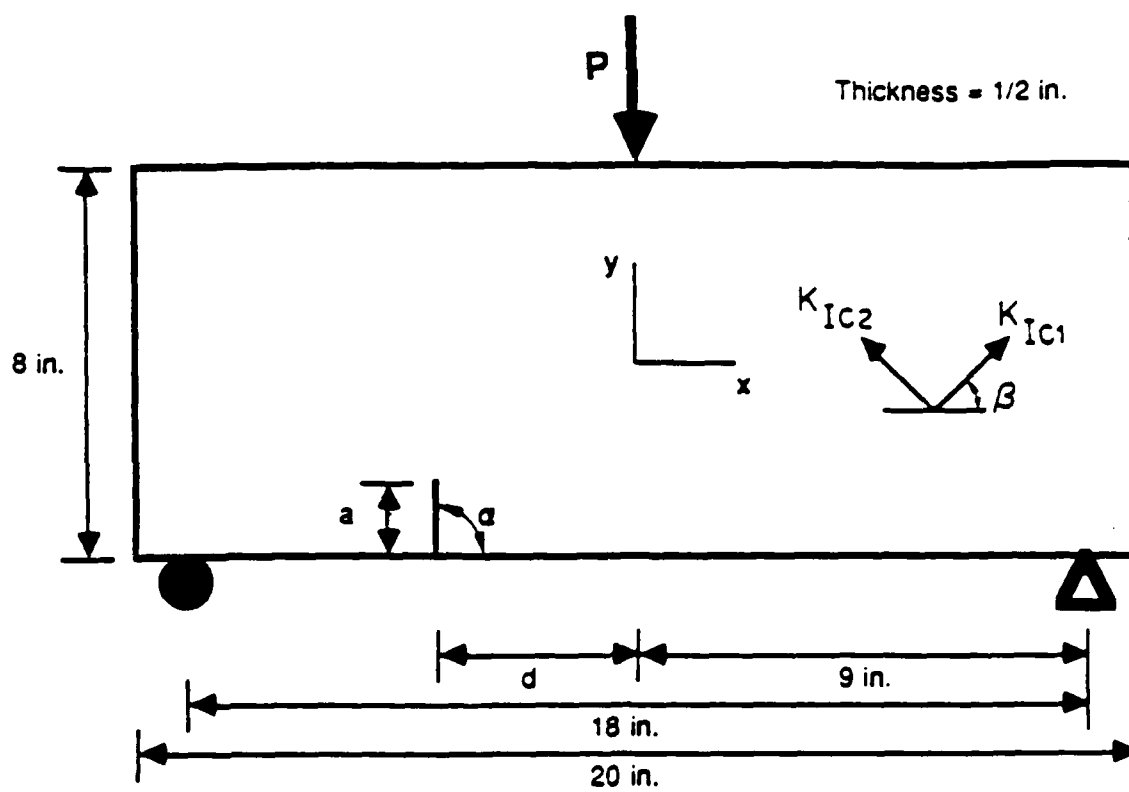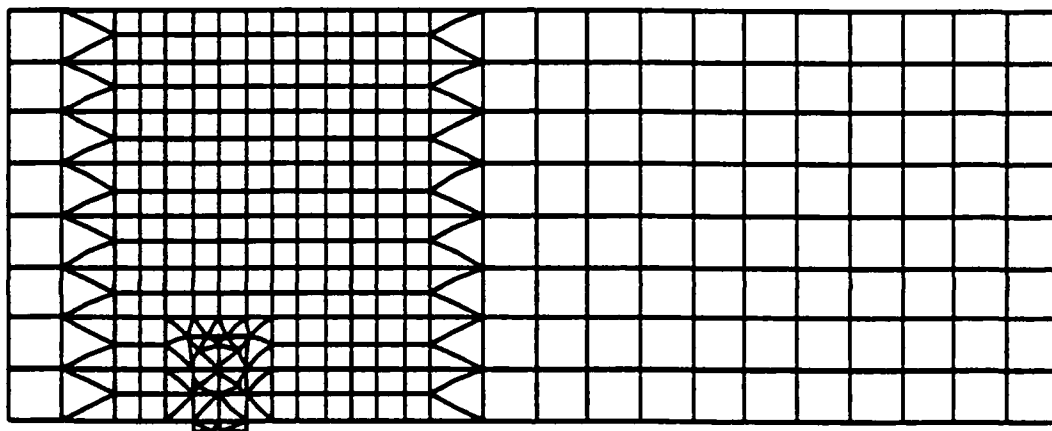
Figure A.1 Configuration selected for testing

Figure A.2   Initial Finite element mesh of specimen #1
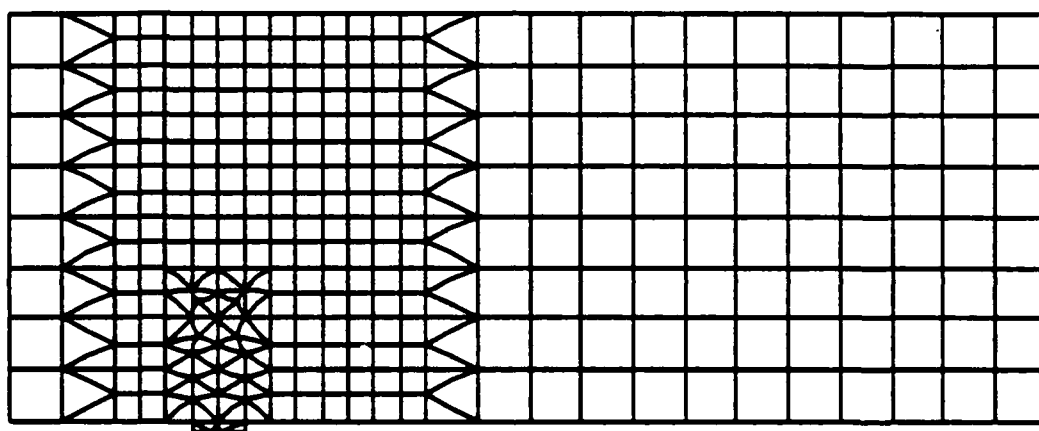(a = 1 inch , d = 6 inches)

Figure A.3   Initial Finite element mesh of specimen #2
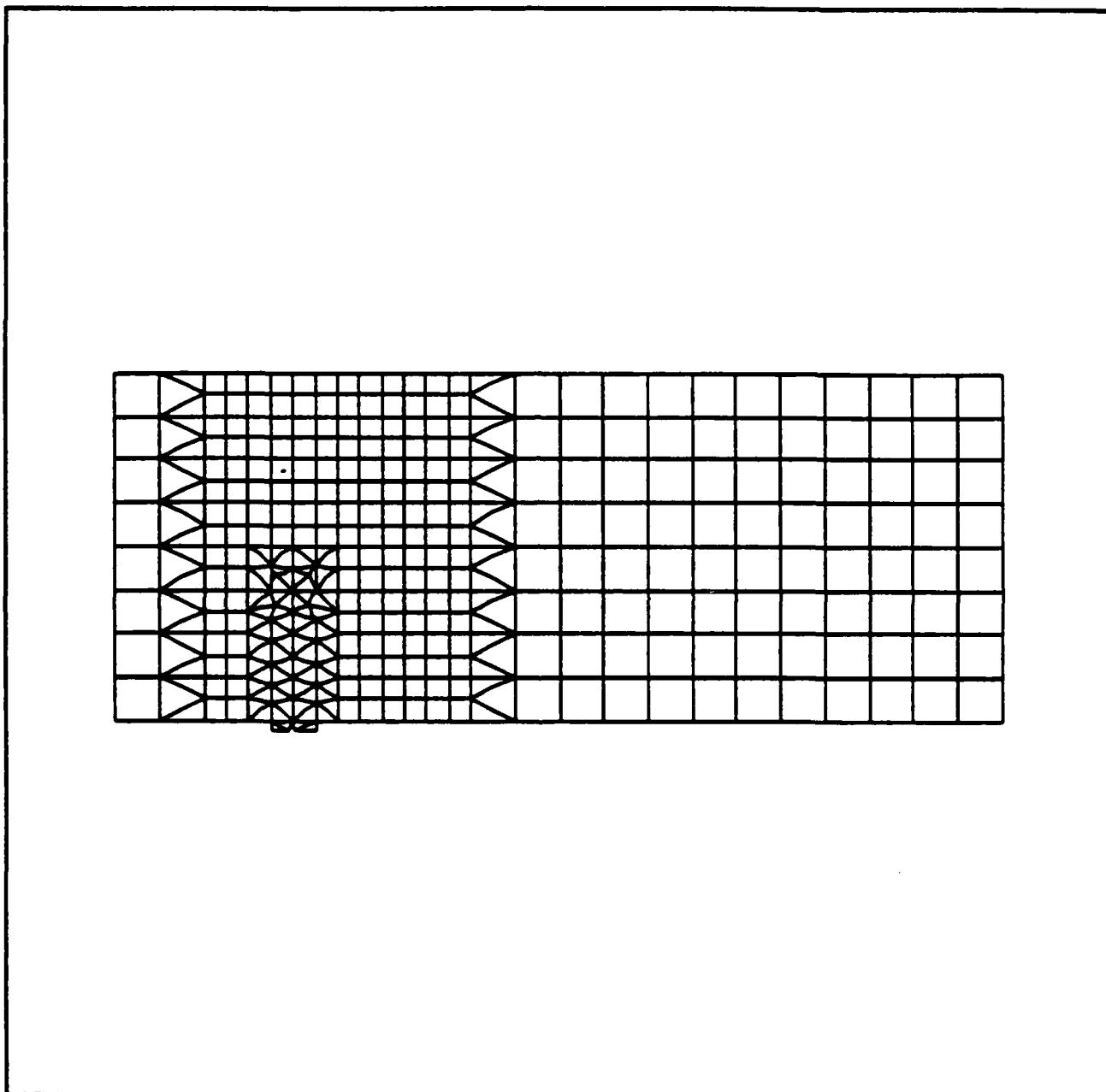(a = 2 inches, d = 6 inches)

Figure A.4   Initial Finite element mesh of specimen #3
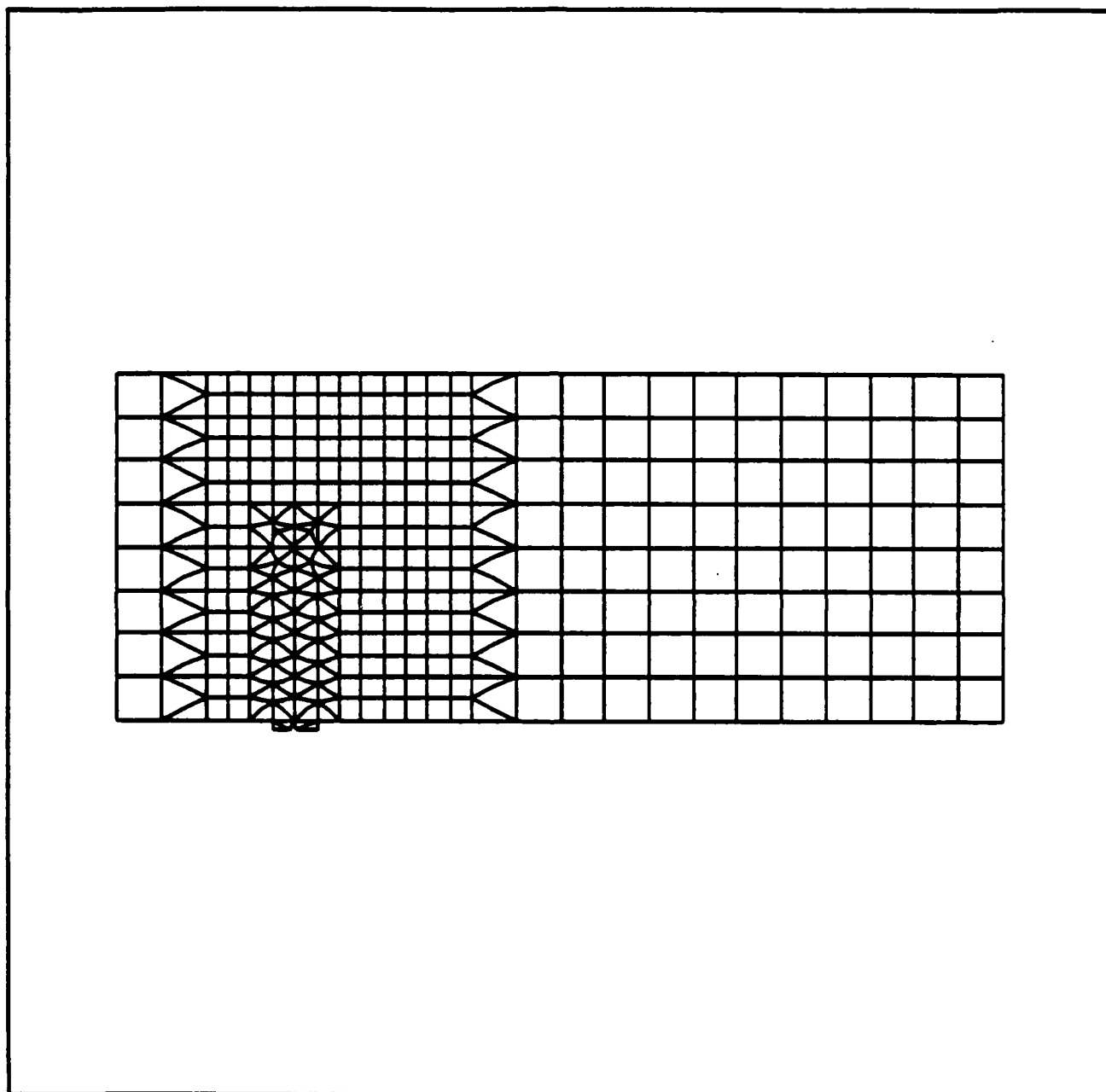(a = 3 inches, d = 6 inches)

Figure A.5 Initial Finite element mesh of specimen #4
(a = 4 inches, d = 6 inches)

computed stiffness equals the modulus of elasticity of the specimen.

Table A.1 shows for each specimen the computed and measured stiffness for each specimen, and the corresponding Young's modulus. The average value of the modulus of elasticity for the four selected specimens is 474,000 psi with a variation of 6% about this value. The observed average modulus of elasticity is very close to the value of 450,000 psi provided by the manufacturer in Table A.2.

Table A.1. Computed and Measured Stiffness and Corresponding Young's Modulus for Each Specimen.

Specimen #	Initial Crack Length (in)	Computed Stiffness (lb/in)	Measured Stiffness (lb/in)	Young's Modulus (psi)
1	1	0.398	186,960	469,295
2	2	0.184	85,653	459,442
3	3	0.097	47,696	491,622
4	4	0.053	25,363	475,998

Note: Computed stiffness is based on a value of 1 for both fracture toughness and Young's modulus.

Property	ASTM Method[a]	Units	Plexiglas MC
Mechanical			
Tensile Strength (¼" specimen- 0.2"/Minute)	D638		
Maximum		psi	10,000
Elongation, Maximum		%	4.5
Modulus of Elasticity		psi	450,000
Flexural Strength (Span depth ratio 16, 0.1"/Minute)	D790		
Maximum		psi	15,000
Deflection, Maximum		inches	0.6
Modulus of Elasticity		psi	450,000
Compressive Strength (0.05"/Minute)	D695		
Maximum		psi	16,000
Modulus of Elasticity		psi	430,000
Impact Strength	D256		
Charpy Unnotched		ft. lbs./ ½" x 1" section	7.0
Rockwell Hardness	D785	—	M-90[*]
Resistance to Stress			
Critical Crazing Stress	ARTC Mod.		
Isopropyl Alcohol	of	psi	1,300
Toluene	MIL-P-6997	psi	1,200

Table A.2 Mechanical properties of plexiglas provided by Rhoms manufacturing company

APPENDIX B

MEASUREMENT OF FRACTURE TOUGHNESS

B.1 Fracture Toughness Testing

A standard plane strain fracture toughness test, based on recommendations of ASTM E399-83 [29], was performed to obtain the fracture toughness of plexiglas. The specimen is shown in Figure B.1. Loading was performed under CMOD control to assure a slow stable crack growth.

Readings of load and CMOD were performed continuously. At fracture initiation, the crack propagated in a slow and stable manner until it stopped. The location of the new crack tip was then approximately recorded using a transparent graph paper. A more accurate crack tip location was later obtained from load-versus-CMOD records using the compliance calibration technique. This procedure was then repeated until the test was completed.

From a single specimen, various combinations of crack length and corresponding fracture initiation load were then used to calculate the material fracture toughness. This is equivalent to testing several similar specimens with increasing initial crack length.

Two different methods were used to calculate the fracture toughness of. The next two sections explain in detail each of these methods, while the last section presents a comparison between them.
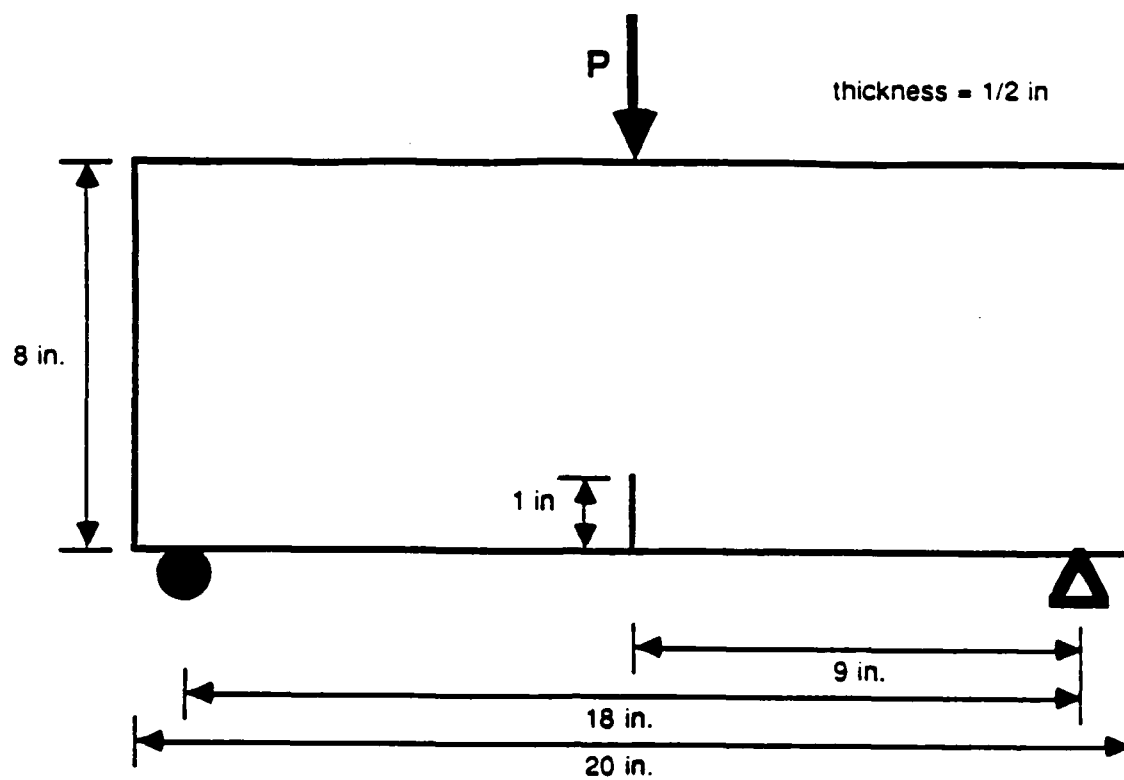
Figure B.1 Single-Edge-Notch (Bend) fracture toughness test

B.2 Description of First Method

The first method used directly the measured crack tip locations from the transparent graph paper. The corresponding fracture initiation loads were obtained by finding the points on the load-versus-CMOD curve at which departure from linearity commenced.

The apparent fracture toughness of plexiglas was computed using the equation proposed by Srawley [30]. The equation is accurate within 0.5 percent over the entire range of crack length:

$$K = \frac{PS}{BW^{3/2}} \ \frac{3\left[\frac{a}{W}\right]^{1/2}\left[1.99 - \frac{a}{W}\left(1 - \frac{a}{W}\right)\left(2.15 - 3.93\frac{a}{W} + 2.7\frac{a^2}{W^2}\right)\right]}{2\left[1 + 2\frac{a}{W}\right]\left[1 - \frac{a}{W}\right]^{3/2}}$$

$$(B.1)$$

where, a: initial crack length

p: fracture initiation load

B: specimen thickness

W: specimen width

S: specimen length

Figure B.2 shows a plot of apparent fracture toughness versus measured crack length. A line fit through the data would give a more or less horizontal line, which indicates that fracture toughness must be the same at all crack tip locations. This means that the apparent fracture toughness computed at each crack tip location is, indeed, the plane strain fracture toughness.
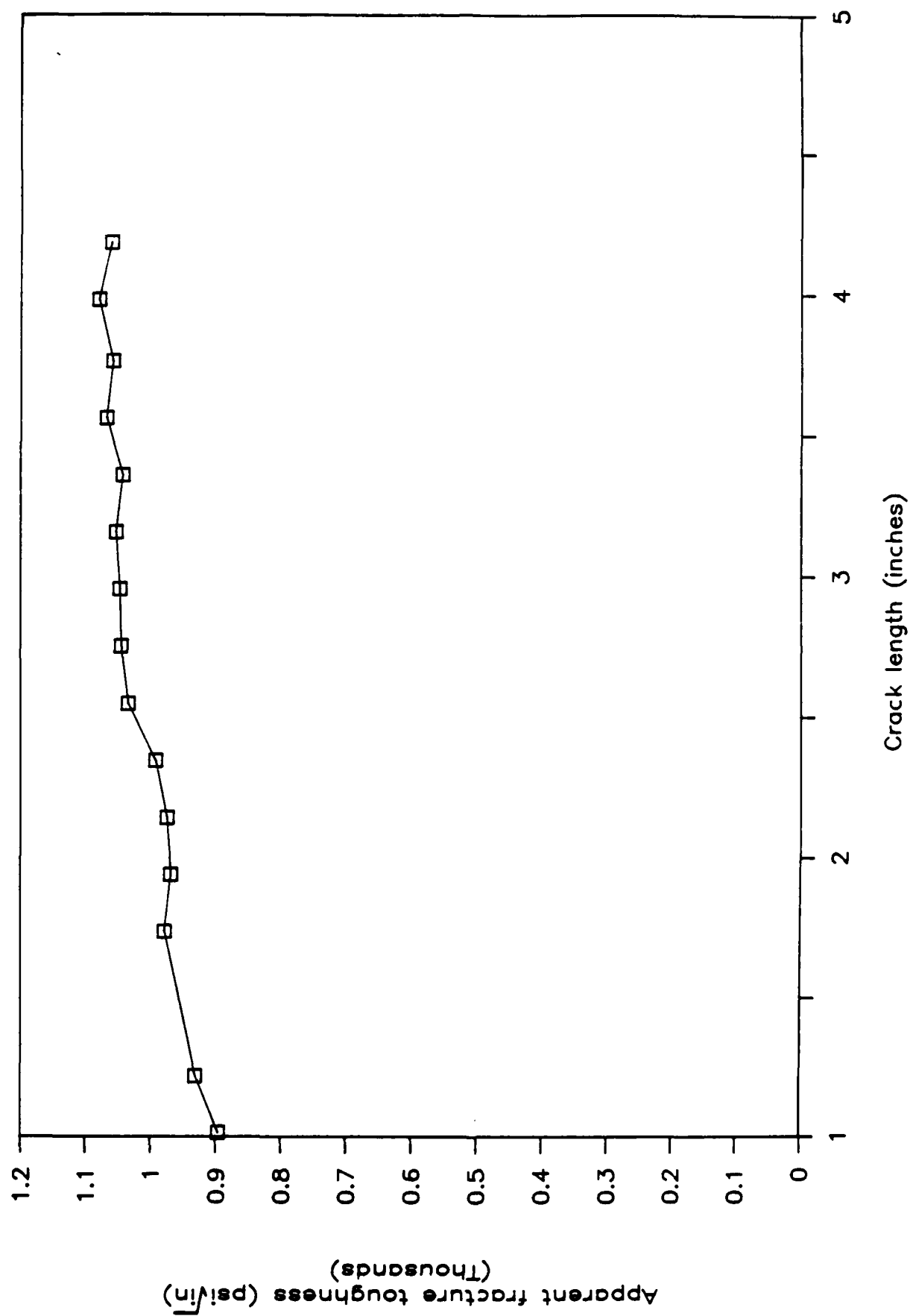
Figure B.2   Plot of apparent fracture toughness versus
measured crack length (First Method)

B.3   Description of Second Method

A compliance calibration technique is used to obtain more accurately the crack tip locations from the load-versus-CMOD records.

The compliance calibration technique consists of obtaining from analysis a plot of compliance versus crack length. The compliance is defined as the inverse of stiffness. A finite element model of the specimen was first prepared, as shown in Figure B.3. After performing an analysis, the crack tip location, and the corresponding CMOD and fracture-initiation load were computed and stored. The crack was then propagated, and the procedure was repeated until the crack reached the boundary prior to complete failure. The compliance of the structure at each crack tip location is defined as the ratio of CMOD to fracture initiation load. Figure B.4 shows a plot of computed compliance versus crack length.

Since continuous readings of load-versus-CMOD were measured during the experiments, the compliance corresponding to any crack length could be easily computed by dividing CMOD by corresponding load. Knowing the compliance from experiments, the corresponding crack length can be obtained from the compliance calibration curve, shown in Figure B.4.

Using the same fracture initiation loads as in the first method and their corresponding CMOD, the compliance at each crack tip location was computed. The corresponding crack length was then obtained from the compliance calibration curve. The
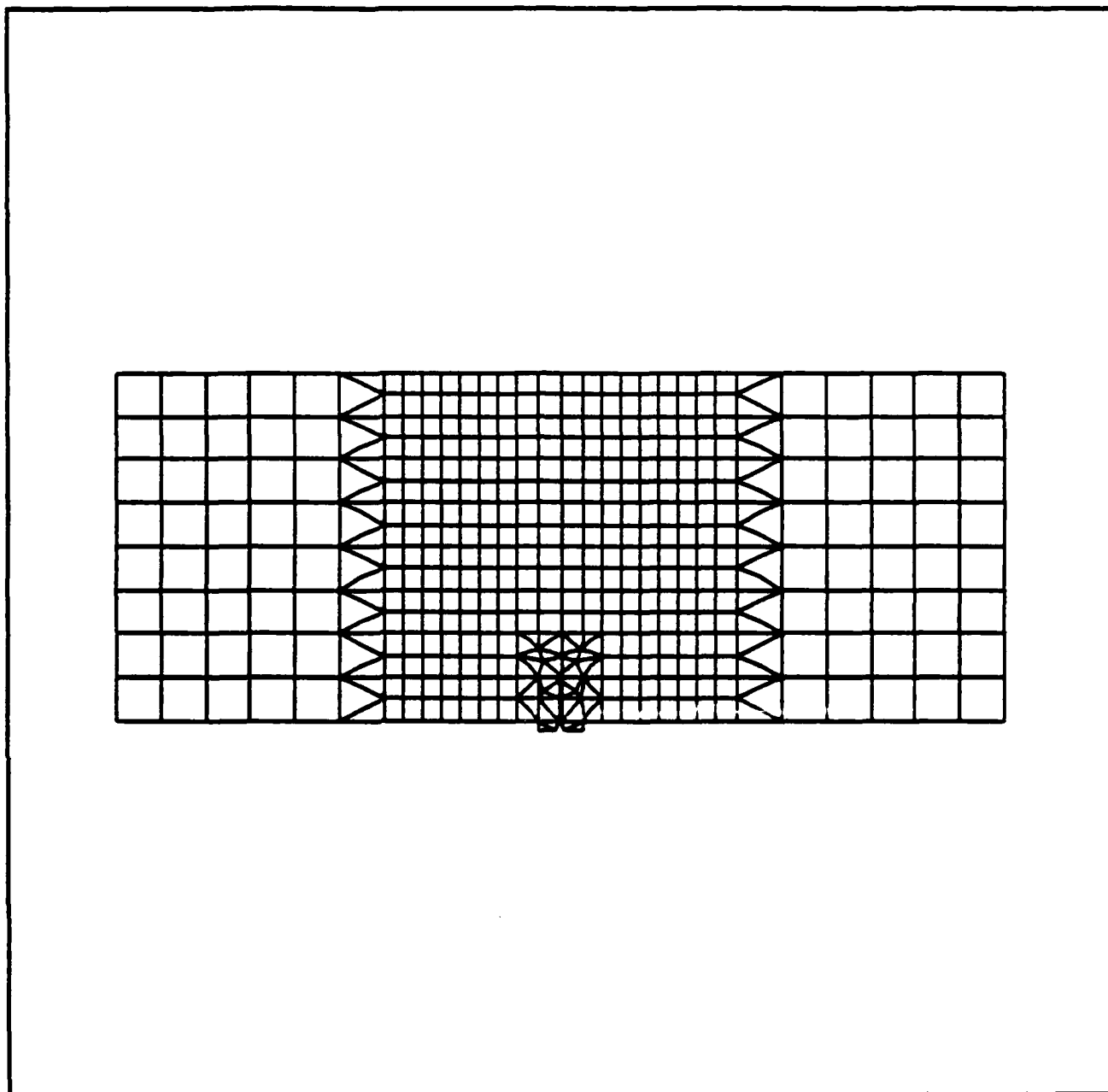
Figure B.3 Finite element mesh of Single-Edge-Notch
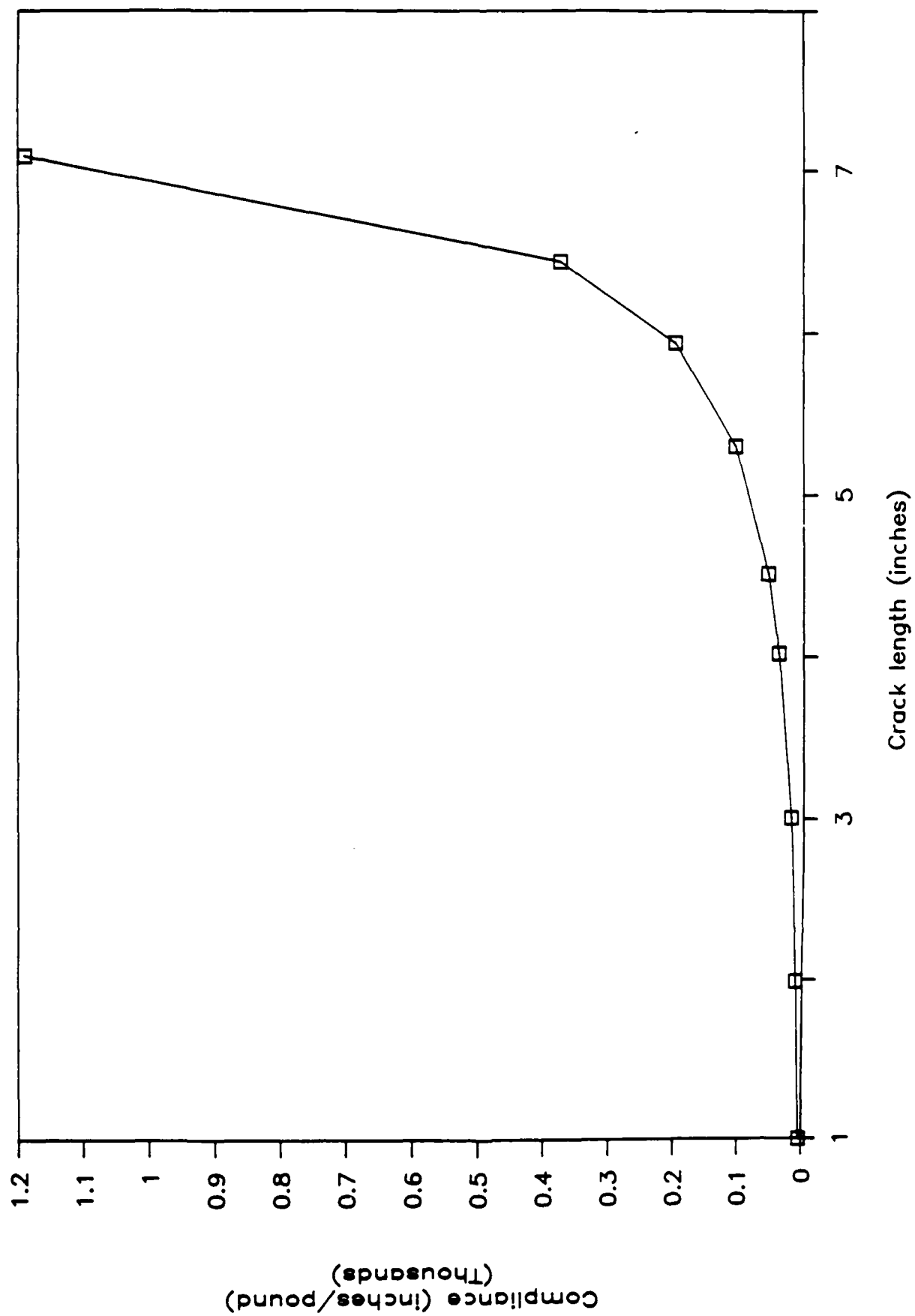(Bend) fracture toughness specimen

Figure B.4   Plot of computed compliance versus crack length

apparent fracture toughness was computed using the same equation used in the first method. A plot of apparent fracture toughness versus computed crack length is shown in Figure B.5.

B.4 Comparison of Both Methods

Intuitively, the second method is more accurate than the first one, because it does not include experimental errors made in crack length measurement. In fact, the maximum relative error between computed and measured crack length was about order of 11%. The second method was, therefore, used to obtain the fracture toughness of plexiglas. The average plane-strain fracture toughness was 944 psi $\sqrt{\text{in.}}$, with a range from 896 to 968 psi $\sqrt{\text{in.}}$.
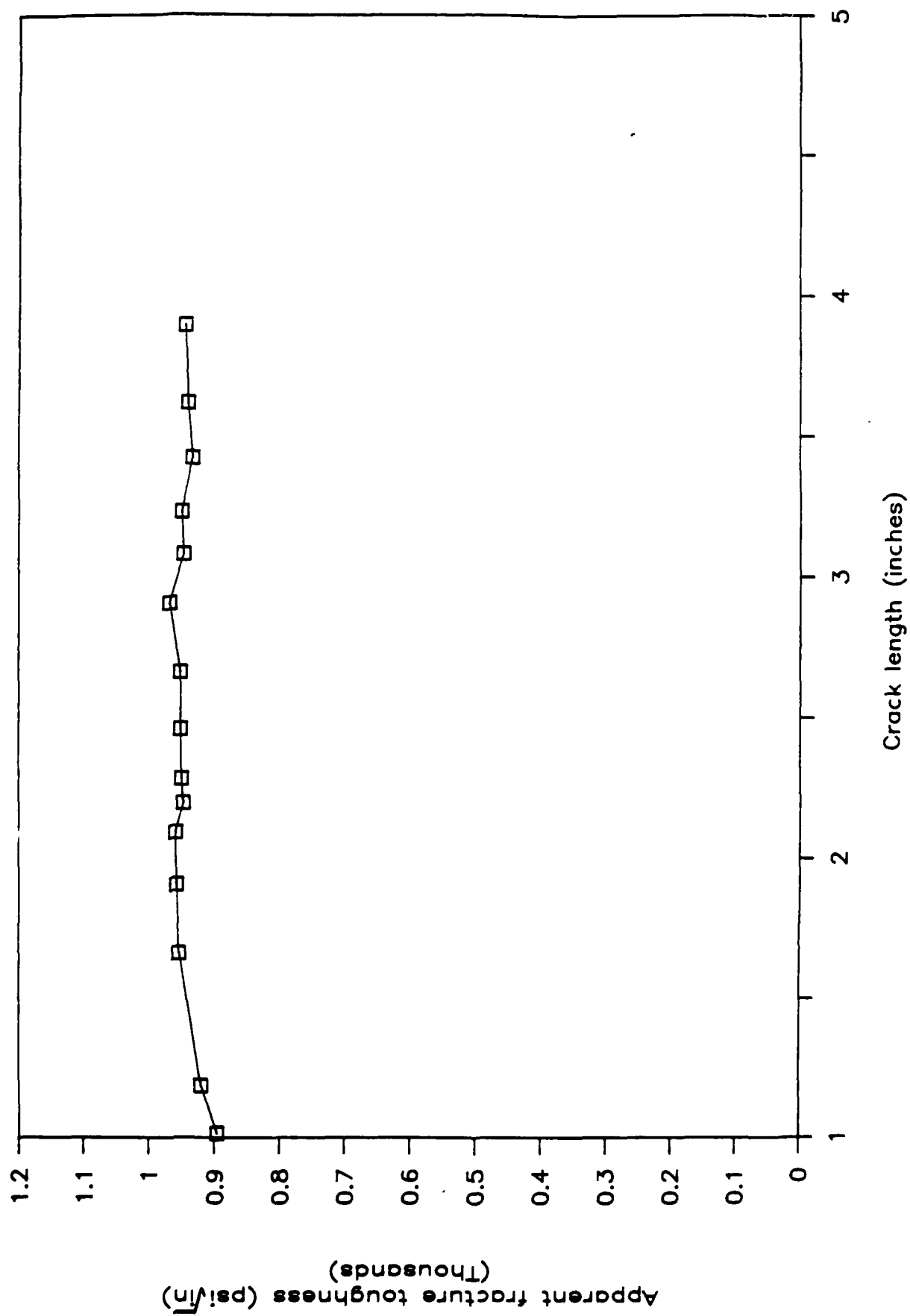
Figure B.5 Plot of apparent fracture toughness versus
computed crack length (Second Method)

APPENDIX C

DESCRIPTION OF AND USER MANUAL FOR

SOFTWARE USED TO CONTROL EXPERIMENTS

C.1 Introduction

The Mixed-mode Fracture Experiment Control Software (MIFECS) is an interactive menu-driven program developed to control testing of mixed-mode fracture specimens. The software was written in QuickBasic language, and is run in the Microsoft QuickBasic environment.

C.2 Choice of Programming Environment

Microsoft QuickBasic is a powerful programming environment in which applications can be created for IBM personal computers and compatibles. It was chosen for several reasons that include:

(i) Support for modular programming that enables one to build applications consisting of several module files.

(ii) An efficient editor that checks syntax and interprets each line of code, and allows one to run the program at any point during the development process.

(iii) Powerful debugging tools that provide efficient ways to check the logic of the program.

(iv) A structured language with many capabilities such as subprograms and functions, a wide variety of structural decisions and loops, records, and structures, etc.

(v) A powerful and versatile graphics package that allows one to write applications with graphics capabilities and efficient system-user interface.

C.3 Description of Software

MIFECS consists of fifteen modules. Each module is assigned a specific subtask in the program; for instance, the "DRAW MENU" module draws the menu page, and the "SAVE_GEO" module saves the specimen geometry in an output file. The modularity of the program allows one to (i) easily modify some parts of the code without changing the remaining parts; (ii) easily expand the present software capabilities; (iii) port the code to other system environments; and (iv) easily translate the code to other languages.

MIFECS allows one to read three different input channels, namely load, load-line displacement and CMOD. The code also can send an output signal through the CMOD channel. The main task of the code consists of simply increasing the CMOD value at constant rate and reading the corresponding input channels. The same procedure is then repeated until the test is completed. At every step, the program waits for the user's response to increase the CMOD value. Figure C.1 shows a flowchart of MIFECS, that explains in more detail the logic of the program.

MIFECS uses a DT 2818 data acquisition system manufactured by Data Translation Company. The program can be easily modified to work with other data acquisition systems. Only three modules need to be modified: "INIT_BOARD" module which initializes the data
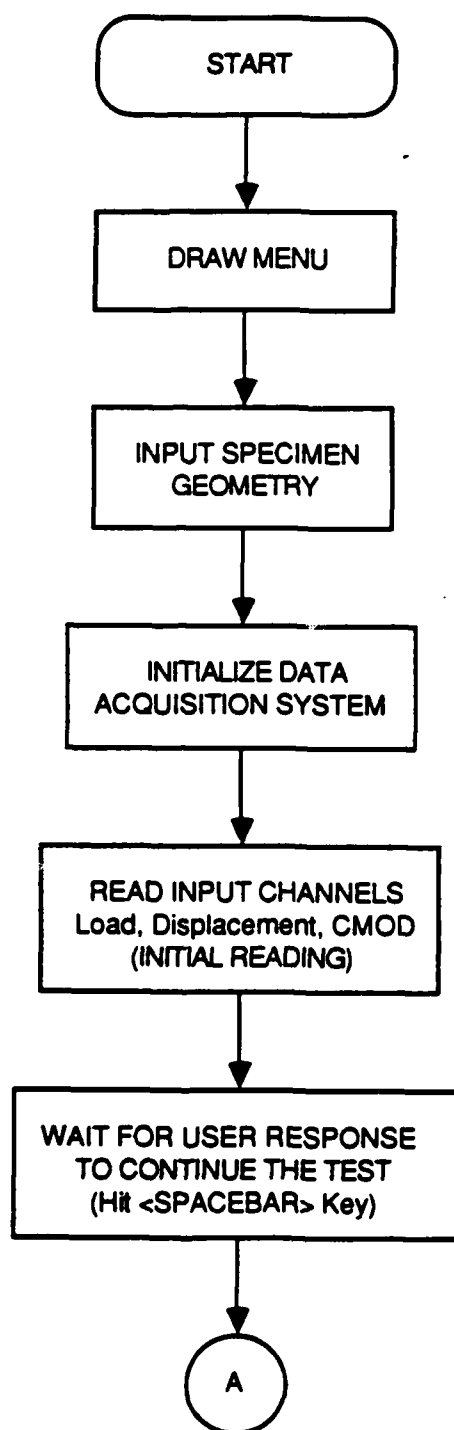
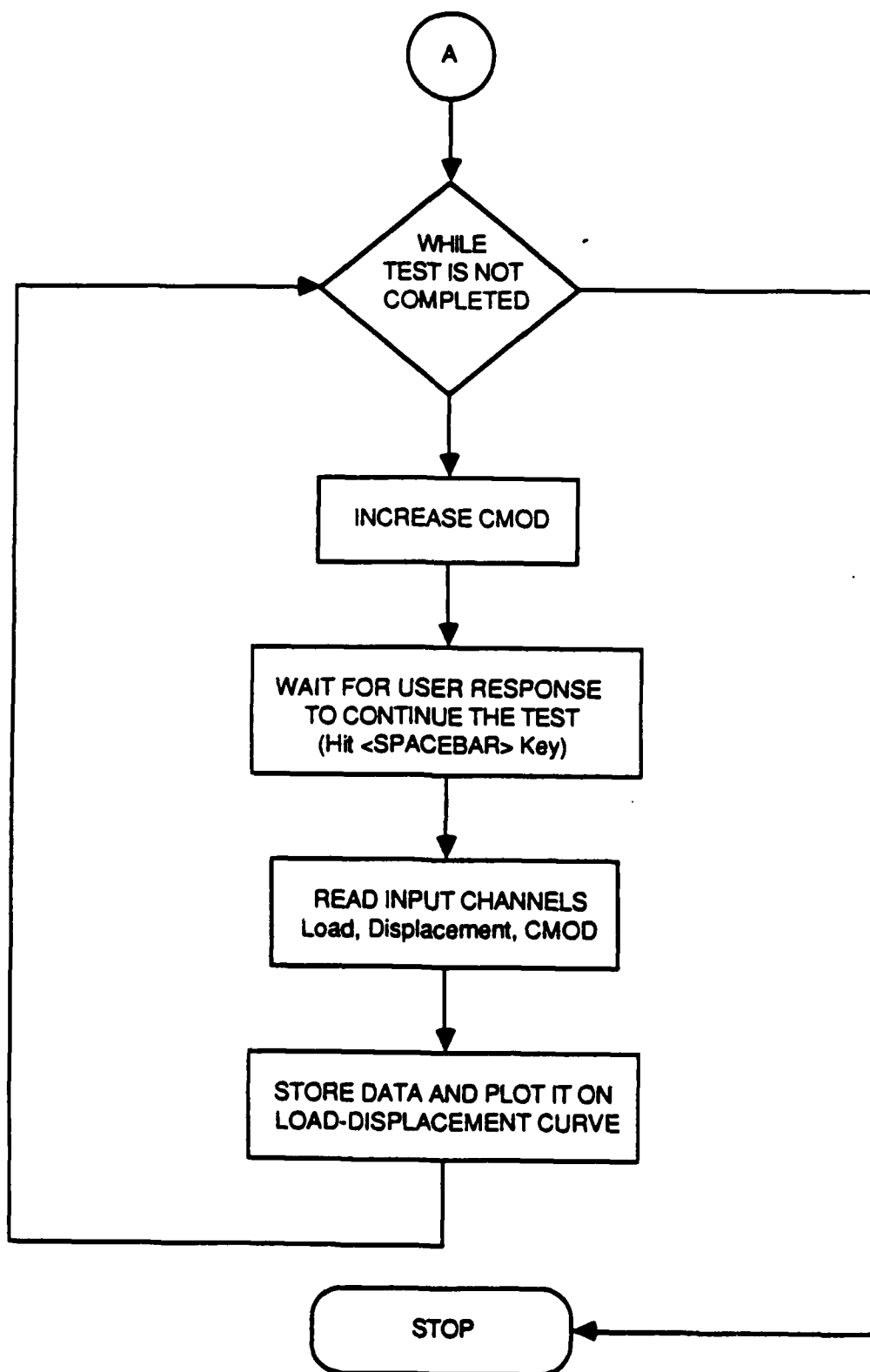Figure C.1   Flowchart of the program MIFECS (Mixed-mode Fracture Experiment Control Software)

Figure C.1   Flowchart of the program MIFECS (Mixed-mode
Fracture Experiment Control Software) (Continued)

acquisition system, "INCR_CMOD" module which sends output signals to increase CMOD, "READ_CHAN" which reads all the input channels (load, load-line displacement and CMOD).

C.3   User Manual

MIFECS is an interactive menu-driven program, whose objective is to control testing of mixed-mode fracture specimens.

To run the software, the user must type "MIFECS" at the MS-DOS level. When the program is activated, the main page, shown in figure C.1 appears on the screen. This page consists of three main windows. The first window contains information requested by the program about specimen geometry. This includes specimen name, length, width and thickness, initial crack location, length and inclination. The second window contains a plot of load versus load-line displacement, that indicates at which stage the testing is. The third window is used to display messages to the user about status of the program.

Prior to testing, the user must input the specimen geometry. The program then makes an initial reading of all three input channels (load, load-line displacement and CMOD), and requests the user to increase the CMOD value. The user can do that by striking the <SPACEBAR> key on the keyboard. The code then makes another set of readings of all input channels, and stores the data in an output file. The procedure is then repeated until the test is completed. To quit the program the user must strike the <F10> key.

After quitting the program, the data is collected in an output file with a name specified by the user and with extension ".DAT". The data can then be analyzed and plotted using any spreadsheet software, such as *LOTUS* or *GRAPHER*.

APPENDIX D

PHOTOGRAPHS OF EXPERIMENTAL SETUP AND

OF A MIXED-MODE FRACTURE TEST

This appendix contains actual photographs of the experimental setup and of a typical mixed-mode fracture test in progress.

Figure D.1 shows a photograph of the experimental setup, while Figure D.2 shows the schematic of the testing system. The configuration selected for testing is shown in Figure D.3. Figure D.4 shows the specimen placed in the load setup. Figure D.5 shows the initial screen image of the control program MIFECS, which gets displayed before starting the test. Figures D.6 to D.11 show photographs of specimen and of screen images obtained during a typical mixed-mode fracture test. In these figures, only three stages are shown:

(i)   Just after fracture initiation

(ii)   When crack is halfway propagated

(iii) When crack is at its final propagation steps.

Figure D.1 Photograph of experimental setup
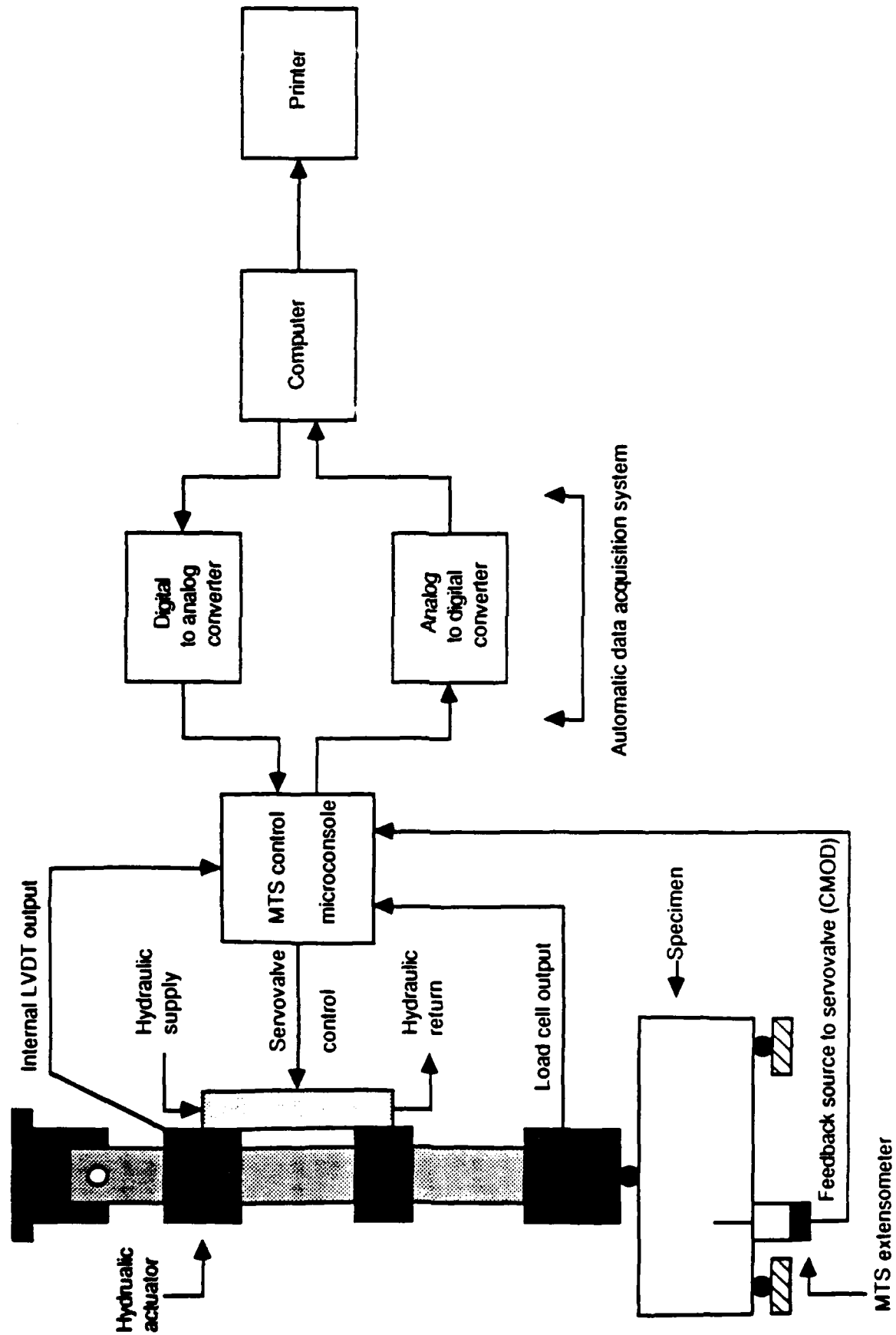
Figure D.2 Schematic of testing system
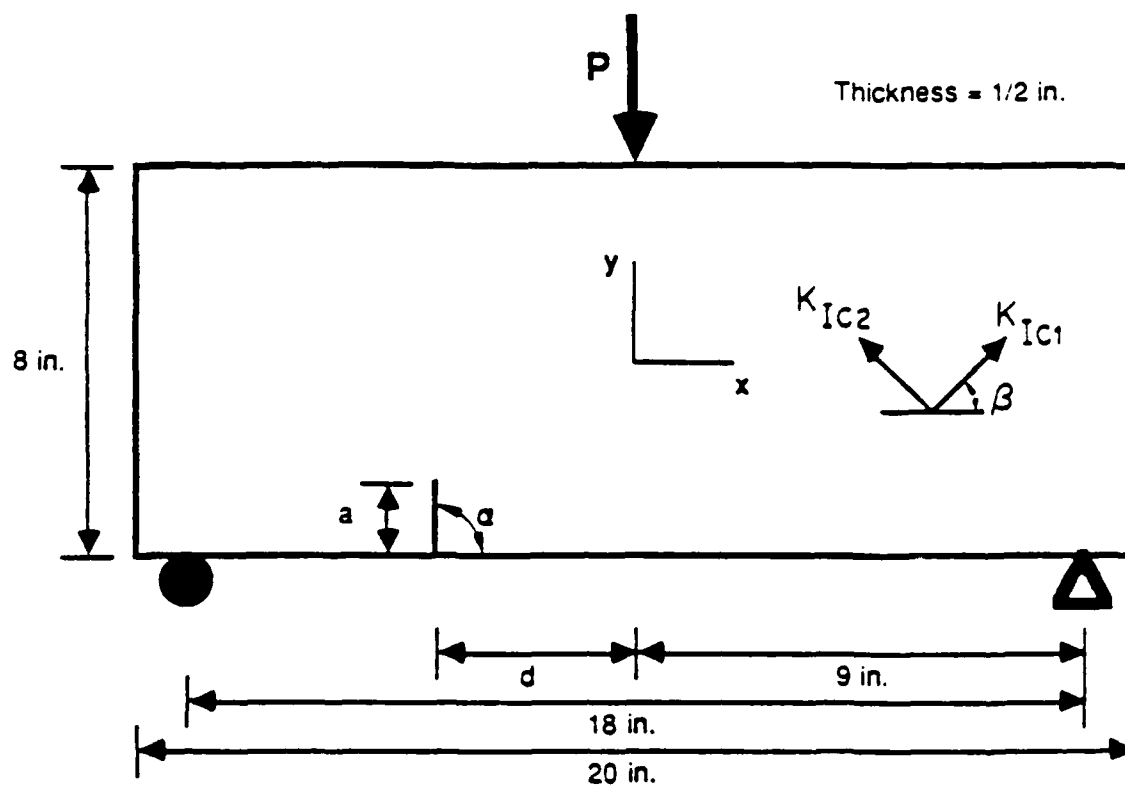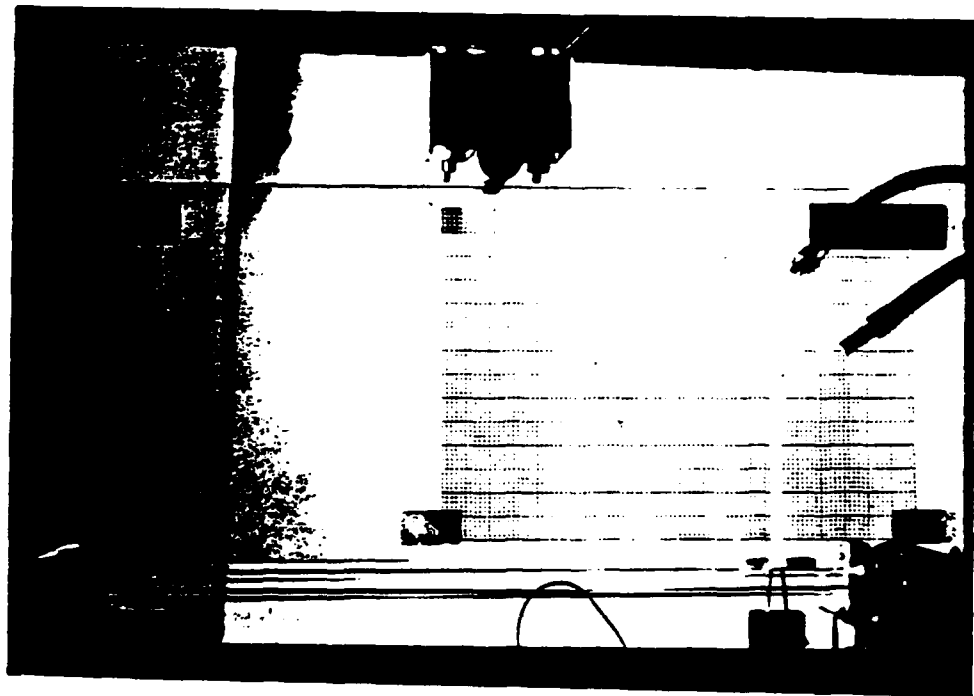
Figure D.3 Configuration selected for testing

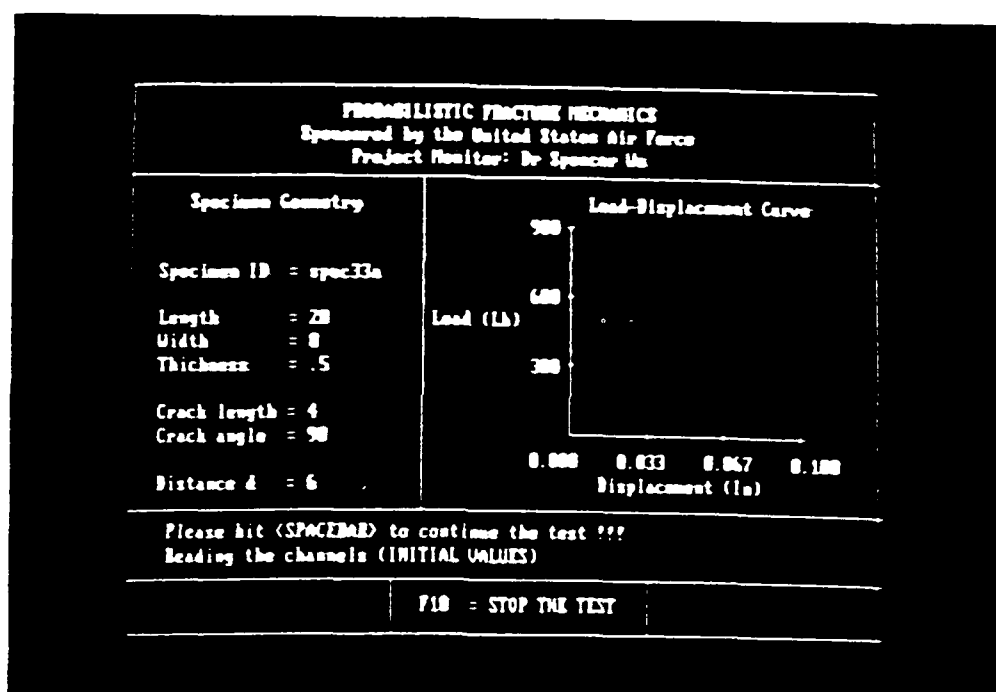Figure D.4 Photograph of load setup

Figure D.5 Photograph of initial screen image of MIFECS

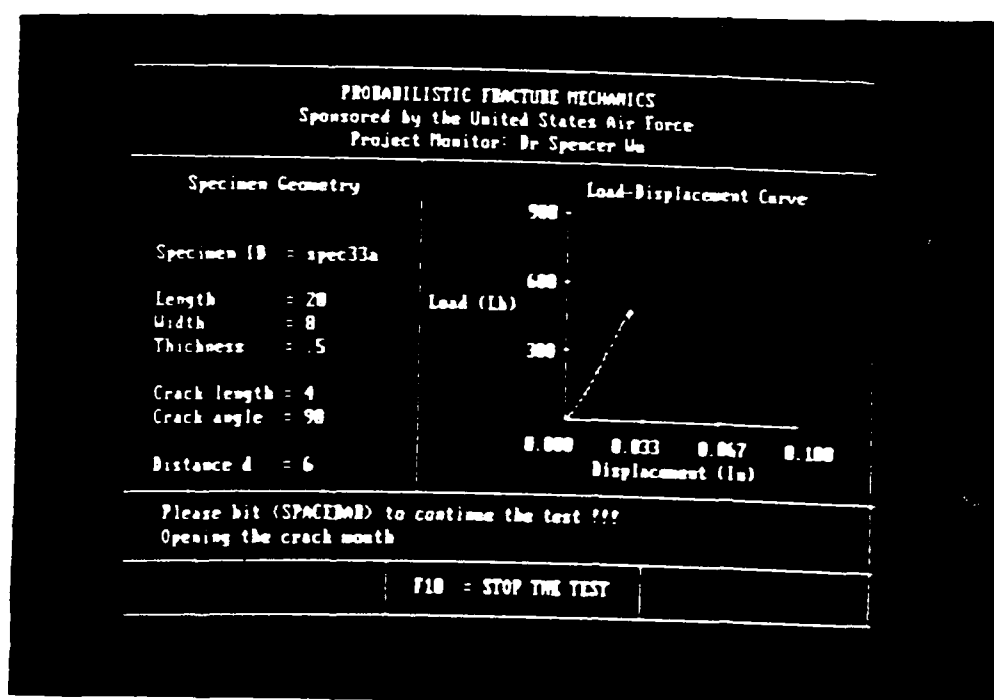Figure D.6 Photograph of specimen just after fracture initiation

Figure D.7 Photograph of screen image of MIFECS just
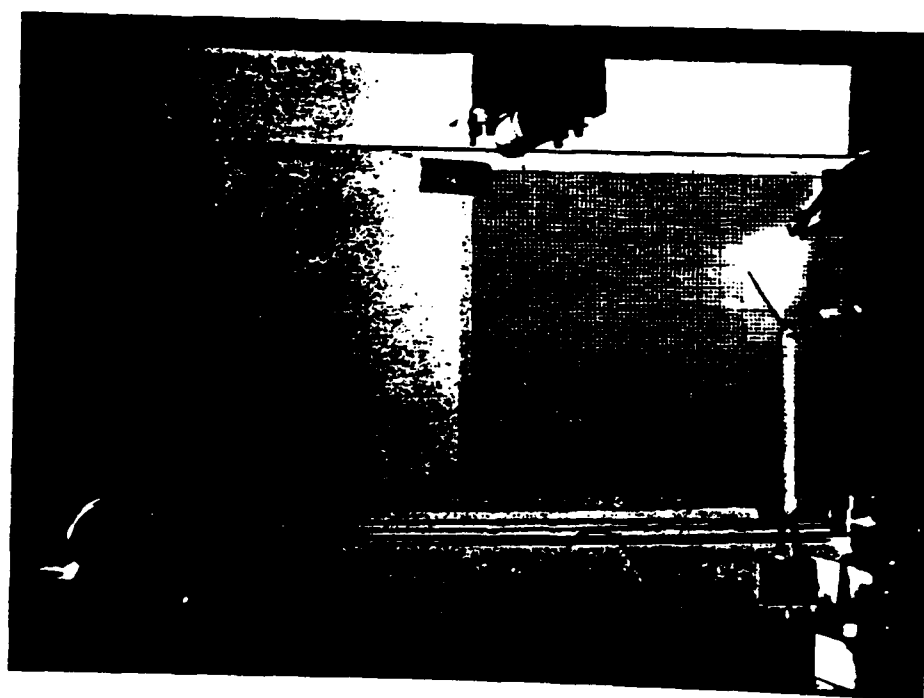after fracture initiation

Figure D.8 Photograph of specimen when crack is half way propagated
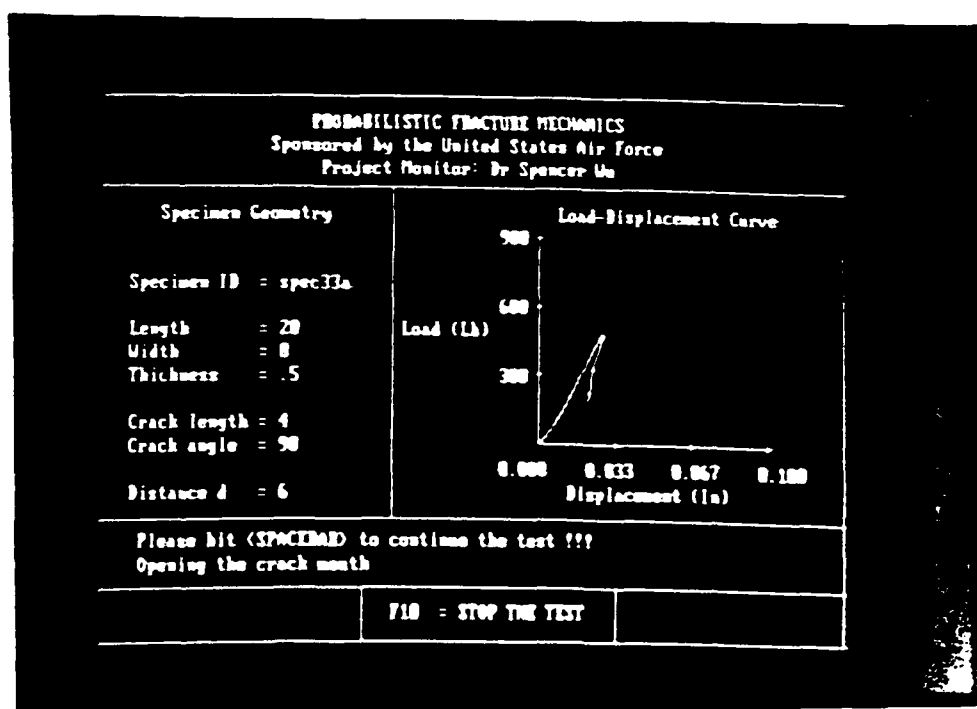
Figure D.9 Photograph of screen image of MIFECS when
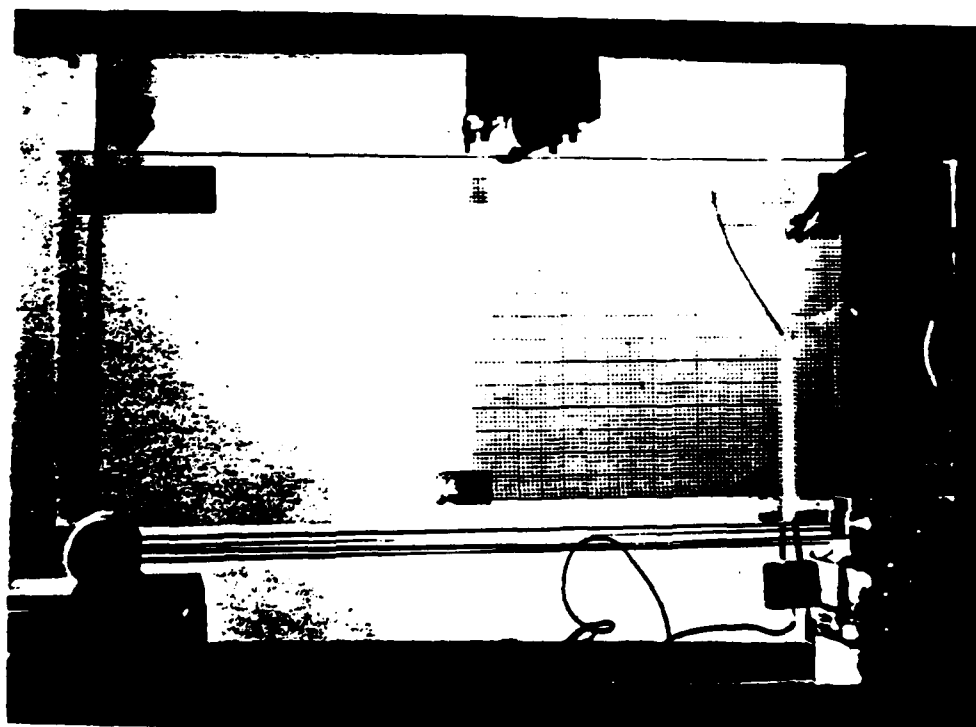crack is half way propagated

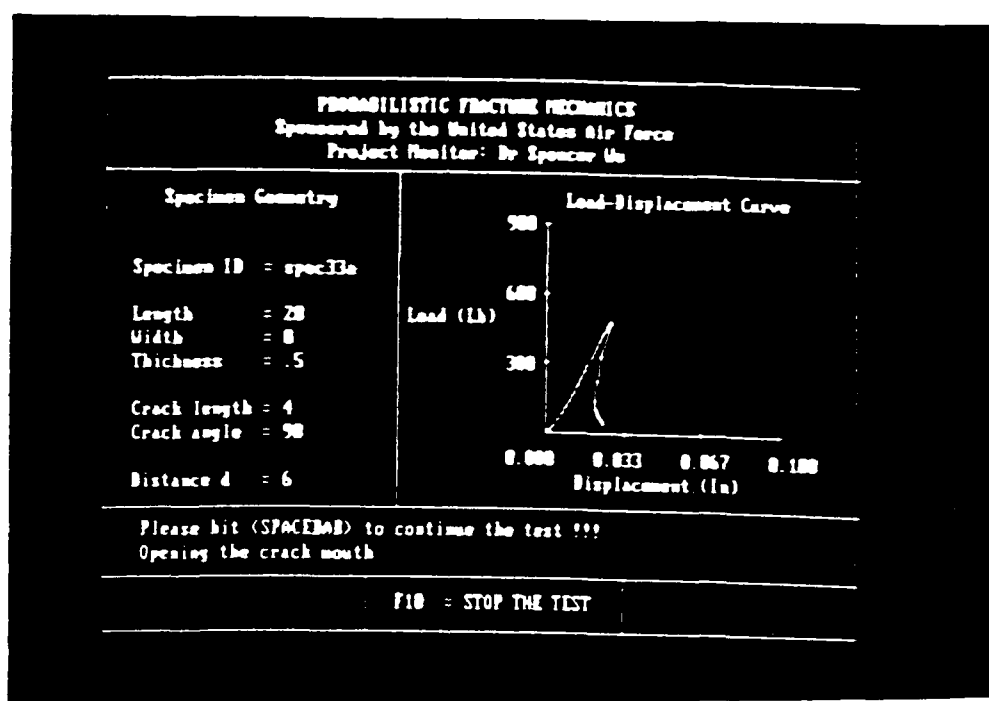Figure D.10 Photograph of specimen at final stage of crack propagation

Figure D.11   Photograph of screen image of MIFECS at final
stage of crack propagation